A DIGITAL TWIN FRAMEWORK OF A MATERIAL HANDLING OPERATOR IN INDUSTRY 4.0 ENVIRONMENTS

by

Abhimanyu Sharotry, B. Tech

A thesis submitted to the Graduate Council of
Texas State University in partial fulfillment
of the requirements for the degree of
Master of Science with a
Major in Engineering
December 2020

Committee Members:

Jesus A. Jimenez, Co-Chair

Francis A. Méndez Mediavilla, Co-Chair

Rachel M. Koldenhoven Rolfe

Damian Valles

FAIR USE AND AUTHOR'S PERMISSION STATEMENT

Fair Use

Duplication Permission

DEDICATION

I would like to dedicate this research work to my family, friends, and professors for their guidance, encouragement, and support throughout this journey.

ACKNOWLEDGEMENTS

I would like to thank my thesis advisor, Dr. Jesus A. Jimenez, for providing me an opportunity to work with him. His immense knowledge and motivation always guided me in the right direction. Always encouraging to explore new opportunities and never stop imagining has been his motto in research. State-of-the-art resources and the environment have always been key to this excellent learning experience.

I would also like to thank Dr. Francis A. Méndez Mediavilla for his immense support and time in the field of statistics for this research. It would not have been possible without assistance from Dr. Rachel M. Koldenhoven Rolfe and her experience in the field of health and human performance. With his excellent knowledge in machine learning and artificial intelligence, Dr. Damian Valles helped foresee this research's vision.

My heartfelt gratitude to Dr. Vishu Viswanathan, Graduate Advisor of the Ingram School of Engineering, and Dr. David Wierschem for their constant support throughout my program. I would also like to thank Sarah Rivas, Chelsea Torres, and John Ivey from Ingram School of Engineering for their kind assistance throughout. A massive shoutout to my research colleagues at CHiPS laboratory for creating a delightful working atmosphere.

Finally, I would like to thank my family, relatives, and friends for their unconditional love and support.

TABLE OF CONTENTS

Page

LIST OF TABLES

Table **Page**

LIST OF FIGURES

Figure **Page**

LIST OF ABBREVIATIONS

Abbreviation	Description
AIM	Automatic Identification of Markers
CI	Confidence Interval
DT	Digital Twin
DTW	Dynamic Time Warping
EWMA	Exponentially Weighted Moving Average
IDE	Integrated Development Environment
LCL	Lower Control Limit
MMH	Manual Material Handling
MoCap	Motion Capture
OC	Out-of-control
QTM	Qualisys Track Manager
ROM	Range of Motion
RPE	Borg Rating of Perceived Exertion
SCC	Shewhart Control Charts
UCL	Upper Control Limit

ABSTRACT

The manufacturing and construction industries around the globe have poor occupational health and safety records. Slip & fall, manual material handling (MMH) moves, and forklift accidents are the top three causes for warehouse injuries. Statistics from the U.S. Department of Labor, Bureau of Labor Statistics show that in manufacturing industries, musculoskeletal disorders accounted for 34% of the "Days Away from Work" cases in 2017. Sprains, strains, and tears accounted for the leading type of injury in the manufacturing industry. This research presents a digital twin (DT) approach to assess fatigue in human operators in the material handling industry. DT is an advanced simulation tool that is an exact representation of a physical object. For data collection and analysis, a simulation-based framework is presented. The proposed methodology consists of three modules: Data Collection, Operator Analysis & Feedback, and Digital Twin Development. An optical motion capture system helps develop the DT, which captures simulated material handling activities similar to those in an actual environment. For a pilot study, participants were selected from the university population to perform a series of 'lifting' MMH activities. The participants' physical attributes, body kinematics, and their rating of perceived exertion were measured throughout the experiment. Fatigue was measured as a factor in the subjects' joint angles and analyzed via a dynamic time warping algorithm. To identify the accumulation of biomechanical fatigue, we use an exponentially weighted moving average control chart.

This research aims to conceptualize a DT of an operator and propose a tool that

enables the understanding and analysis of the factors that influence human variability and error while performing MMH tasks. The proposed methodology was able to detect biomechanical fatigue in subjects performing MMH tasks and justify the need for a true DT of an operator for fatigue evaluation in the Industry 4.0 era.

1. INTRODUCTION

1.1 Background

The first industrial revolution began in the 18th century with the introduction of mechanical production facilities. This revolution, identified as Industry 1.0, was dedicated to water and steam-powered machines, reducing human labor and effort with increased productivity [1]. Industry 1.0 began industrialization, which was followed by the introduction of electricity at the beginning of the 20th century. More efficient machines were invented to increase the productivity, quality, and efficiency of manufacturing products, giving birth to the term Industry 2.0, i.e., the second industrial revolution. Industry 2.0 also gave humankind its first assembly line, introduced by Henry Ford, and produced the iconic Ford Model T [1]. This innovation reduced the production time per vehicle from more than twelve hours to two hours and thirty minutes [2]. Frederick Winslow Taylor contributed by further optimizing the manufacturing process by developing tools for workforce optimization [3]. Other production management techniques, such as the Toyota Production System with lean manufacturing and just-in-time production, developed ways to optimize the system by reducing waste associated with overproduction, excess inventory, and defective products, to name a few [4]. By the mid-20th century, humans started broad-scale mass production of items, allowing large society sections to afford products because of lower production costs. Meanwhile, the research and development of electronic components introduced automation into the field of manufacturing processes. Development of Programmable Logic Controllers (PLC), transistors, integrated circuits, and computers led the shift to the third industrial revolution, i.e., Industry 3.0. As a result of this, automation of machines was possible,

resulting in reduced demands on the human workforce and increased production through increased speed and accuracy. As an outcome of this hardware enhancement, there was a significant rise in the software development sector: controlling hardware, management resources such as Enterprise Resource Planning (ERP) tools, logistics, simulating product flow in the factory, and supply chain management [1].

Towards the end of the 20th century, with the boom in the internet and telecommunication industry, collecting, storing, analyzing, and exchanging information evolved. Technologies developed to integrate traditional production systems into the cyber world, linking the physical and virtual world allowing the machines to communicate intelligently and make decisions. This technological advancement in machines' capabilities to make decisions, store, and analyze large amounts of data was the introduction to the fourth industrial revolution, i.e., Industry 4.0. This current era of Industry 4.0 that we live in is the era of digitalization and is evolving at an exponential pace as compared to the previous advancements [5]. Technologies such as the Internet of Things (IoT), cyber-physical systems (CPS), enterprise architecture (EA), artificial intelligence (AI), robotics, autonomous vehicles, and 3-D printing have been vital components in the development of this era of industrialization [5]. With the goals of customer-centric and customized products, advanced optimization levels, higher operational efficiency & productivity, and creating intelligent and self-sufficient factories of the future, everyday new technology is developed [6]. Another critical player of technology in this era, which is transforming manufacturing processes, is the digital twin (DT). Although mathematical models have been used since the eighteenth century to evaluate a system’s performance, Industry 4.0 tools such as IoT, big data, cloud

computing, artificial intelligence, and digital reality have made the interaction of physical and digital systems possible.

A DT is the virtual and exact representations of physical objects or systems over their life cycle [7]. The main characteristics of DT include scalability (analyze varying information), interoperability (track multiple variables in real-time), expansibility (ability to extend on the go), and fidelity (similarity to the real physical system). DTs add real-time capabilities for visualization, analysis, prediction, and optimization [8].

The futuristic Industry 4.0 manufacturing environment focuses on shorter delivery times, increased levels of customization, product variety, quality, and demand variability. With the transition in manufacturing to more technologically advanced and automated systems, it is essential to understand the role of the human operators who work in these environments. Industry 4.0 is accompanied by a change in the range of worker tasks and demands in the factory context [9]. The operators now are multi-skilled and perform jobs at several workstations capable of responding to mass-customized products and processing large amounts of information [10]. Romero et al. [11] has defined this smart generation of operators as Operator 4.0, i.e., humans assisted by machines and technology to enhance their physical, cognitive and sensorial capabilities to perform their manufacturing tasks.

A significant amount of manufacturing and material handling activities are highly manual [12]. Material handling is one of the most physically demanding tasks, and thus, can quickly become a leading factor contributing to operators' accumulation of both mental and physical fatigue [12]. According to the Bureau of Labor Statistics, 114 million people were employed in the Warehousing and Storage Industry Group in 2018

[13]. These statistics show that 22% of the workforce are “Laborers & freight, stock & material movers, hand,” and 17% work in stocking, order filling, or packaging by hand. According to Reeve et al. [14], the industry sectors “Construction,” “Transportation & Warehousing,” and “Manufacturing” reported a cumulative total of 13,782; 10,952; and 5,177 fatalities from 2003 to 2016, respectively. The study also listed that ‘Back – including spine – spinal cord’ was the most frequently injured body part, with 17% of cases involving days away from work and about 36% of cases involving sprains and strains. The research highlighted that human operators need a safer environment to work. The substantial reduction of fatalities over-time proves the use of safer practices but still corroborates the need for research in this field.

Factors such as personal characteristics, training, experience, and health conditions can influence the accumulation of fatigue in workers, which impacts the performance of activity [12]. While performing basic manual material handling tasks, workers experience physical fatigue, which occurs due to repetitive activities such as lifting/loading and leads to a high risk for low back, trunk, spine, hip, and knee injuries [15].

1.2 Research Objective

This research attempts to identify opportunities to track biomechanical fatigue caused by traditional repetitive Manual Material Handling (MMH) lifting activity. Using fundamentals of Industry 4.0 and DT technologies as a foundation, this research aims to conceptualize a DT of a human operator and propose a framework that enables the understanding and analysis of body fatigue while performing their material handling tasks.

1.3 Research Summary

A methodological framework, enabling the creation of a personalized digital twin to analyze and detect biomechanical fatigue, was presented. The framework used a dynamic time warping (DTW) algorithm and exponentially weighted moving average (EWMA) control charts to analyze the change in the human operator's joint angles performing a lifting MMH task.

Prior research by [16] [17] [18] provides a framework to conceptualize the DT of an MMH operator. The framework (Figure 1) includes the following three modules: 1) Data Collection Module, 2) Operator Analysis & Feedback Module, 3) Digital Twin Module.

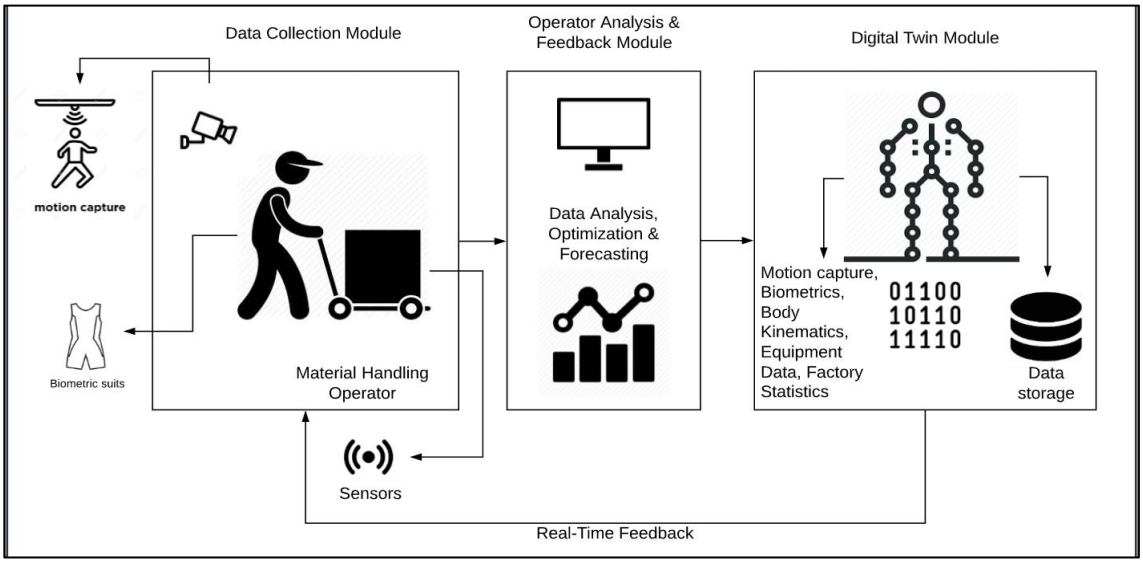

Figure 1. The framework of operator centric Industry 4.0 environment.

The Data Collection module uses a motion capture (MoCap) system to record human motions while performing a lifting MMH task in a laboratory environment. The system tracks reflective marker positions attached to a human subject's body and provides accurate x-y-z coordinate data at a frequency of 100 Hz as output. Coordinate

data for all the respective joint locations are stored in a database for further analysis.

Operator Analysis & Feedback Module conceptualizes the data analysis, optimization, and forecasting based on joint movements [19], type of motion [18], and biometric factors [20]. This thesis adds additional capabilities to the original module design [16]. Expanded capabilities of the module include the incorporation of joint angles to measure biomechanical fatigue. Data collected from the first module is analyzed using Qualisys Track Manager MoCap software [21] for calculating joint angles and is processed post-capture using R statistical software [22] for implementing the developed algorithm. The algorithm uses concepts of DTW to compare the change in joint angles during the lifting activity. DTW metrics are analyzed via an EWMA control chart for out-of-control (OC) points above the upper control limit (UCL). The occurrence of these OC points is compared with the subject's Borg's Rating of Perceived Exertion (RPE) [23]. The final analysis tests for the assumption that the OC points in the control chart will help identify the workload in a human while performing a vigorous activity that gets the heart pounding and increases the breathing rate, i.e., RPE level 15. As a result of the analysis, the need for a personalized DT for an MMH operator will be justified.

The Digital Twin module presents the vision of analyzed operator statistics in a simulated environment as feedback to the operator and stores the operator activity metrics for further research and development.

1.4 Expected Outcomes

This research is expected to achieve the following outcomes:

- Detect biomechanical fatigue in subject performing MMH lifting activity as a factor of change in joint angles.

- Prove that different individuals show signs of body fatigue via *different* body joints.
- Justify the need for personalized digital twin for an operator performing MMH lifting task.

1.5 Research Hypothesis

Keeping the idea of creating a true DT of an operator, this study may provide insights on the following research hypothesis:

"Different human subjects reveal biomechanical fatigue via *similar* body joints."

Formulating the hypothesis, a binary metric β_{ij} was defined for the detection of fatigue via the proposed methodology, i is the subject number. The value of j ranges from 1 to 6, linked to left back (1), right back (2), left elbow (3), right elbow (4), left knee (5), and right knee (6) joints.

Null (H_0) hypothesis (Equation 1) tests for equality in the rate of detecting fatigue by the proposed methodology for two different individuals (i), considering the same body joint (j). Alternative (H_1) hypothesis checks for the dissimilarities.

$$H_0 : \beta_{1j} = \beta_{2j} \; \forall \; \mathrm{j} = 1,2,3,4,5,6 \qquad (1)$$

$$H_1 : \beta_{1j} \neq \beta_{2j} \; \forall \; \mathrm{j} = 1,2,3,4,5,6 \qquad (2)$$

1.6 Organization of Thesis

This thesis is organized as follows: Chapter 2 provides a detailed literature review on the use of DT technologies and the preexisting methods to analyze human biomechanical fatigue prevailing in industrial environments. Chapter 3 explains the developed methodology to analyze fatigue as a factor of change in joint angles. Chapter 4 discusses the experiments carried out to validate the proposed methodology of the DT

development and the results. Subsequently, Chapter 5 states the summary and conclusions of this research. Chapter 6 presents the author's opinions on future research scope. Appendices present additional relevant details to this research.

2. LITERATURE REVIEW

2.1 Preamble

This research presents a digital twin concept and prototype to represent human operators in the material handling industry. A simulation-based framework led to the development of a digital twin for data collection and analysis. The framework consists of three modules: Data Collection Module, Operator Analysis and Feedback Module, and Digital Twin Module. This chapter summarizes the literature review on different modules for the digital twin (DT) development. It presents an overview of published work in manual material handling (MMH), DT, and operator ergonomic analysis. Section 2.2 summarizes the evolution of DT technology and its use in current scientific advancements. Section 2.3 reviews the techniques and tools used to analyze an MMH operator's activity in the current factory environment.

2.2 Digital Twin Technology

Simulation is a copy of an existing system, manipulated logically to identify how it behaves in varying conditions. Whereas, DT is a virtual and precise depiction of a system, allowing real-time analysis for detection, prediction, prevention, and optimization to increase productivity.

Some practitioners have used digital twins and simulation interchangeably. However, we point out the following differences between simulation and digital twins. Simulation provides an understanding of a physical system using numbers. It leads to time and cost advantages by helping developers to understand better real-world product behavior and elevating product lifecycle management [24].

While a simulation provides static information like design elements, materials,

and operating conditions, starting its life as a static model, a DT simulation becomes active. Its ability to change with the flow of data dynamically yields more valuable information not generated by a traditional simulation [25]. A simulation model does not involve the other parts of business beyond research & development. In contrast, the continuous flow of data with a DT keeps the business provider in perfect synchronization with the business operations. To summarize, DT's use allows the developers, supply chain managers, and customers to ‘drive’ and experience the product in real-time, as it grows.

Common challenges in the development of a DT include data analysis, enhanced manufacturing process, and effectiveness of predictive analysis [26]. The economic value of DT varies widely based on factors like development, implementation, and maintenance costs. The abstraction level of DT ranges from the lowest component (data received & analyzed from an individual part) to asset (data from a machine e.g., tool life for predictive maintenance), system or unit (production line in a facility) and the highest component, process (business-level view) [27].

DT technology is increasingly penetrating the manufacturing and logistics sectors. It is beneficial to the researchers and technology companies to provide a digital representation of the material handling facility and supply chain system or find the optimal conditions for enhanced performance [28]. Estimating the real system's response to identify the factors affecting its environment and allowing communication and collaboration between other simulation models and DTs, companies such as TESLA, GE, and DHL have been working towards building DT versions for vehicles, engines, and warehouses, respectively [8] [29].

In 2017, the global DT market size was valued at USD 2.26 billion, with an estimated compound annual growth rate of 38.2% from 2018 to 2025 [30]. International Data Corporation (IDC) anticipates 70% of manufacturers will use DT technology to conduct simulations and scenario evaluations by 2022. In Brazil, Unilever achieved a one to three percent increase in productivity by using DT to cut down its facility's energy use, which led to a savings of approximately $2.8 million [31]. Besides using DT technology in 'Automotive & Transport' and 'Manufacturing' industries, scarce research has been done to use the concepts of DT to evaluate well-being of human operators in the industry.

2.3 Real-time Ergonomic Evaluations & Feedback

Since 1972, collecting data from the 'Injuries, Illnesses, and Fatalities' program of the U.S. Bureau of Labor Statistics shows that injuries and fatalities incurred by workers have decreased [14]. However, the results show that there is still a need for research to make workers safe on the job. The social integration in cyber-physical systems is still considered a societal challenge [32]. As the human involvement plays an essential role in the productivity of the system, risks related to MMH tasks associated with the nature of the load, type of task, work environment & the operator [33] allow the use of technology to analyze the ergonomics of the work environment to reduce worker fatigue [17] (Figure 2).

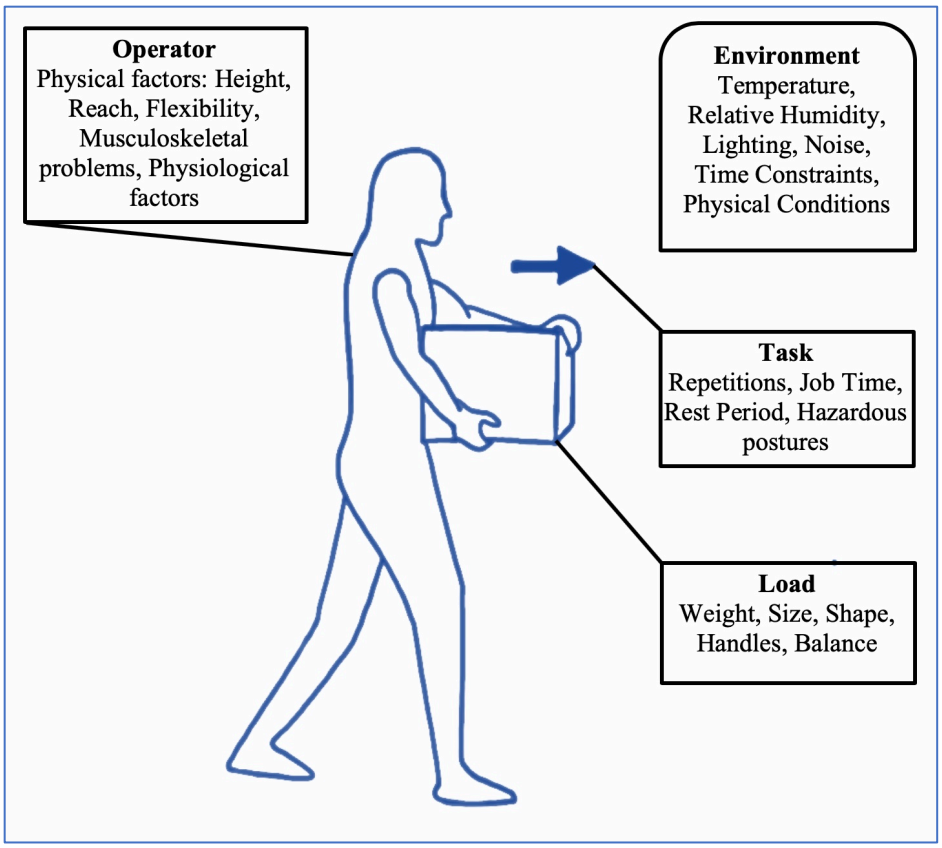

Figure 2. Operator environment with factors leading to MMH hazards.

Multiple tools have been introduced to measure fatigue in the workforce. Methods such as standard questionnaires after completing a job or using on-body sensors have been used in the past to analyze fatigue in construction workers [34]. Despite their use, the on-body sensors tend to cause discomfort for the human workforce while performing tasks.

Various ergonomic assessment tools such as Rapid Upper Limb Assessment (RULA) and the job strain index method are commonly practiced in industries to identify repetitive movements [35] [36]. In order to identify strained postures, observational tools like Rapid Entire Body Assessment (REBA) and the Ovako Working Assessment System (OWAS) provide feedback based on an experienced user's scoring system [37] [38]. The

National Institute for Occupational Safety and Health's (NIOSH) lifting equations, Snook tables, and Liberty Mutual tables provide information on safe load capacity [39] [40]. The commonly used Borg scale assess fatigue by subjective worker feedback [23].

The majority of the methods described above require post-experiment evaluation, resulting in an inability to provide real-time feedback to the operator. Lack of including the object's weight, a significant component of MMH tasks, as a decision variable is considered another limitation of currently used methods.

In recent times, virtual human factor (VHF) tools such as virtual reality, digital human models, and discrete event simulation allow the user to perform an ergonomic assessment to systems not yet constructed. A novel tool created by Greig et al. [41] used methods like biomechanical regression modeling and Methods-Time Measurement to predict worker demand and element-time, along with assisting the user inline layout and task balancing. However, this tool possesses the limitation of being used only in the design stage of the process. The study was also restricted to light assembly work and only considered loads at the shoulder joint.

Research by Visentin et al. [12] proposed using energy expenditure to measure MMH workers' physical fatigue. The study induced a model for fatigue accumulation and rest allowance but was limited to less demanding activities. Activities where workers experience high energy expenditure rates due to repetitive movements were regarded as drawbacks of this methodology [12].

The study by Vignais et al. [42] and Boocock et al. [15] have proven real-time feedback for ergonomic evaluations to reduce the risk of musculoskeletal injuries. Using sensors, auditory and visual feedback by the operator reduces injury risk.

A personalized digital athlete was built by [43] as an approach to creating a digital version of on-field athletic performance. The use of big data architectures allowed the creation of a personalized 'digital athlete.' Based on extensive datasets, missing individual data was estimated to reduce the use of traditional experimental designs to evaluate humans' ergonomics in the sports biomechanics community. Researchers proposed using a Deep Learning Neural Network (DNN) scheme to estimate the missing data (ground reaction forces) using only motion capture (MoCap) trajectories as the input. Romero et al. [11] introduced the concept of Operator 4.0, i.e., humans assisted by machines and technologies to enhance their physical, cognitive, and sensorial capabilities to perform their manufacturing tasks. Discussions on the use of wearable tracking, Augmented Reality (AR), Virtual Reality (VR), robots, exoskeletons, and data analytics to enhance worker's capabilities were included.

Jimenez [28] explains the opportunities of building industrial digital twins of material handling operators. These include: 1) training based on digital copies of highly skilled operators, 2) real-time ergonomic evaluations and feedback, 3) workplace optimization and testing, 4) personalized health plans, and 5) communication between human-based and equipment-based digital twin agents. Hernandez et al. [44] proposed Recurrent Neural Networks (RNN) to predict the human body's motion, predicting human operators' fatigue for the specific material handling operation.

Since the literature shows that fatigue has a protective function against irreversible muscle damage, it plays a vital role in the redistribution and reorganization mechanisms of the human body, optimizing active muscle fibers and multi-joint coordination [45].

Objective measures for muscle fatigue include surface electromyography (sMEG), mechanomyography (MMG), and ultrasound strain imaging. A limitation of using sMEG is that it can only provide measurement for the muscles the sensor is attached to. Another human factor that is influenced by fatigue is postural control and movement coordination. With the accumulation of muscular fatigue, changes are observed in movement kinematics such as range-of-motion (ROM) and angular velocities [46]. To measure an accurate change of body kinematics, an optical MoCap methodology with infrared cameras is preferred. Tracking individual joints with MoCap technology allows an in-depth analysis of the movement. As concluded by M. Golan et al. [47] and M. Peruzzini et al. [48], the lack of standard datasets makes it challenging to validate standard human behavior and the real-time mapping of operator movements in a factory environment. Using the MoCap system to track the change in body kinematics would make it possible to determine, evaluate, and create the required datasets for operator movement analysis.

2.4 Literature Decision Matrix

The literature decision matrix summarizes the studies discussed in the previous section. This matrix classifies tools used for MMH activity assessment on a factory floor based on the following factors: evaluation of human ergonomics (EE), feedback to the workers (WF), ability to detect upper and lower body biomechanical fatigue (UB/LB-BF), real-time capabilities or applications (RT), consideration of repetitive motions (RM) and handling of loads (HL) while performing the MMH task. Table 1 presents the literature decision matrix showcasing the identified research gaps, opportunities, and contributions.

Table 1. Literature decision matrix.

Research article	EE	WF	UB-BF	LB-BF	RT	RM	HL
[34]	✓	✓	✓				
[35]	✓	✓	✓			✓	
[36]	✓		✓				
[37]	✓		✓	✓		✓	
[38]	✓	✓	✓	✓			
[39]						✓	✓
[40]						✓	✓
[41]		✓	✓				
[42]	✓	✓	✓		✓		
[43]			✓	✓	✓		
[45]			✓	✓			
[46]				✓		✓	
[47]	✓			✓			
[49]				✓	✓		
Current research	✓	✓	✓	✓	✓	✓	✓

EE: Ergonomics Evaluation, WF: Worker Feedback, UB-BF: Upper Body Biomechanical Fatigue, LB-BF: Lower Body Biomechanical Fatigue, RT: Real-time capabilities/application, RM: Repetitive Motions, HL: Handling of Loads

The matrix represents that research by [34], [35], [36], [37], [38], [42] and [47] presents various tools for ergonomics evaluation of an operator performing a MMH task. Comparing the literature, not all the proposed methodologies focus on real-time worker feedback, fatigue analysis based on all body joints, and repetitive motions done by an

operator. [34], [35], [38], and [42] hold the capabilities to provide worker feedback but only [42] tends to provide real-time feedback. Research by [15] indicated the significance of real-time biofeedback for a repetitive lifting task. The feedback enables the correction of body motion as the individual performs the task. It significantly reduces the risk of injury and educates the operator on correct methods. The weight of load also plays a critical role in MMH tasks. Experiments conducted by [39] and [40] present recommendations on allowable loads for an MMH operator. Other included research in the matrix fail to consider the weight of the load in their respective analysis. [37], [38], [43], and [45] presented tools to evaluate all the upper and lower body joints, whereas others considered either upper body or lower body only. Current research attempts to fill the gaps in recent research to develop a personalized and real-time ergonomics assessment tool for MMH operators.

3. METHODOLOGY

This chapter discusses a methodology to conceptualize the DT framework for an MMH operator. The Data Collection module discusses the methods used to collect and measure human biomechanical data using optical motion capture technology while performing a repetitive lifting task. The collected data acts as an input to the Operator Analysis & Feedback module. This module analyzes the collected data for change in joint angles over time using a dynamic time warping (DTW) algorithm. The results are then evaluated via EWMA control charts to detect fatigue as a change in body joint angles.

3.1 Data Collection Module

3.1.1 Objective

Collect human kinematic data for fatigue detection during MMH lifting experiments.

3.1.2 Outcomes

This module will generate the human joint angle data using MoCap technology for left elbow, right elbow, left back, right back, left knee, and right knee (Figure 3).

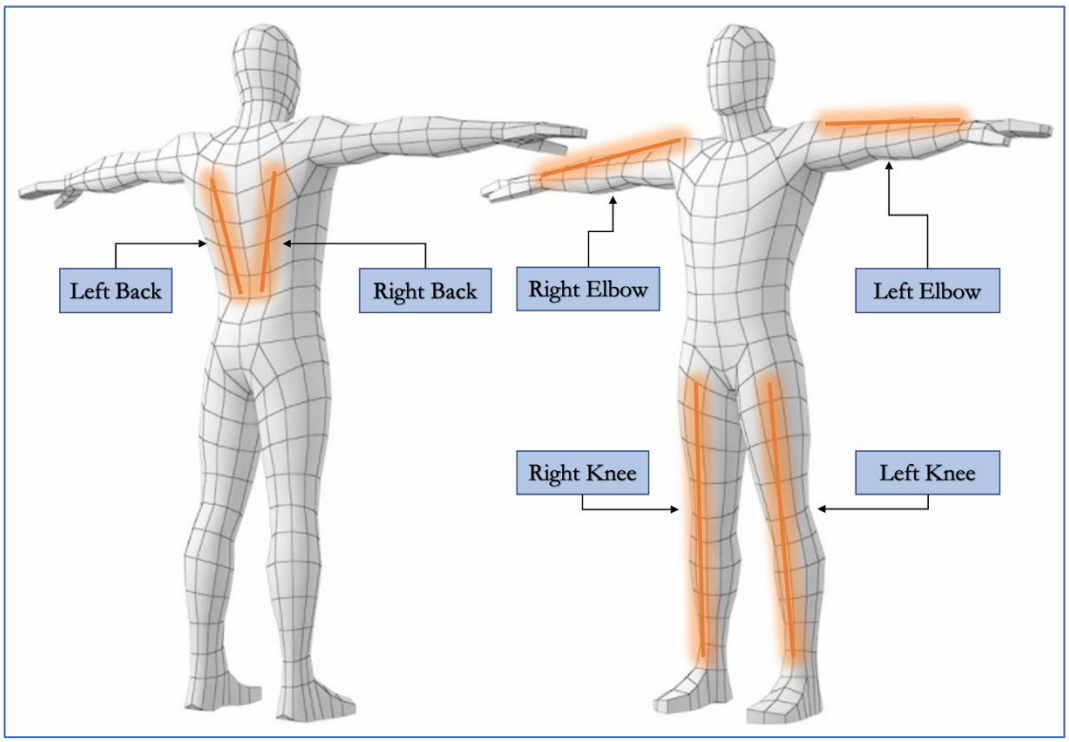

Figure 3. Human body joints in consideration.

From the data collected we analyze the change in joint angles as the human subject performs a repetitive lifting task using DTW algorithm.

3.1.3 Methodology

DT development features advanced big data architectures, using passive & active imaging, multi-sensor integration, data mining, real-time image processing, and non-linear data science analytics [43]. Researchers have made conclusions regarding the lack of standard datasets in material handling, which acts as a barrier for validating operator behavior [47] [48]. In a study by Johnson et al. [49], a significant number of data captures have been carried out for sport-specific applications, providing access to about 20,066 motion capture files. The sports-specific exercises include walking & running trails, football kicking, and baseball pitching; these exercises do not follow the motion patterns

found in industrial MMH applications. Hence, the data collection module is focused on creating structural databases and training sets to develop a DT vision of an industrial MMH operator.

To accomplish the vision of a true DT of an operator, it is necessary to build specific datasets with required variables. Body kinematics of the individual has been identified as essential factors to determine body fatigue. This novel approach collects data specific to the motions carried out by a MMH operator while performing such tasks on the shop floor. The data collection process simulates an actual MMH operation in a controlled environment, collecting the motion and biomechanical data. Figure 4 summarizes the data flow of the 'Data collection Module.'

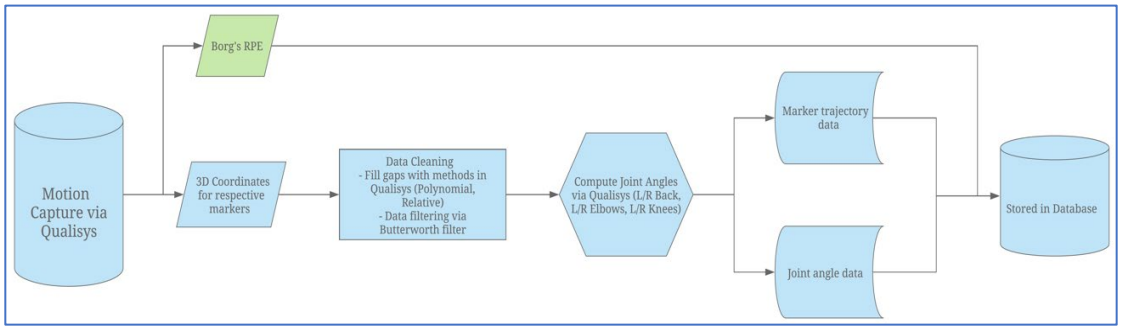

Figure 4. Data collection process.

Previous research by Karg et al. [45] concluded that, as humans accumulate fatigue, observable changes are reflected in joint kinematics such as ROM, angular velocities, and angular acceleration. Hence, optical motion capture methodology with infrared cameras can be used to compute body kinematic parameters. MoCap technologies provide more accurate measurements than computer vision and inertial measurement units (IMU) [50].

3.1.3.1 Motion Capture

Motion capture (MoCap) is the technology developed to track and record an entity's live movements in a given space. Roots of this technology can be dated back to the nineteenth century with humans' urge to understand animal and human locomotion. Later in the early twentieth century, the concept of rotoscoping was introduced by the animator Max Fleischer to record and trace the performances frame-by-frame. This concept played an important role in animated movies. MoCap technology was first used to understand human motion in the 1980s. Since then, this technology is widely used in animal & human biomechanics, sports sciences, engineering, and entertainment [51]. To capture motions performed in a predefined space, many methods of MoCap exist. The flowchart in Figure 5 presents the different types of MoCap technology.

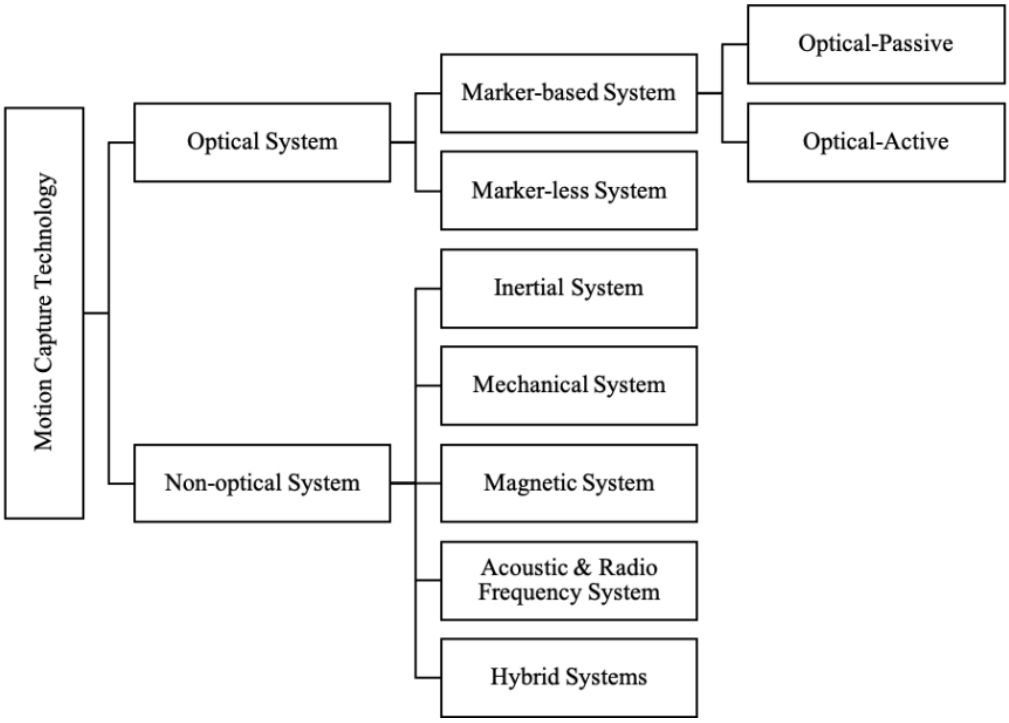

Figure 5. Types of motion capture technology.

Passive optical MoCap is the most accurate method with limitations such as restricted area, highly sensitive, and necessary line-of-sight [52]. Due to its high accuracy, the optical-passive MoCap was selected as the chosen methodology for this research.

The MoCap cameras (Figure 6A) use human vision concepts to see the world in three dimensions. Two or more cameras tracking and observing the same object provides the relative 3D position in the software. The marker-based system allows the cameras to observe reflective markers (Figure 6B) placed on a subject's body and track the markers' trajectories in a 3D space using ROM concepts. As a result of the MoCap session, the computer software provides precise x-y-z coordinates of the reflective markers at a frequency of 100 Hz.

For this study, researchers used the Qualisys AB MoCap system [53] for experimentation, including a cluster of cameras and Qualisys Track Manager (QTM) computer software [21]. The MoCap environment requires a series of pre-capture set up to ensure the system's optimum performance.

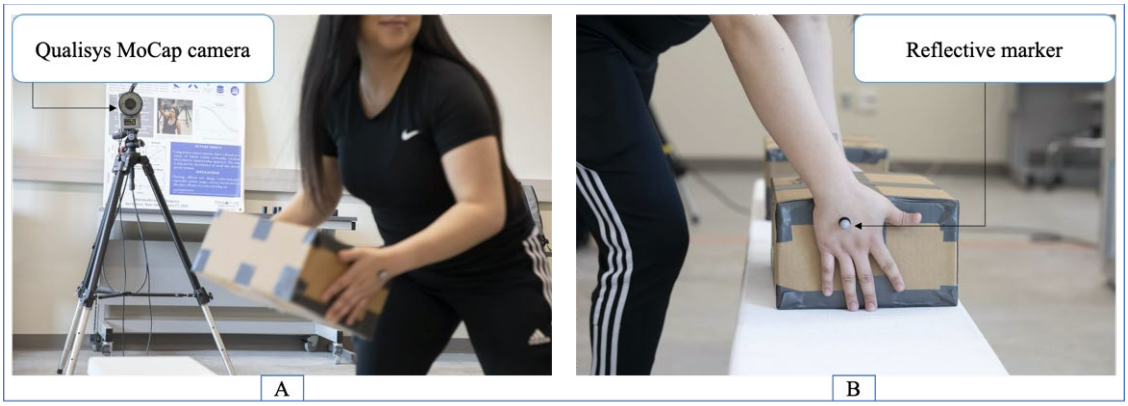

Figure 6. Qualisys camera (A) & reflective marker (B).

The flowchart in Figure 7 shows the series of necessary steps required before the final activity capture.

Figure 7. Pre-capture routine.

Once the system is turned ON and the computer software identifies the camera cluster, the first step is to calibrate the environment. The calibration environment is the space where the subject will perform the required activity. Calibration allows the system to identify where the cameras stand with respect to each other and the experiment space. The carbon fiber calibration kit (Figure 8) provided by the manufacturer includes an L-frame and a wand with reflective markers attached to them.

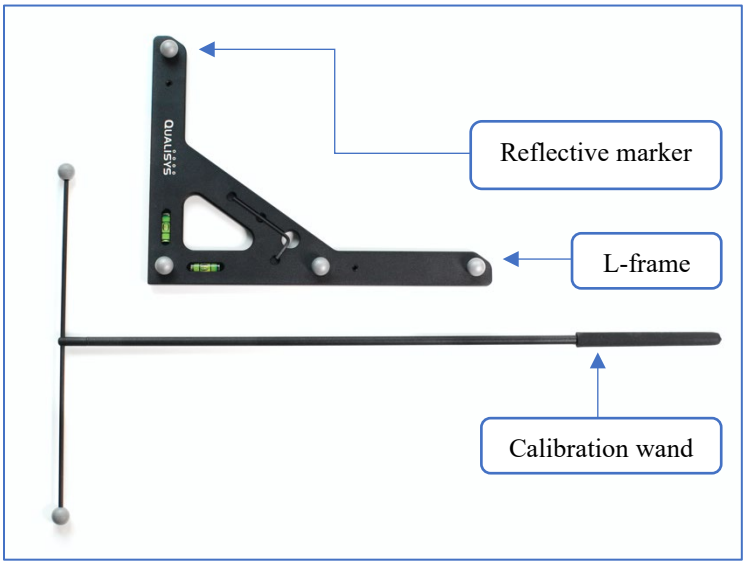

Figure 8. Qualisys calibration kit.

The corner of the L-frame defines the origin position of the experiment space. The L-frame's long and short arm defines the x-axis and the y-axis of the experiment area, respectively. The z-axis will be coming out of the L-frame. Hence, creating the base for all marker positions. The calibration wand defines the experiment volume. Once the L-frame is setup at the origin, the specific dimensions of the calibration (distance between markers) wand is input in the software, allowing the system to optimize the calibration setup. Once calibration is started using the software, the wand is held by its handle and waved around the experiment space in various directions for 60 seconds (calibration time). The calibration results screen displays the number of points detected by the cameras and the average residuals. If the average residuals lie in the same range, the calibration is successful. In the case of any outliers, it is recommended to re-do the calibration.

After a successful calibration, the next steps include subject and experiment preparation followed by the Automatic Identification of Marker (AIM) model development and final capture. Details of the following components are discussed in the next section.

3.1.3.2 Experiment Environment & Data Collection

This study's test environment is located in the Center for High Performance Systems (CHiPS) laboratory at the Ingram School of Engineering at Texas State University, San Marcos, Texas, USA.

A fleet of twelve MoCap cameras by Qualisys AB [53] was set up to capture and record the human subject's activity. Table 2 summarizes the specifications of the MoCap cameras used for this study.

Table 2. MoCap camera specifications.

Camera	Quantity
Oqus 1+	3
Oqus 210c	1
Oqus 5+	6
Miqus M3	2

For the pilot experiments, subjects were recruited from the university student population. The subjects were not trained in performing MMH activities in their routine work. Participants with any muscular injury or primary treatment were excluded from the study. Ethical approval for this study was obtained from Texas State University's Institutional Review Board (IRB).

Since we identified that the MMH activities lead to fatigue, the experiment focuses on simulating one of the fundamental skills moves related to MMH, i.e., lifting [39]. Lifting is defined as the activity performed to raise an object to a higher level. Lifting is performed manually or using a tool. Figure 9 shows a manual lift process, which is identified as a manual material handling (MMH) activity.

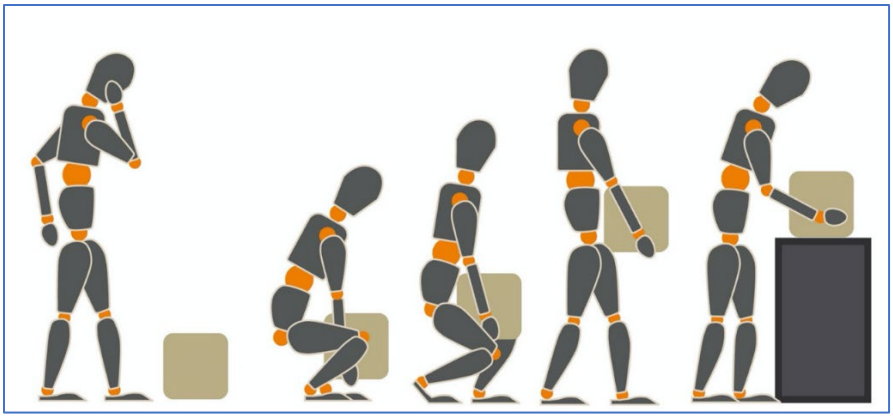

Figure 9. Process of performing a manual lifting task.

Factors summarized by [54], making an MMH activity dangerous for humans include poor lifting techniques, lifting at inappropriate distance/height, short rest period, and uncomfortable clothing. Improper MMH can lead to health hazards such as occupational fatigue, muscular and joint injuries. Figure 10 presents factors contributing to various injuries caused by repetitive lifting MMH activity [55].

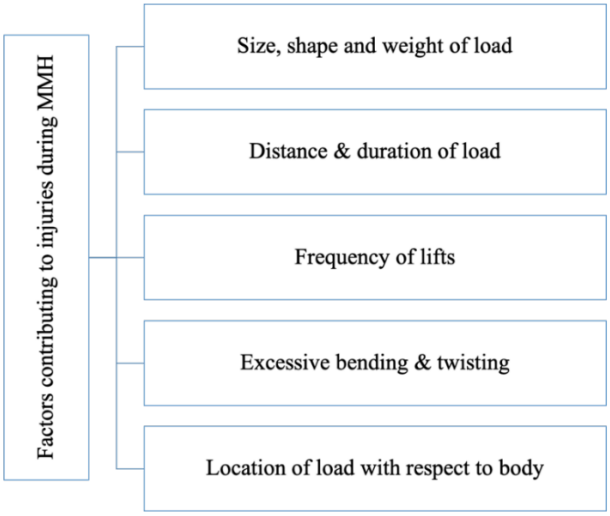

Figure 10. Factors contributing to injuries during lifting MMH activity.

In the current research, participants performed a prescribed 'lifting and lowering' task to induce muscular fatigue [15]. However, only the 'lifting' task was analyzed as the

scope of this research.

The experiment setup includes identifying the weight of lift by the subject. It is determined using Snook Tables [40]. Snook Tables provide design goals for lifting tasks. Research by [40] identified the acceptable conditions to perform an MMH lifting task for a determined percentage of the population, causing a lower risk of injuries. Hence, for the lifting experiments, factors such as the height of lift, frequency of lift, and weight of load were identified via Snook Tables.

During the experiment setup, a wooden table with a 51 cm height and a box with a 24 kg weight is set up in the calibrated area. Meanwhile, the subject is set up with reflective markers on the body joints (Figure 3). The reflective markers' position was based on recommendations by Color Atlas of Skeletal Landmark Definitions [56]. Figure 11 shows the position of the 18 reflective markers taken into consideration for this study.

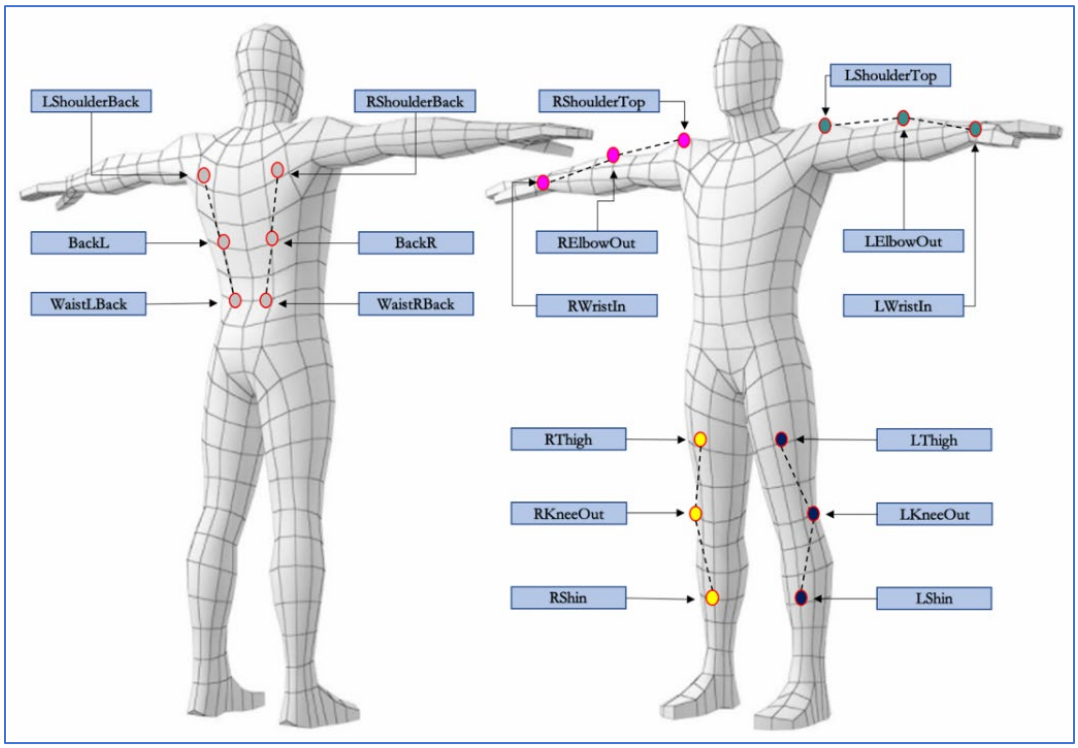

Figure 11. Subject reflective marker position with the naming convention.

The subjects also wore back support and a smart suit, Hexoskin® Shirt [57]. The suit contains body sensors and is paired with a Hexoskin® Smart Device for monitoring the biometrics of the subject at 60 Hz [57]. However, the data analysis of the subject's biometrics is not part of the scope of this study.

The experiment coordinator ensured there was no reflective surface on the subject's shorts & shoes and followed the proper calibration and subject setup procedure.

Once the subject is prepared for the experiment, the last stage of the pre-capture routine (Figure 7) is creating an Automatic Identification of Markers (AIM) model of the subject. Creating an AIM model allows the MoCap system to identify the individual reflective markers during the experiment's main capture.

In the MoCap procedure, the system tracks the reflective markers and records the experiment's respective x-y-z coordinate data. This data is used to calculate and analyze the required metrics. To observe good quality of data, i.e. 100% of the data for a marker, techniques such as proper camera placement, optimum number of cameras, and number of reflective markers play an important role. The proximity of markers on the subject led to issues related to the switching of markers during the MoCap experiment. Hence, optimizing the capture quality was achieved by using the AIM feature of QTM. To achieve the goals of this research, the MoCap experiments must capture 100% data for all markers on the body. Pre-identifying the markers allowed ensuring no switching of markers and reduced the post-processing time of the MoCap experiment.

An AIM model saves the pre-identified marker trajectories relative to each other, allowing its use during the final MoCap experiment. Once the markers are placed on the subject, to create the AIM model, the subject enters the experiment space and performs a

simulation of MMH activity as instructed by the coordinator. Upon completion, the markers are identified in the QTM software and given a specific naming convention (Figure 11). The AIM model is saved and applied to the experiment. With this setup, the pre-capture routine ends, ensuring the subject and experiment are ready for the final MoCap.

Other challenges faced during the MoCap experiments include recurring phantom markers and sudden loss of markers on the subject. The bounding box was defined via QTM to reduce the number of phantom markers in the experiment space. It allows the MoCap cameras to only consider the area defined by the bounding box parameters. Hence, allowing the system to neglect any markers/reflective surfaces outside the bounding box. A black screen was installed to separate the experiment area from the other laboratory space, leading to reduced phantom markers. To reduce the falling off of markers from the subject, the author recommends using good-quality skin-friendly double-sided tape. For major concern areas, i.e., wrists, thighs, and shins, unique fixtures were modeled using SolidWorks [58] and 3D-printed (Figure 12). These fixtures were strapped to the subject's joint of concern and proven effective during the experiments. The reflective marker was screwed in the base for optimum grip, leading to a significant decrease in falling markers at concern areas.

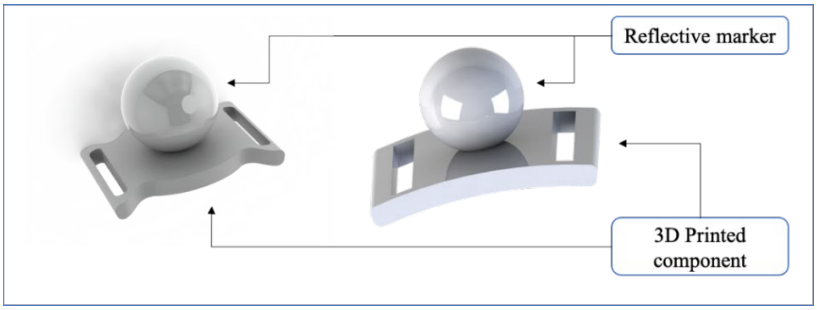

Figure 12. 3D-Printed marker base for wrist, thigh & shin.

Before the final MoCap experiment, the subject was educated on proper lifting and lowering techniques, ensuring the subject's health and safety [59].

Figure 13 shows the beginning of the activity in the QTM environment [21]. The colored dots are the reflective markers on the subject. The list of markers on the right is a result of the AIM model discussed above. The QTM environment also shows the cameras with their respective numbers, camera view cones, origin, and the bounding box.

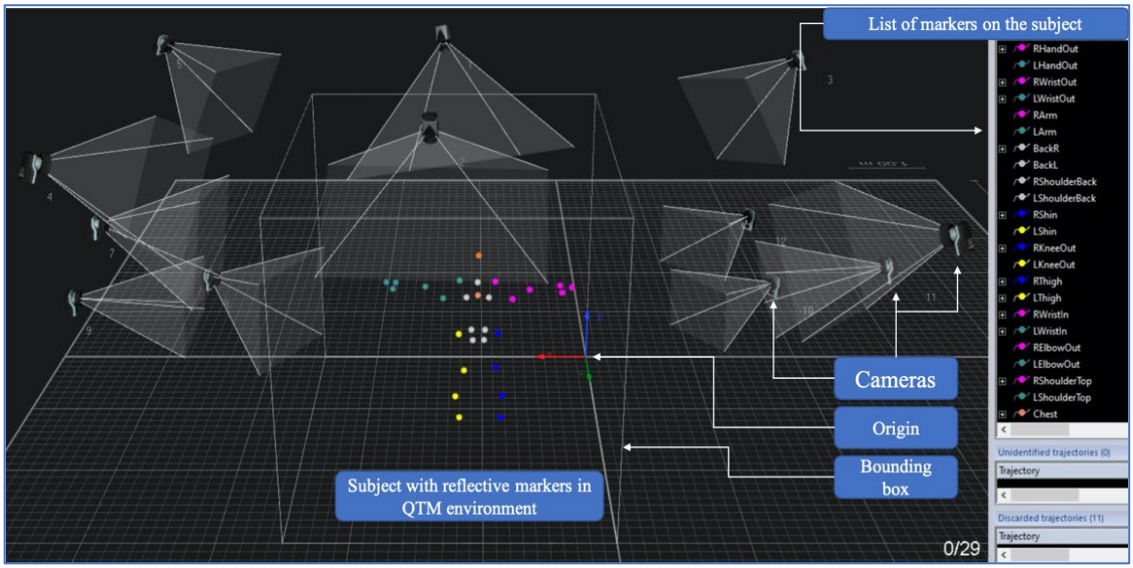

Figure 13. QTM software environment.

The MoCap experiment starts at a T-pose by the subject in the calibrated area. An audible cue is provided to the subject to initiate each lifting and lowering task in the loop at the selected time interval.

Performing repetitive lifting and lowering tasks by the individual, the fatigue level was estimated using Borg's Rate of Perceived Exertion (RPE) [23]. During the experiment, at intervals of one minute, the subject was asked to provide info on RPE using the RPE scores [60].

Borg's RPE is the scale defined by Dr. Gunnar Borg [23], which runs as a discrete

scale from six to twenty to measure an individual's physical activity intensity. Physical sensations like sweating, increased heart rate, and muscle fatigue, experienced by a person while performing a physical activity are considered in the scale. The RPE scale tends to estimate the individual's heart rate. Table 3 represents Borg's perceived exertion scale stating the level of exertion, RPE scores, and an example of the activity [60].

Table 3. Borg's scale of perceived exertion.

Level of exertion	**Borg's RPE score**	**Example of activity**
None	6	Sitting, reading a book
Very, very light	7 to 8	Tying shoes
Very light	9 to 10	Walking slowly
Fairly light	11 to 12	Activities that do not speed up your breathing
Somewhat hard	13 to 14	Brisk walking
Hard	15 to 16	Bicycling or activities taking vigorous effort that makes breathing very fast
Very hard	17 to 18	Highest level of activity you can sustain
Very, very hard	19 to 20	Finishing leg of the race, most strenuous activity ever done

While performing an activity, the individual must concentrate on the body's overall feelings rather than a single joint. Multiplying the Borg scale score by ten provides an approximation of actual heart rate for activity level [23].

The subject was asked to continue the 'lifting' and 'lowering' task until sensed

exhaustion (fatigue) or informed the value of 18 on the RPE scale. Figure 14 shows the flow of activity done by the subject.

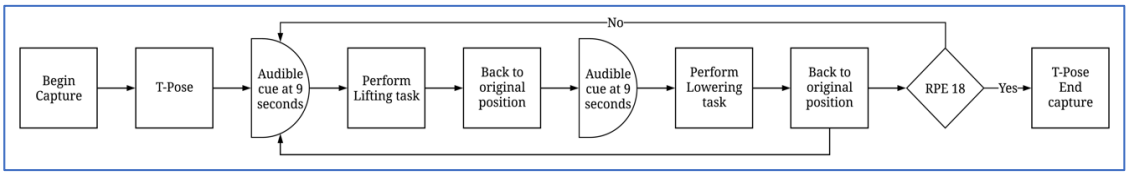

Figure 14. Subject activity flow during the experiment.

Figure 15 shows the laboratory environment with a male subject performing the lifting task at a floor – knuckle range of 25 cm. A table of different height from the actual experiment is displayed in the image for demonstration purposes only.

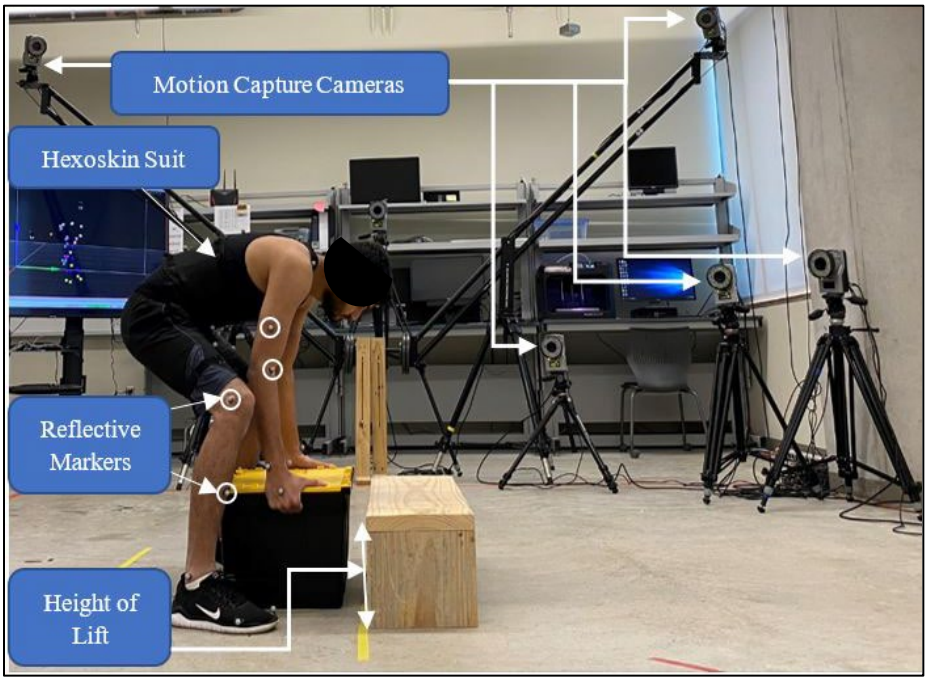

Figure 15. A subject performing the MMH task.

Upon completing the experiment, MoCap coordinate data at 100 Hz (100 values per second) and RPE data at one value per minute are stored in a database for further analysis.

3.1.3.3 Motion Capture Data Post-processing

The MoCap experiment provides the coordinate data for reflective markers on the subject. During the post-processing of the MoCap data, one needs to ensure (1) the captured data is free of phantom markers, (2) the marker trajectories are free of spikes, and (3) all the marker data is at a fill level of 100%.

The first step of post-processing a successful capture includes removing the phantom markers and matching the unidentified markers to their respective names. Unidentified markers are a result of the MoCap system not being able to identify the marker while capturing. Due to the activity's complexity and a limited number of MoCap cameras, all the subject markers are not identified to the respective AIM model markers. Hence, the user has to identify such instances and identify the markers manually.

Another reason for the unidentified markers is the temporary loss of markers, which does not include instances when the marker falls off the subject due to unavoidable reasons. The marker's temporary loss can be caused due to an obstruction between the marker and camera pointing towards it. Methods like static, linear, polynomial, relational, virtual, and kinematic fill such trajectory gaps [21].

Figure 16 shows the left thigh (LThigh) marker trajectory before and after the gap fill using the polynomial technique in the QTM environment. Image before gap-fill presents the marker LThigh with 18 gaps (the region in brown color) in the coordinate trajectory from frame 17203 to 17220. Plots in red, green, and blue represent the x, y, and z coordinates of the marker location. Applying the polynomial gap-fill technique via the ‘Fill’ section completes the gaps in marker data successfully.

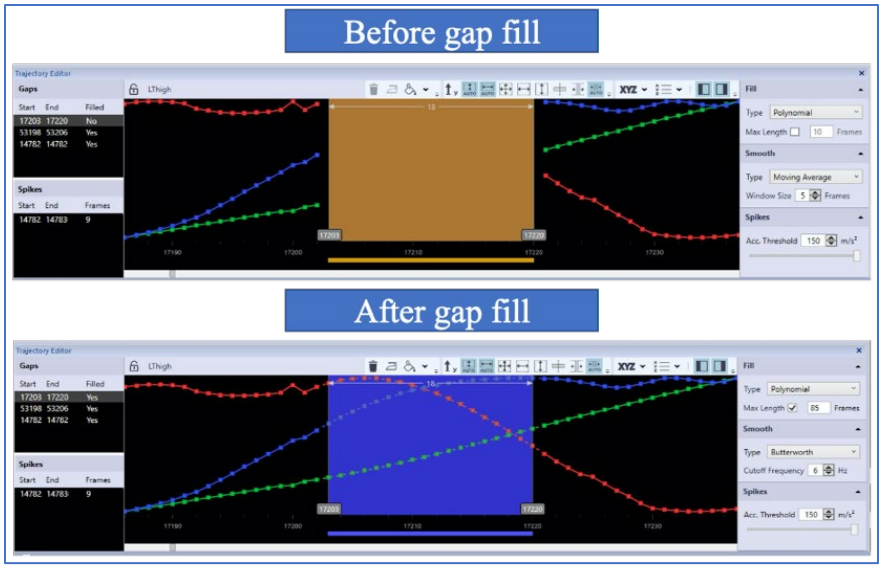

Figure 16. Marker trajectory before and after gap-fill via QTM.

In the MoCap process, at times, noise is received in data at unwanted frequencies. Capturing marker motions at such frequencies is irregular for humans to perform or is caused by the irregularities in the data processing by the MoCap system. The process of filtration is applied to remove such irregularities. Data filtration is used to smoothen the data received by the MoCap systems. The filtering technique allows the removal of unwanted noise and smoothening the data. Fourth-order low-pass Butterworth filtering at a frequency of 6Hz was used to smoothen the data. Figure 17 shows an instance of marker trajectory before and after filtering. A case of spikes in the left thigh (LThigh) marker x, y, and z coordinates are displayed. The QTM software detects an unwanted spike in data for the x coordinate (red) position. The inappropriate noise is removed after smoothening the data via the Butterworth filter via the ‘Smooth’ option in QTM Trajectory Editor.

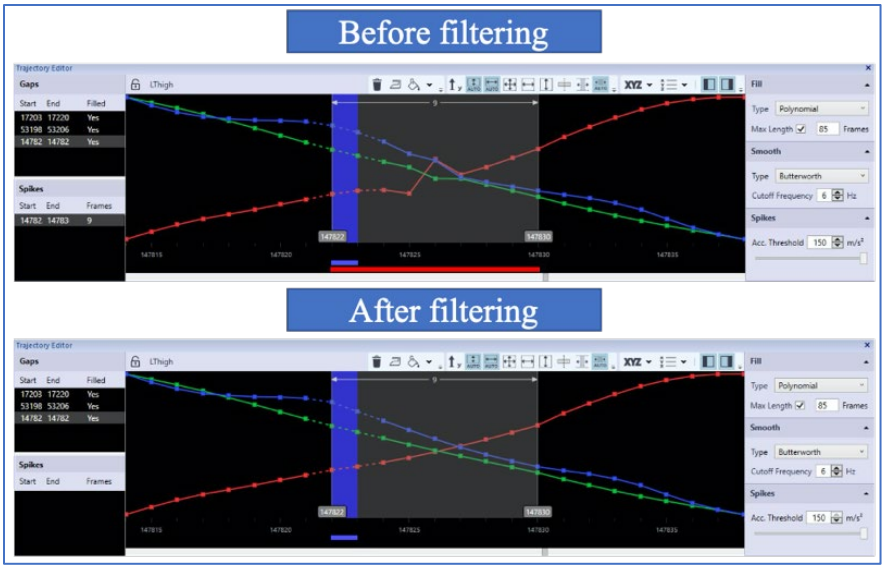

Figure 17. Marker trajectory before and after filtering.

Ensuring the required markers for analysis are 100% filled and there are no unwanted spikes in the trajectories, the marker x-y-z coordinate data can be used to measure respective joint angles. The ‘Analyze’ tool of QTM (Figure 18) [21] is used to measure the study's respective joint angles. The tool uses an inverse kinematics concept to measure angles from the 3D motion capture data [34]. The respective marker locations were defined in the QTM Analyze tool by selecting the markers required for measuring the joint angles. As a result, all the recorded frames' joint angles were calculated and exported in the database for further analysis. Figure 18 shows the selection of markers required to calculate the left knee joint angle. Upon selection, the left thigh, left knee, and left shin markers are selected for reference in the ‘Analyze’ tool. The left knee joint angle is displayed as a result.

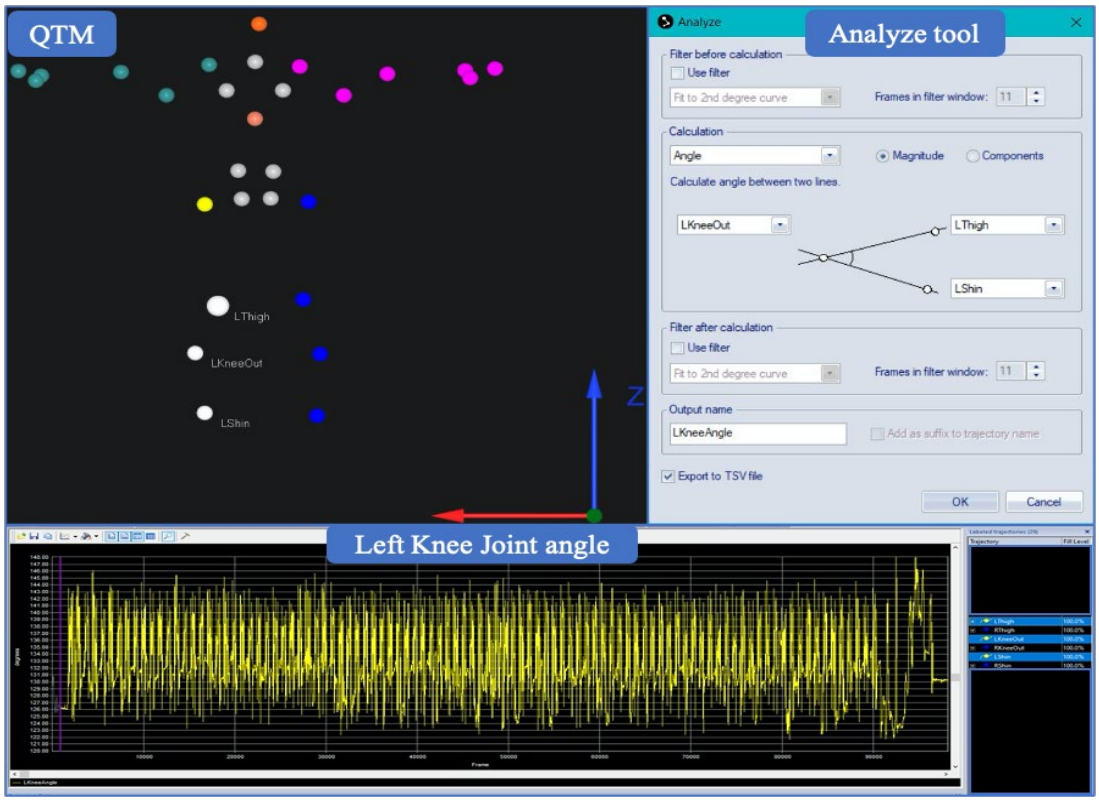

Figure 18. QTM Analyze tool for joint angles.

Similarly, required joint angles for the right knee, left elbow, right elbow, left back and right back joints (Figure 3) were calculated and saved in the database for further analysis.

In this section of the 'Data Collection Module,' the methodology of MoCap, including subject and experiment environment setup, was discussed. As a result of this section, joint angles for the subject were calculated and stored in the database for future analysis.

3.2 Operator Analysis and Feedback Module

3.2.1 Objective

Analyze the subject's joint angles performing the ‘Lifting’ MMH task using the dynamic time warping (DTW) algorithm.

3.2.2 Outcomes

This module will give an analysis of change in joint angles over time.

3.2.3 Methodology

This module of the DT framework conceptualizes data analysis and optimization based on data collection in the first module (Figure 1). Industries have identified human involvement as an essential factor in the productivity of the system. MMH task risks are associated with the nature of the load, type of task, work environment, and the operator [33] (Figure 2). Characteristics of the operator include physical factors like the height of the human, reach, flexibility, musculoskeletal health history, and physiological factors, among many others. Environmental conditions such as temperature, relative humidity, lighting, noise levels, time constraints, and physical conditions are some of the other factors affecting human operator productivity. Among the above-listed factors, task conditions like repetitions, work time, resting period, hazardous postures, handles, and weight of the load are a few recently researched conditions that create a safe environment for the operator.

The proposed framework currently aims to incorporate fatigue evaluation based on changes in joint angles. Body joints of concern were identified as: left elbow, right elbow, left back, right back, left knee, and right knee (Figure 3). The marker data collected in real-time via optical MoCap technology (3.1 Data Collection Module) are

analyzed to measure the change in these joint angles as the subject accumulates fatigue. This fatigue accumulation influences the postural control and movement coordination of the subject [45].

Joint angles and marker trajectory data stored in the database will be used in this section to perform the analysis. Data analysis was performed via the statistical software R [61], deployed via an integrated development environment (IDE) RStudio [22]. The flowchart in Figure 19 shows the steps covered in this module.

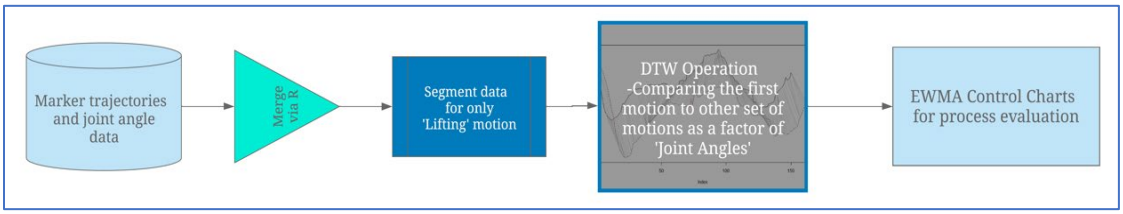

Figure 19. Operator Analysis & Feedback module data flow.

3.2.3.1 Data Segmentation

Six joint angles and marker trajectory data for the performed experiments were merged via R to proceed with segmentation. The experiment methodology includes lifting and lowering motion performed by the subject. The scope of this research is limited to the 'lifting' motion only. A segmenting filter [62] was developed in R [61] and implemented via RStudio [22] using the plyr library [63] to trim the activity performed during the lifting task. The activity was divided based on 'Motion with Load' and 'Motion without Load.' 'Motion with Load' is the activity carried out by the subject as they grab the lifting container and then lift it to its location of placement at the required height. This 'Motion with Load' is identified as a 'segment.' The segmenting filter identifies and splits the data for analysis into the desired lift segments.

Figure 20 shows the change of left elbow joint angle in degrees, taking the whole set of motion by subject into consideration, i.e., normal stance, proceed to lift, lift the box with weight (Motion with Load) and move back to the original position. A segment in this set of motion, i.e., 'Motion with Load' (lifting), ranges from frame number 2749 – 2885.

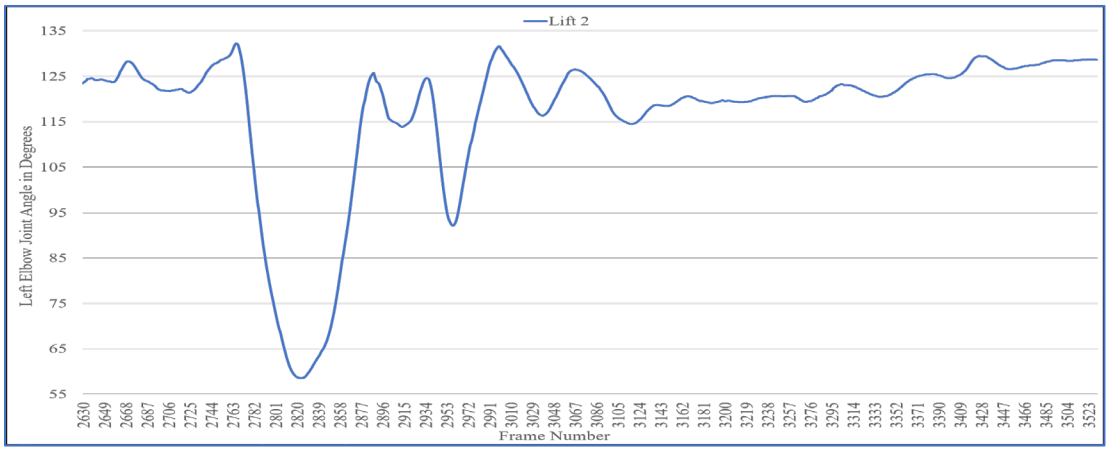

Figure 20. Change in left elbow joint angle segments with time.

The segmenting filter is applied to the dataset including marker trajectories and joint angles. As a result of this filter, the joint angles of segments, including only the lifting motion, are attained. The segmented lift motion is further displayed as 'Seg2' in Figure 21. Summarizing the segmentation concept: a subject performs consecutive 100 repetitive lifting and lowering motions. The segmenting filter will filter out the 50 lifts and 50 lowering motions with respective marker trajectory and joint angle data associated with each frame.

Segmented data (Motion with Load), results for ten individual segments, extracted from the original complete motion file are displayed in Figure 21. Solid lines depict the change in angles during the first five segments (first five iterations of the activity) at RPE

6. The dotted lines show the last five segments (the last five iterations of the activity) of the recorded activity at RPE 18.

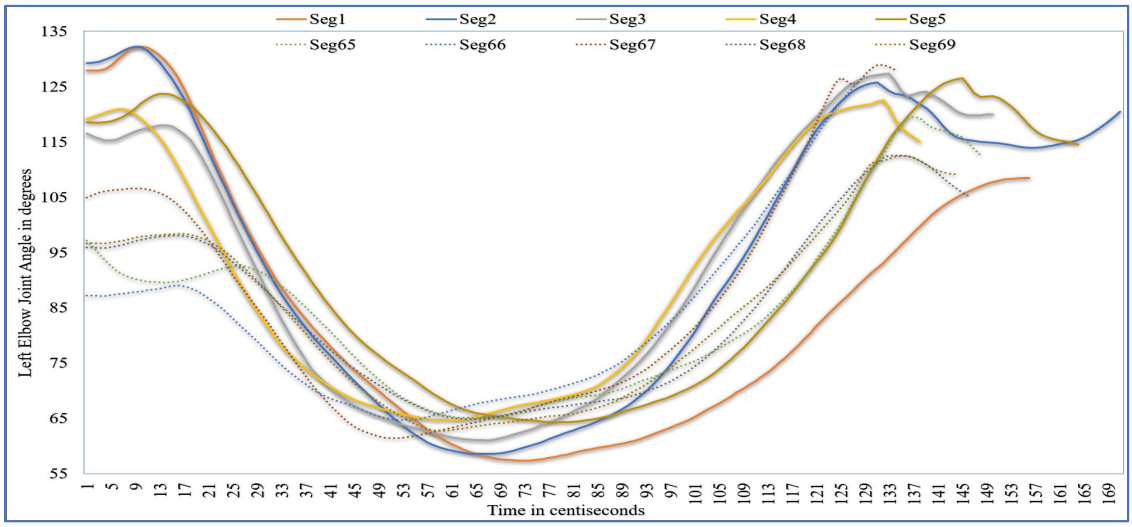

Figure 21. Change in left elbow joint angle at the beginning and end of lifting activity.

Comparing the data plotted in Figure 21, it can be deduced that a substantial change in angle is observed, and the duration of each lift varies. At the beginning of the lifting experiment, the subject's elbow joint angle varies between 116° and 129.3°, whereas at the end of the experiment, the same angle lies between 87.22° and 105.41° (towards 180° = elbow extension; towards 0° = elbow flexion). As a result of this change in the joint angle, we infer that in the initial five lifts (Seg1 – Seg5), the individual started with their elbows more extended and moved through a greater ROM. Towards the end of the activity (Seg65 – Seg69), the elbow extension reduces towards the beginning of 'lift,' but the elbow flexion remains almost similar. Overall, the ROM was less when the subject was fatigued. The R script developed to implement the data merge, segmentation, and analysis is available for reference in APPENDIX A.

3.2.3.2 Dynamic Time Warping

Once the segmented joint angle data is in the database, Dynamic Time Warping (DTW) concepts are used to analyze the change of joint angles during the activity.

DTW is a technique of analyzing similarity between two selected time series. It calculates the overall distance between the two-time series as the series is 'warped' non-linearly in the similar time domain [64]. DTW's concept emerged from the field of speech recognition in the late twentieth century [64]. Although the concept is widely used in speech recognition, its use in human kinematics is still scarce. Previous uses of DTW in analyzing body kinematics include research by Hu et al. [65] as a classification tool for basketball playing movements. Research by Ameli et al. [46] used DTW in analyzing physical fatigue in twenty subjects, performing a stair-climbing test. The joint of concern was the knee, and the study indicated positive results regarding DTW's use in determining fatigue.

Multiple successful attempts have been made by researchers using the DTW algorithm in the field of activity classification, developing rehabilitation exergames [66] [67] and gait recognition [68] [46] [65]. DTW's simplicity in real-time scenarios and low requirements for training and optimizing the algorithm makes it a suitable choice for the current application [69]. Hence, building the base for the use of the DTW algorithm in the field of MMH.

The change of joint angles with time can be considered as time series, and each segment is considered an individual series for this DTW analysis.

Given two time series of change in concerned joint angle, Query Index (Q) and Reference Index (R) (Figure 22) such that

$$Q = q_1, q_2, \dots, q_i, \dots, q_n \qquad (3)$$

$$R = r_1, r_2, \dots, r_j, \dots, r_m \qquad (4)$$

DTW aligns the two sequences by constructing an $n \times m$ matrix where the element (i^{th}, j^{th}) in the matrix contains a distance $\left(q_i - r_j\right)^2$.

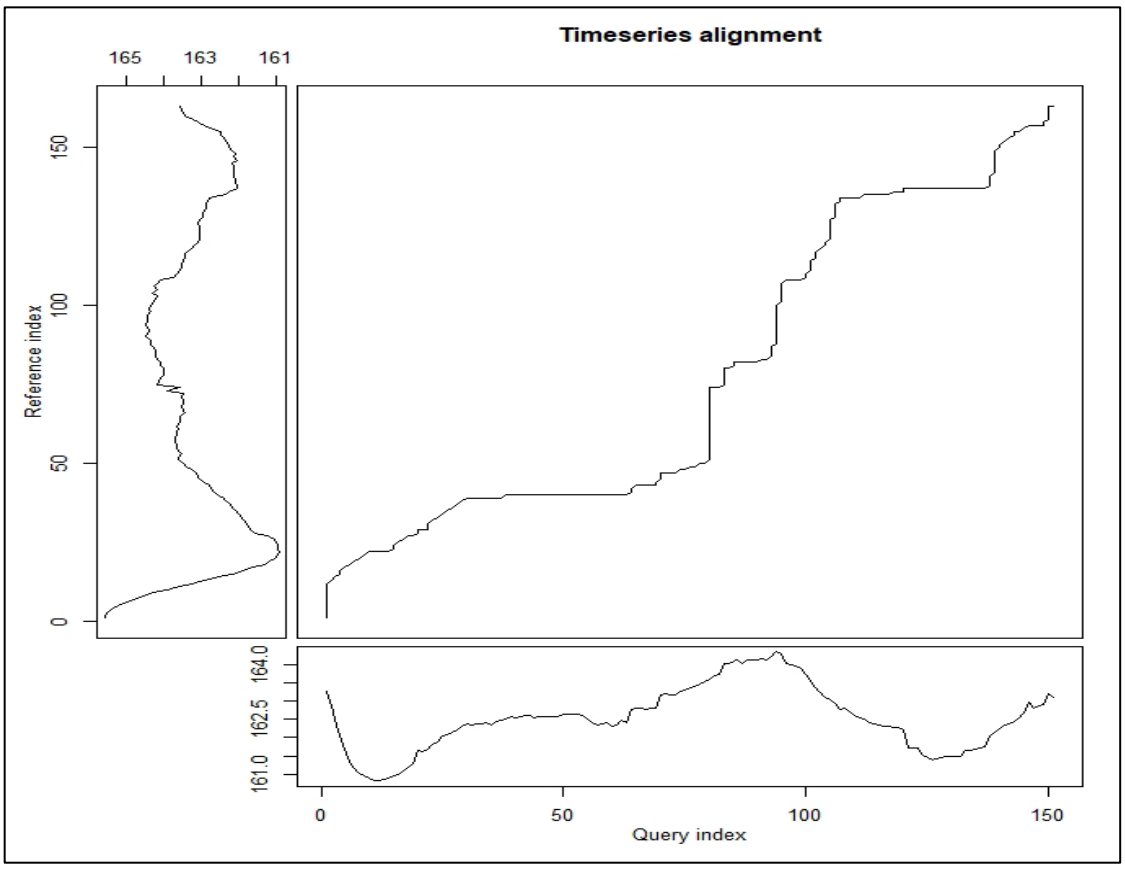

Figure 22. DTW time series alignment.

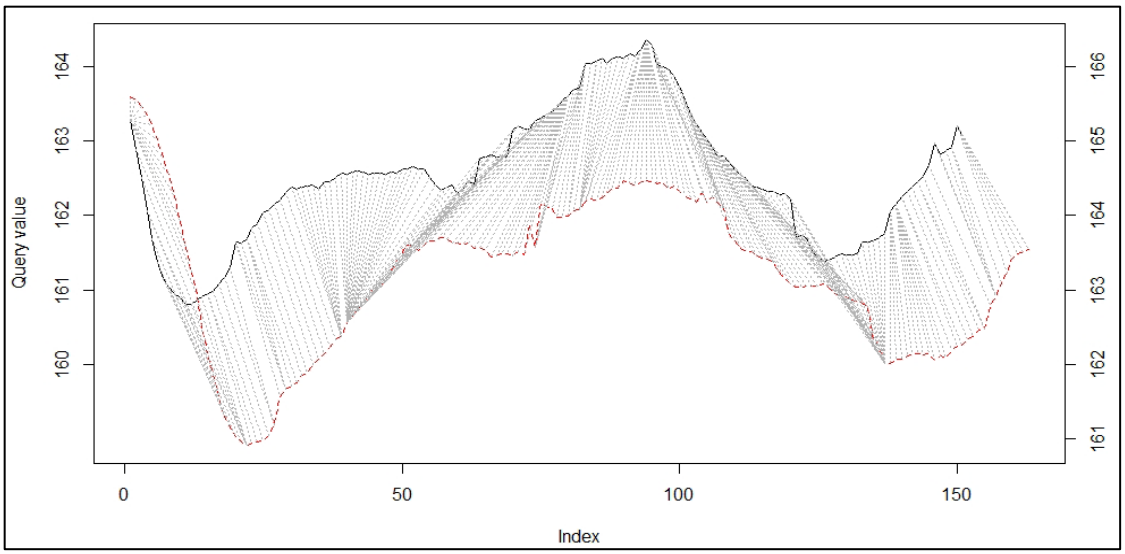

Figure 23. Q and R time series aligned for DTW.

The best match between series Q and R is the path through the matrix that results in lowest total cumulative distance between them. DTW can be stated as

$$DTW(Q,R) = \min \sqrt{\sum_{l=1}^{L} w_l} \tag{5}$$

where w_l corresponds to a matrix element $(i^{th}, j^{th})_k$ which belongs to the contiguous set of elements along the path that minimizes the cumulative distance between the Query Index (3) and Reference Index (4). Figure 22 represents the alignment of two time series, outlining the process of calculating the minimum distance. Figure 23 shows the scenario when Q (solid line) and R (red dotted line) are aligned for DTW for comparison.

In this research, the subject's first lift motion is considered as the Reference Index, calculating the DTW metrics for all respective joints. DTW distances for all the joints were computed using the 'dtw' library [70] available in the R software [61].

For this mathematical model representation, the first segment's left knee joint

angle data corresponds to the 'Reference Index,' and the future occurring segments in the time series are selected as 'Query Index.' Using the first lift motion as a reference in the DTW algorithm makes the algorithm perform under an assumption. The algorithm assumes that the very first lifting motion performed is the correct motion performed by the subject. In a rare scenario, if the subject does not bend his/her knees in the first lift and performs the second lift with bent knees, the DTW algorithm will lead to a higher DTW value. The variation in knees' joint angles will be higher when both the motions are compared as a factor of change in joint angles.

In the discussed example of the activity, the subject performed a set of 215 lifts in 33 minutes (#Segments = 215), i.e., duration of the activity till the subject reaches RPE 19 (Table 3). Figure 24 shows the calculated DTW distances of the activity performed by the individual. The DTW values range from 92 to 925.

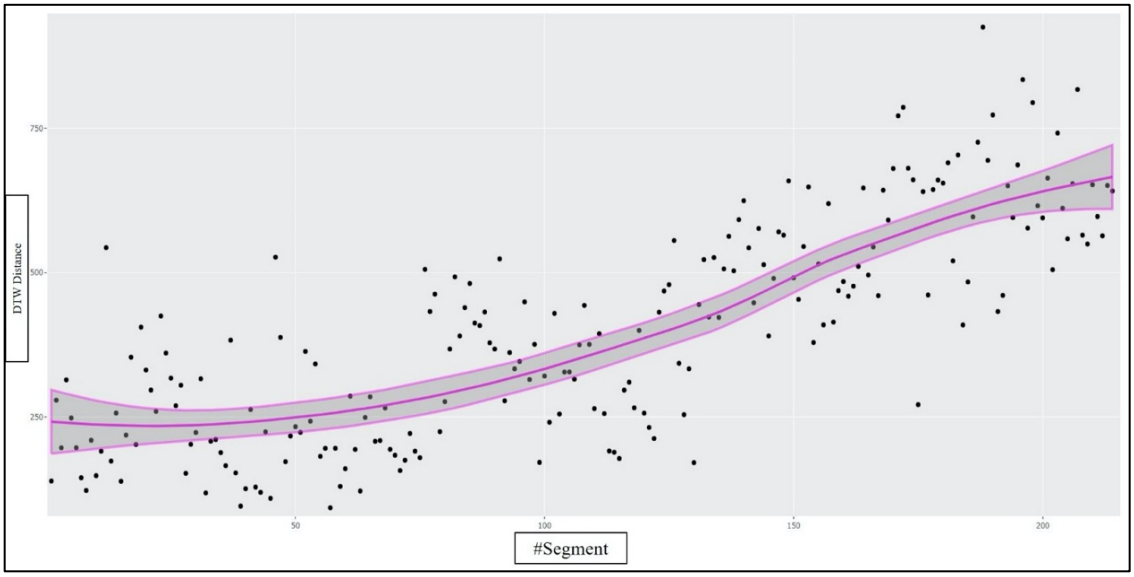

Figure 24. DTW distances for the Left Knee joint angle for the performed activity.

DTW distance in the y-axis represents the minimum distance computed by the algorithm using Equation 5. The length of distance when left knee joint angles for the first lift are considered as the 'Reference Index' and change in joint angles for the second segment onwards considered as 'Query Index.' X-axis presents the segment number corresponding to the DTW value.

Lower DTW values at #segment 1, 8, 39, and 57 represent that the joint angle (left knee) was similar to the individual's first activity. Higher values at points beyond 150 on the x-axis represent deviations towards the activity's end. The solid pink line displays an upward trend line.

This change of the DTW distances can be associated with fatigue in the subject performing the activity [46]. Figure 25 shows the subject's RPE scores at a frequency of 1 minute during the activity performed for 33 minutes, segmented into 215 iterations.

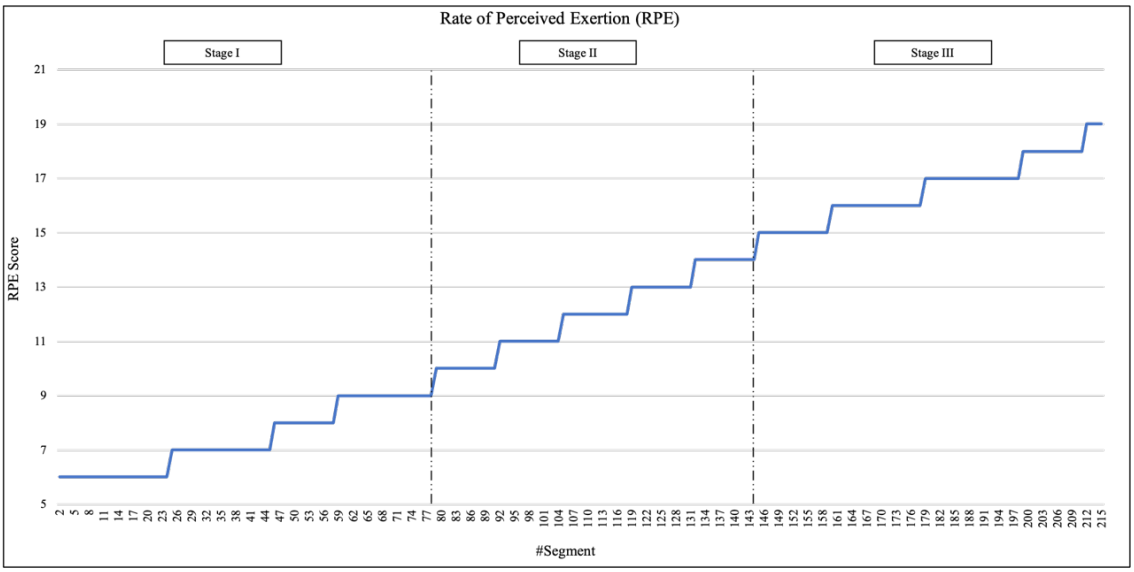

Figure 25. Rate of Perceived Exertion (RPE) values.

3.2.3.3 Exponentially Weighted Moving Average Control Chart

Considering the exponentially weighted moving average (EWMA) control chart to analyze the computed DTW distances, the EWMA parameter (z_i) is defined as:

$$z_i = \lambda x_i + (1 - \lambda) z_{i-1} \quad (6)$$

where,

λ is the weight constant with $0 < \lambda \leq 1$

x_i is the sample at i

$i = 1$ denotes the first sample

Starting value of z_0 is the target mean. Therefore,

$$z_0 = \mu_0$$

In some cases, the average of initial data is used as the starting value.

$$z_0 = \bar{x}$$

The upper control limit (UCL), centerline, and lower control limit (LCL) for the EWMA control chart are as follows.

$$UCL = \mu_0 + L\sigma\sqrt{\frac{\lambda}{(2-\lambda)}[1-(1-\lambda)^{2i}]} \quad (7)$$

$$Center\ line = \mu_0$$

$$LCL = \mu_0 - L\sigma\sqrt{\frac{\lambda}{(2-\lambda)}[1-(1-\lambda)^{2i}]} \quad (8)$$

Parameter $\left[1-(1-\lambda)^{2i}\right]$ in equations 7 and 8 tends to reach unity as its value gets larger. Hence, upon running for several periods, the control limits of the EWMA chart will be steady. L is the width of control limits. Value of L and λ are chosen based on the required shift in mean as a multiple of the standard deviation (σ) [71] as it leads to a

shorter average run length (ARL). As recommended by [71], the fair values for L and λ are 3 (three sigma limits) and 0.2, leading to detect a shift of three standard deviations in the mean of 2.4 ARL. In this analysis, the EWMA chart was plotted using the 'qcc' library [72] available in the R statistical software [61]. Figure 26 shows a sample EWMA chart for the DTW metrics of the left knee joint.

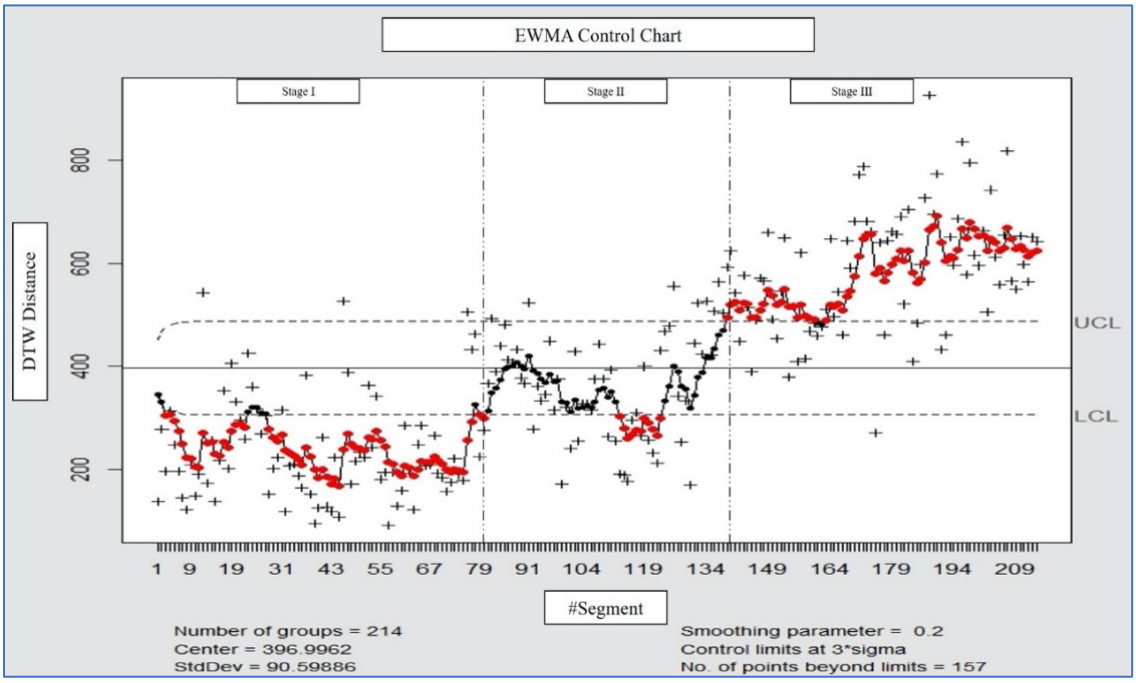

Figure 26. EWMA control chart for left knee joint angle DTW distances.

The EWMA control chart considers the weighted average of the past and current observations, making it the ideal control chart for the computed DTW distance observations. EWMA control charts serve as an excellent alternative to Shewhart Control Charts, detecting small shifts in the process [71]. With performance capabilities similar to cumulative sum control charts and its ease of setup and operation, the EWMA control chart was chosen for this analysis.

The subject's activity is divided into three stages based on the RPE levels for the

analysis. The Stage I (RPE 6 – 9), Stage II (RPE 10 - 14), and Stage III (RPE 15 – 19) include segments 1 – 78, 79 – 144, and 145 – 214, respectively.

Similarly, the EWMA control charts' parameters are calculated for the DTW metrics computed over the experiment. The EWMA chart in Figure 26 shows that the out of control points in Stage I and Stage III points lie outside the lower and upper control limits, respectively.

To enhance EWMA charts' performance, the next step of processing is estimating the control limits based on DTW values until the subject's RPE 10 rating, i.e., Stage I. The Stage I data points are taken as the 'Calibration data' for the EWMA control charts. EWMA control charts allow defining the upper and lower control limits based on the calibration data. Next, the data points in Stage II and Stage III are combined and scaled as 'New data' and analyzed for the EWMA control chart. Figure 27 presents the final EWMA control chart.

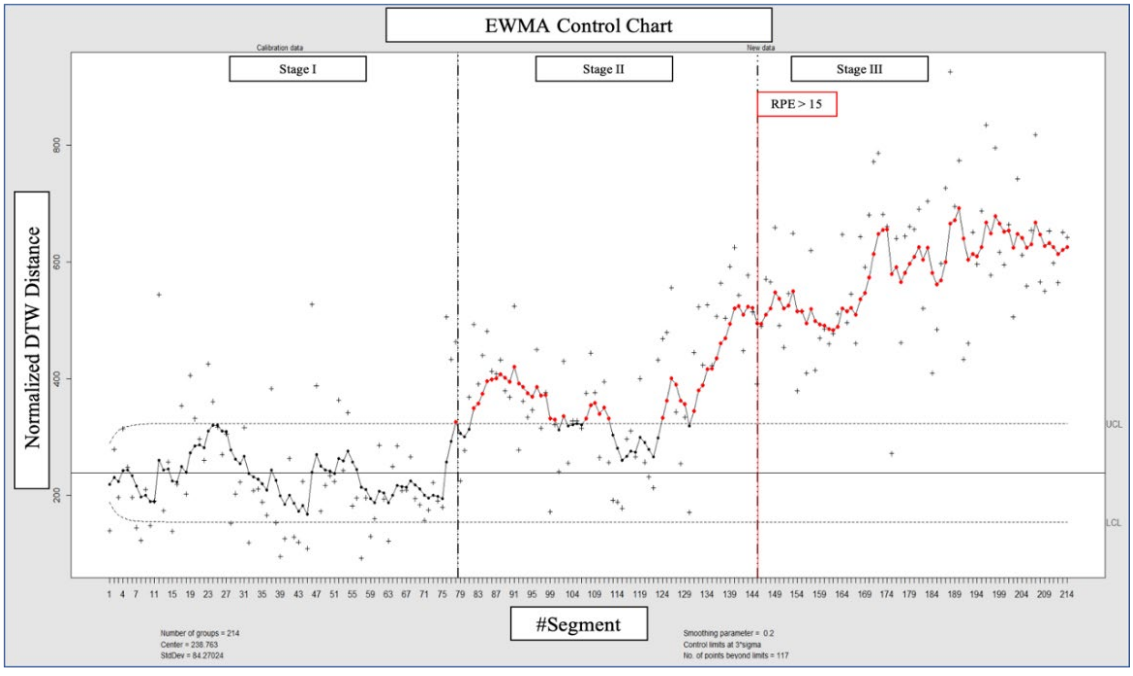

Figure 27. Processed EWMA control chart for left knee joint angle DTW distances.

As the EWMA chart represents, there are 117 points above the defined control limits. This result, when aligned with the RPE values, depicts that the DTW distances tend to go out of control (OC) when the subject accumulates fatigue (RPE > 15). The red line in Figure 27 is aligned as an indication from the subject's RPE data at RPE 15.

Hence, the EWMA control chart with the defined process was selected for detecting the change in the variability of a subject's joint angles while performing the MMH lifting activity.

4. EXPERIMENTS & RESULTS

4.1 Objective

Perform MMH 'lifting' experiments and analyze the data collected via the proposed methodology.

4.2 Outcomes

As a result of the experiments conducted, a final verdict on the research hypothesis will be presented.

4.3 Preamble

In this section, the MMH experiments were conducted using the methodology presented in the 'Data Collection Module' and 'Operator Analysis and Feedback Module.' Table 4 presents the design of experiments. Two male subjects with similar physical characteristics and daily level of activity were chosen for the study. The lift height was chosen as 51 cm (20.08 inches) with a time interval of 9 seconds between consecutive lifting and lowering motions [40]. The weight of the box was 24 kg (52.91 pounds). Subjects performed seven replicates of the activity each. The activity was performed as per the sequence displayed in Figure 14. As a result of the MoCap experiment, absolute joint angles at the left elbow, right elbow, left back, right back, left knee, and right knee (Figure 3) were calculated at 100 Hz in degrees. Upon integration of joint angle data with marker coordinate data, the segmenting filter was applied. Calculations for estimating the required sample size are discussed in the following section.

Table 4. Design of experiments.

Experiment	Subject	Height of lift (cm)	Time interval between consecutive lift & lower (seconds)	Weight of box (kg)	Replicate
1	1	51	9	24	1
2	1	51	9	24	2
3	1	51	9	24	3
4	1	51	9	24	4
5	1	51	9	24	5
6	1	51	9	24	6
7	1	51	9	24	7
8	2	51	9	24	1
9	2	51	9	24	2
10	2	51	9	24	3
11	2	51	9	24	4
12	2	51	9	24	5
13	2	51	9	24	6
14	2	51	9	24	7

4.4 Sample Size Estimation

Minitab Statistical Software® was used to determine the sample size for the experiment [73]. Pre-requisites to determine the required sample size for estimation were standard deviation, margin of error at desired confidence interval, and power of the test. The required metrics were calculated from the first three experiments. Standard deviation for the estimation was taken as the maximum standard deviation of DTW distances from the three experiments, i.e., 369.64. Power of test is defined as the probability of a hypothesis test to detect an effect; hence a value of 0.9 was chosen. The difference was

chosen double of the standard deviation, as we are interested in detecting the shifts at least twice as large as the standard deviation. Sample size estimation for the 1-Sample t-test was used with inputs listed in Table 5.

Table 5. Power and sample size metrics.

Test	1-Sample t-Test
Assumed standard deviation	369.64
Alpha value (α)	0.05
Difference	739.28
Target Power	0.9

Results from Minitab Statistical Software® are presented in Figure 28.

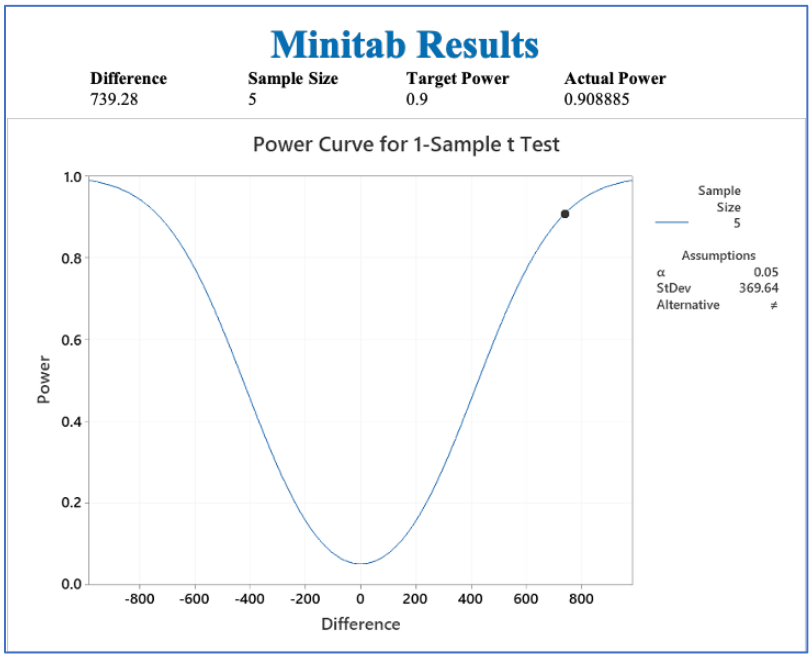

Figure 28. Results for sample size estimation.

The results (Figure 28) indicate that *at least* a sample size of five is needed for testing the hypothesis at the desired levels. For this study, seven experiments were conducted for each subject, i.e., a total of fourteen experiments.

The following section summarizes the results and the author's insights on the experiments.

4.5 Results

Previous research by [74], [75] and [76] shows that in a repetitive task, with the accumulation of fatigue, different muscles causes variations in body joint angles. A significant decrease in knee and hip motion was identified by [75], and an increase in trunk flexion and knee angle was observed by [76] while analyzing subjects performing repetitive lifting tasks.

The variations in joint angles can be visualized in current research via box plots. The box plots provide an outlook on the distribution of the data. The solid box presents an upper and lower quartile range of data. The solid line in the box represents the median of the dataset. The whiskers show the minimum and maximum values except for the outliers. Outliers in the data are presented as points beyond the whiskers.

Figure 29 represents the behavior of change in DTW values for six joints of experiments 1 to 7. The plots are set up to compare the variability in each joint for the seven experiments.

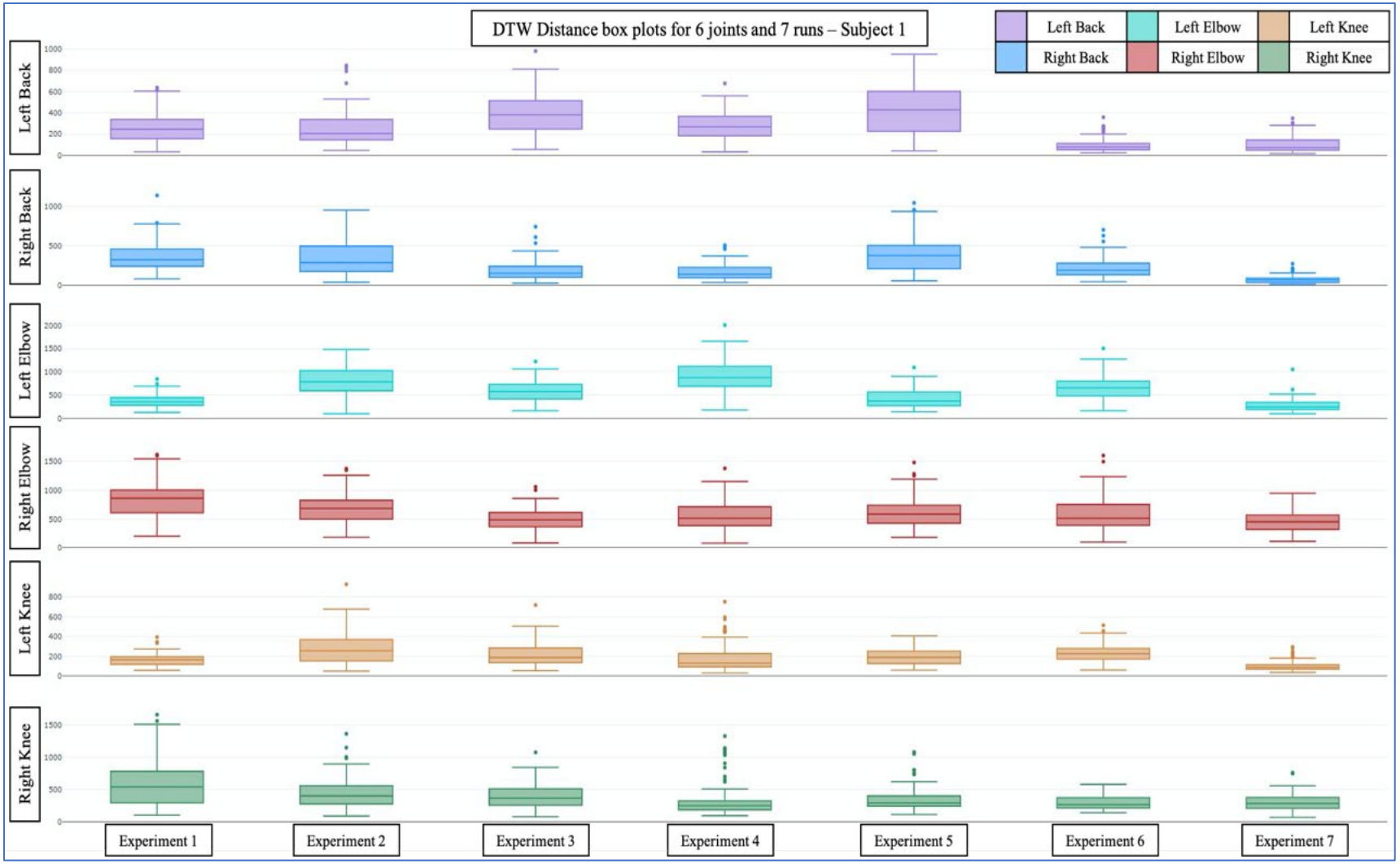

Figure 29. Joint angle DTW distance box plots: Experiment 1 – 7.

Considering the left back joint, the variability reduces in experiments 6 and 7. However, experiments 2 and 6 show a higher number of outliers in this joint's DTW values. In the right back joint, considering the marker positions on the subject (Figure 11), similar behavior is expected. The DTW points lie in the same range of 0 to 1000, but in experiments 3, 6, and 7, the box plots show less variability. This depicts that the DTW distances lie within a shorter range, i.e., the change in left and right back angles for these runs was almost similar to the individual's first lifting motion.

Left elbow DTW distance box plots show reduced variability in experiments 1, 5, and 7, whereas the points lie in almost similar ranges for the other four experiments. On the other hand, right elbow box plots lie in a shorter range than left elbow points and closer to the initial motion. The points seem to lie in the same range in the right elbow throughout seven experiments with not more than three outliers. The maximum values of the left elbow DTW parameter lie between 1500 to 2000. In contrast, the maximum limit is attained around 1500 in the right elbow, indicating that the subject's left elbow joint shows higher DTW values with accumulation of fatigue as recorded by change in RPE score from 6 to 18.

Left knee joint DTW values range from 0 to 900, whereas the maximum values for the right knee were around 1500, implying higher deviations in the right knee joint angle. A higher number of outliers can be seen in experiment 4 in both knee joints. We infer that with higher dissimilarities in left and right knee DTW values, the subject used one knee more than the other while performing the experiments. However, the current analysis does not provide insights into the use of a specific joint to analyze fatigue. Summarizing experiments 1 to 7, Table 6 shows the activity statistics.

Table 6. Activity statistics of Experiments 1 to 7.

Experiment	1	2	3	4	5	6	7
Number of Lifts	98	72	89	113	96	97	107
Left Back DTW SD	136.77	176.93	190.63	132.66	229.00	66.88	76.95
Right Back DTW SD	185.95	212.55	124.73	93.42	220.34	123.07	45.60
Left Elbow DTW SD	130.35	328.00	225.90	317.46	196.64	253.94	127.61
Right Elbow DTW SD	299.80	259.64	184.05	243.84	259.17	271.60	177.50
Left Knee DTW SD	62.96	181.06	111.30	134.56	81.87	89.95	51.10
Right Knee DTW SD	369.64	249.93	180.10	246.43	173.66	107.91	130.89
Left Back DTW Mean	256.64	260.74	401.82	276.84	422.50	98.92	104.23
Right Back DTW Mean	370.70	343.86	190.26	165.45	384.20	216.46	73.79
Left Elbow DTW Mean	376.12	803.82	594.85	885.07	427.39	646.19	273.83
Right Elbow DTW Mean	840.23	697.46	502.21	552.97	624.04	578.41	467.85
Left Knee DTW Mean	168.98	294.72	217.92	187.91	194.82	234.14	101.97
Right Knee DTW Mean	602.27	459.99	401.00	323.83	345.24	300.80	298.99
Maximum Standard Deviation	Right Knee	Left Elbow	Left Elbow	Left Elbow	Right Elbow	Right Elbow	Right Elbow

Table 6 shows the number of lifts performed in each experiment, standard deviation, and mean of computed DTW distances for the consecutive joints. The last row presents the body joint with a maximum standard deviation for each run. Based on the maximum standard deviation of DTW distances for the joints and considering research by [74], [75] and [76], the right knee, left elbow, and right elbow can be identified as the joints of concern for the respective individual. However, this is not the scope of this research and shall be considered for future research. Evaluating the joint angle characteristics for experiments 8 to 14, box plots in Figure 30 represent the behavior of DTW values.

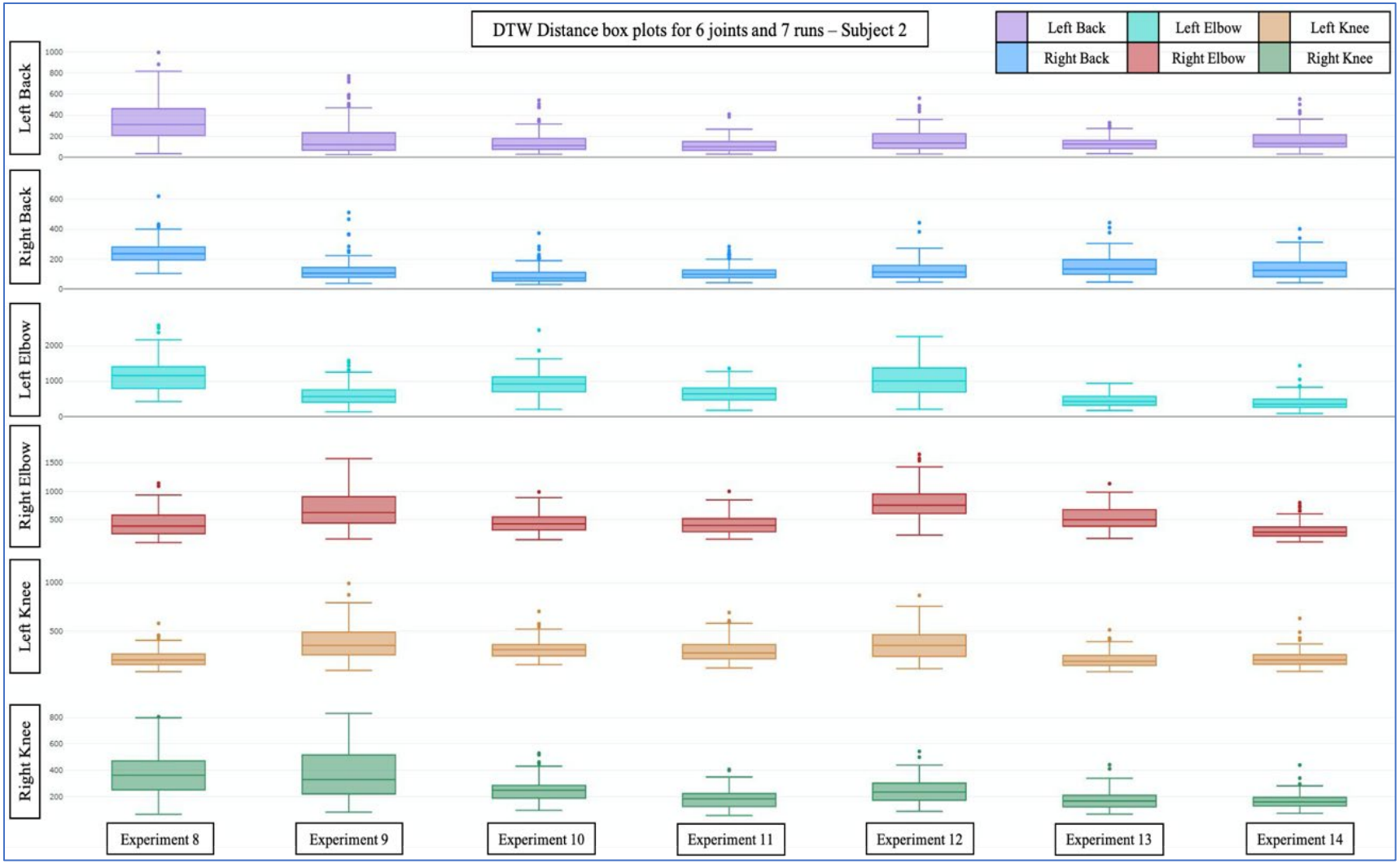

Figure 30. Joint angle DTW distance box plots: Experiment 8 – 14.

The left back joint displayed large variability in experiment 8, compared to the other experiments. However, many outliers were recorded in experiments 9, 10, 12, and 14. Considering the left back and right back joints' position, similar variations were expected from the joint. The results show that the right back joint has less variability as compared to the left back. The DTW values for the left back reach a maximum at 1000, whereas the highest DTW distance of 600 was recorded for the right back joint. A possible reason for this variability being, the subject twisted the back while lifting, causing a higher degree of change in angle for one specific side.

Left elbow DTW values lie at a higher range than the values for other joints, as the highest values reach beyond 2000. DTW values for experiments 8, 10, and 12 lie in the same range, whereas experiments 9, 11, 13, and 14 tend to follow close ranges. Less variation was noted in the right elbow joint DTW values as the maximum values lie around 1500. Experiment 9 and 12 had spread out data when compared to other experiments.

Left knee joint DTW parameters lie in the range close to the right knee. The higher variation in data was recorded in experiments 8 and 9 for the right knee compared to experiments 10 to 14. Table 7 presents the activity statistics for experiments 8 to 14.

Table 7. Activity statistics of Experiments 8 to 14.

Experiment	8	9	10	11	12	13	14
Number of Lifts	143	145	135	130	126	88	116
Left Back DTW SD	183.85	156.97	96.91	66.99	103.2	63.73	99.03
Right Back DTW SD	73.06	70.25	58.49	48.13	65.03	80.97	66.82
Left Elbow DTW SD	431.6	287.64	340.44	246	442.87	165.92	222.88
Right Elbow DTW SD	220.17	318.56	160.24	163.47	277.43	203.58	134.22
Left Knee DTW SD	81.32	167.02	100.03	112.9	153.98	78.64	85.76
Right Knee DTW SD	158.4	188.97	79.64	68.71	95	74.94	56.86
Left Back DTW Mean	344.21	178.22	140.62	116.03	163.67	132.05	164.29
Right Back DTW Mean	244.48	120.49	93.31	110.29	125.8	153.86	134.35
Left Elbow DTW Mean	1140.46	610.14	919.96	633.48	1032.21	443.92	405.89
Right Elbow DTW Mean	427.72	693.31	439.78	417.03	793.4	533.96	304.10
Left Knee DTW Mean	223.57	388.37	321.86	300.96	368.67	207.83	222.81
Right Knee DTW Mean	378.01	367.63	243.99	179.5	246.55	174.09	165.38
Maximum Standard Deviation	Left Elbow	Right Elbow	Left Elbow	Left Elbow	Left Elbow	Right Elbow	Left Elbow

Body joints with maximum standard deviation from the experiments 8 to 14 were left elbow and right elbow. Upon calculating DTW values for all experiments' respective joints, the proposed methodology's next step is to test the DTW points via the EWMA control charts. The following sections discuss the results of the analysis and tend to answer the following questions:

1. Do control charts detect fatigue in an individual?
2. Can *similar* joints be used to detect fatigue in different individuals

4.6 Do control charts detect fatigue in an individual?

To examine if EWMA control charts detected fatigue in an individual, the out of control (OC) points in control charts for all experiments were analyzed. The proposed model was evaluated based on its sensitivity (recall) metric [77].

The model's sensitivity can be stated as the parameter defined to calculate the fraction of correct detections of fatigue performed by the model [77]. It is indicated as:

$$Sensitivity = \frac{True\ detections}{Sum\ of\ true\ detections\ and\ undetected\ points}$$

Mathematically, sensitivity can be expressed as:

$$Sensitivity = \frac{True\ Positive}{True\ Positive + False\ Negative} \qquad (9)$$

A True Positive (TP) detection is defined as the EWMA point in the control chart, which lies in RPE 15 to RPE 17 range and beyond the Upper Control Limit (UCL). False Negative (FN) is defined as the point which lies in the same range (RPE 15 to RPE 17) but below the UCL. Figure 31 demonstrates the TP (True +), and FN (False -) points in an EWMA control chart for the left back joint in experiment 1.

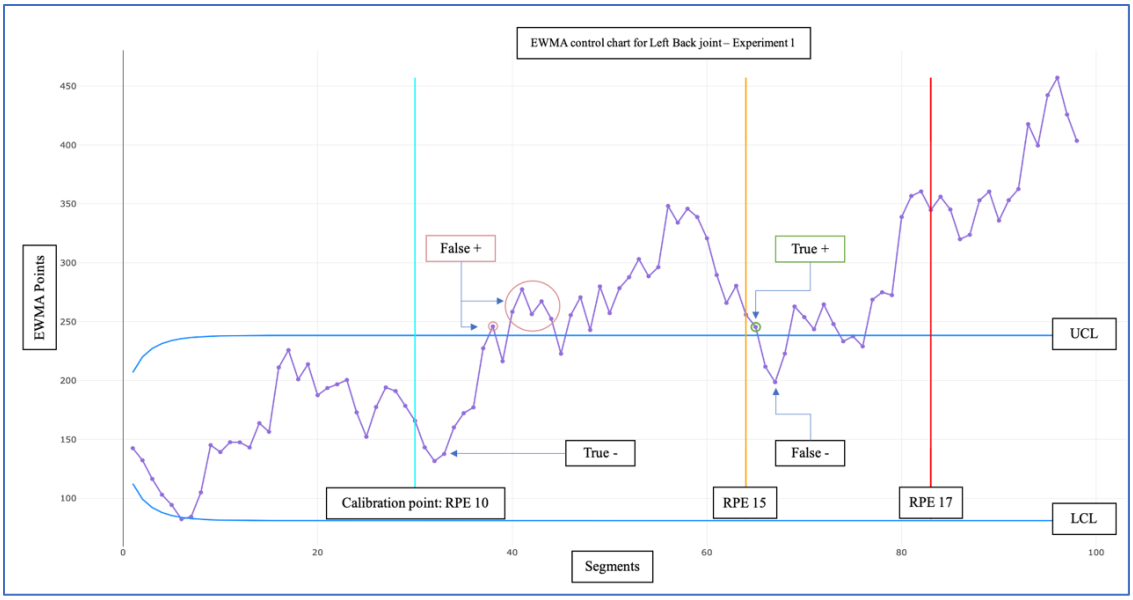

Figure 31. EWMA control chart for left back joint: Experiment 1.

The vertical line (cyan) presents the segment when the subject reaches RPE 10. The data points before this point are considered as the calibration points. EWMA control chart's mean, standard deviations, and control limits are decided based on the calibration data. The orange and red vertical lines in the control charts present the segments at which the subject declares RPE 15 and RPE 17, respectively. The points lying between these lines are of concern, as those points indicate that the subject reached a hard exertion level.

In the displayed control chart, the process goes out of control (OC) at an early stage, i.e., at segment 38. Montgomery identified that a single OC point in the EWMA control chart concludes that the process is OC [71]. EWMA control charts for all the joints and experiments were plotted (APPENDIX B).

A sensitivity score ranges from 0 to 1. A score of 0 denotes that there were no OC points detected by the control chart in the desired range, making TP zero. A score of 1

indicates that the model detected no FN values. Hence, the higher the sensitivity score, the better the model behaved in detecting OC points. Since a single point out of UCL can lead to an OC process in the EWMA control chart [71], a sensitivity score greater than zero implies that the proposed methodology worked in detecting points in the hard exertion range. Using the formula in Equation 9, the number of TP and FN points were calculated for each EWMA control chart using the statistical software R on IDE, RStudio (APPENDIX A). Sensitivity results for all experiments for the proposed methodology are presented in Table 8.

Table 8. Model sensitivity results.

Experiment	Left Back	Right Back	Left Elbow	Right Elbow	Left Knee	Right Knee
1	0.70	0.30	0.30	0.20	0.70	1.00
2	1.00	1.00	1.00	0.83	0.00	0.00
3	0.71	0.59	0.41	0.00	0.00	0.06
4	0.54	0.00	0.08	0.00	0.00	0.54
5	1.00	1.00	0.47	1.00	0.00	0.24
6	0.48	0.22	0.87	0.70	0.00	0.13
7	0.00	0.00	0.36	0.00	0.00	1.00
8	0.00	0.09	0.78	0.00	0.26	1.00
9	1.00	0.39	0.00	0.00	1.00	1.00
10	1.00	0.23	0.00	0.00	0.38	0.00
11	0.05	0.00	0.90	0.33	0.00	0.00
12	0.20	0.00	1.00	0.00	0.10	0.40
13	0.00	0.00	0.00	0.38	0.94	0.00
14	0.50	0.00	0.00	0.00	0.00	0.00

At instances with a sensitivity score of greater than 0, the proposed method correctly identified the OC points (highlighted in green). At a score of 0, no points were detected OC by the control charts in RPE 15 to RPE 17 range.

In experiment 1, the left back joint's sensitivity, 0.70, represents that out of all the EWMA points in RPE 15 to RPE 17 range, 70% of the points lie above the UCL. Thus, if the sensitivity is greater than 0, it shows that the model detected fatigue in the subjective RPE 15 to RPE 17 range.

For experiments 1, 2, 5, 7, 8, 9, 10, and 12, a sensitivity score of 100% was observed in at least one body joint. The results show that EWMA control charts could detect fatigue in all the experiments by at least one body joint. Combining the sensitivity scores of all fourteen experiments for six joints each, the EWMA control charts detected fatigue in 78.5%, 57%, 71%, 42.8%, 42.8%, and 64% experiments for left back, right back, left elbow, right elbow, left knee, and right knee, respectively.

Since we have established that EWMA control charts can detect biomechanical fatigue in an individual, the following section tests the second research question.

4.7 Can *similar* joints be used to detect fatigue in different individuals?

This section tests the proposed hypothesis, i.e., different human subjects reveal biomechanical fatigue via *similar* body joints.

Restating the null (H_0) hypothesis (Equation 1):

$$H_0 : \beta_{1j} = \beta_{2j} \; \forall \; \mathrm{j} = 1,2,3,4,5,6$$

Where, β_{ij} is the rate of detecting fatigue by the proposed methodology. i is either 1 or 2, linked to subject 1 and subject 2, respectively. The value of j ranges from 1 to 6, linked to left back (1), right back (2), left elbow (3), right elbow (4), left knee (5), and

right knee (6) joints. The hypothesis test was performed to check if the rate of detection of biomechanical fatigue for the two subjects, using the proposed methodology was either due to chance or not.

We have established that the model's sensitivity considers the number of OC points after RPE 15, and one OC point in the EWMA control chart can identify the OC process. Re-evaluating the results in Table 8, entries with sensitivity greater than 0 were marked as true detection, i.e., 1 and 0 remained the same. Table 9 summarizes the data for hypothesis tests.

Table 9. Data for hypothesis testing.

	Left Back		**Right Back**		**Left Elbow**		**Right Elbow**		**Left Knee**		**Right Knee**	
Run	**S1**	**S2**	**S1**	**S2**	**S1**	**S2**	**S1**	**S2**	**S1**	**S2**	**S1**	**S2**
1	1	0	1	1	1	1	1	0	1	1	1	1
2	1	1	1	1	1	0	1	0	0	1	0	1
3	1	1	1	1	1	0	0	0	0	1	1	0
4	1	1	0	0	1	1	0	1	0	0	1	0
5	1	1	1	0	1	1	1	0	0	1	1	1
6	1	0	1	0	1	0	1	1	0	1	1	0
7	0	1	0	0	1	0	0	0	0	0	1	0

The columns represent seven replicates of experiments performed by the two subjects (Subject 1 = S1, Subject 2 = S2). The data were analyzed via Minitab Statistical Software®. The 2 Proportions statistical test aimed to check for a significant difference between sample data of an event for two groups. Each sample was presented in a column

as an entry to the software (Table 9). Checking for similarities in the null hypothesis, 0 was selected as the hypothesized difference value. The alternative hypothesis stated that the difference was not equal to the hypothesized difference. The pooled estimate of proportion was chosen as the testing method.

As stated by [78], testing for multiple null hypotheses (current case) with the same probability values (p-value) increases the risk of type 1 error. To adjust the p-value (alpha) for such scenarios, Bonferroni correction is used. Taking the alpha value of 0.05, based on the calculation of Bonferroni-adjusted p-values by [79], the value required for significance is 0.00833. Thus, defining the confidence interval (CI) at 1-0.00833, i.e., 99.167%.

Properties for the two sample proportions test in Minitab Statistical Software® are presented in Figure 32.

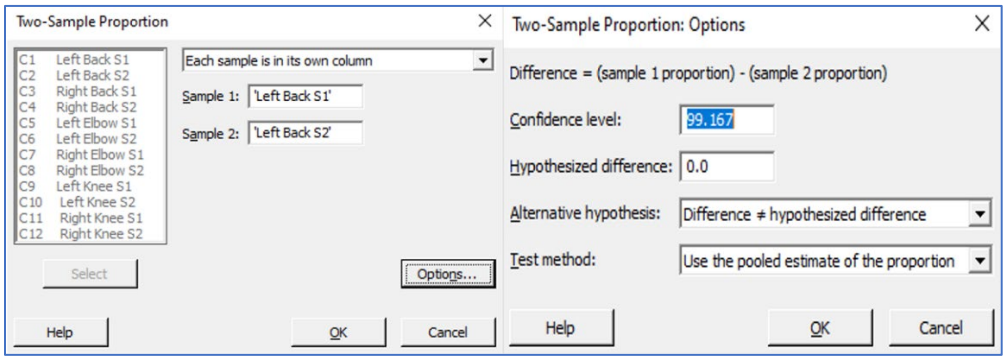

Figure 32. Two-sample proportion hypothesis test.

Equation 10 presents the first null hypothesis considering the left back joint (j = 1).

$$H_0 : \beta_{11} - \beta_{21} = 0 \qquad (10)$$

Upon analysis, the hypothesis test presents the method used, descriptive statistics, estimation for difference and test results z-value, p-value based on normal approximation, and the Fisher's exact. The results are summarized in Figure 33.

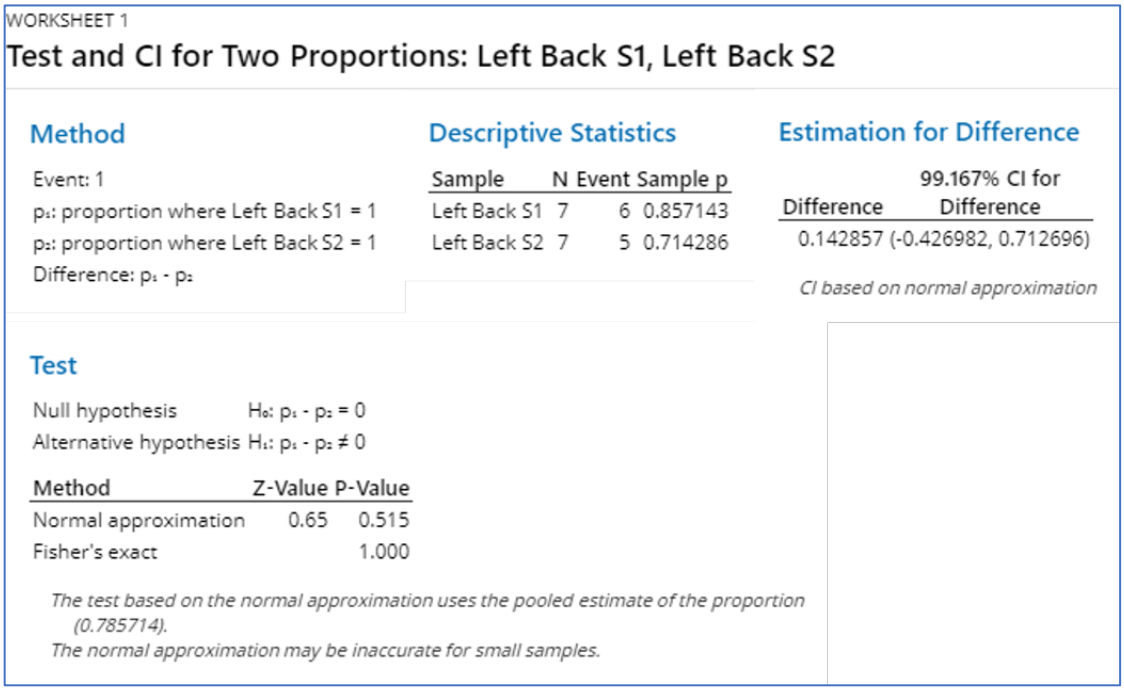

WORKSHEET 1

Test and CI for Two Proportions: Left Back S1, Left Back S2

Method

Event: 1
p_1: proportion where Left Back S1 = 1
p_2: proportion where Left Back S2 = 1
Difference: $p_1 - p_2$

Descriptive Statistics

Sample	N	Event	Sample p
Left Back S1	7	6	0.857143
Left Back S2	7	5	0.714286

Estimation for Difference

Difference	99.167% CI for Difference
0.142857	(-0.426982, 0.712696)

CI based on normal approximation

Test

Null hypothesis H_0: $p_1 - p_2 = 0$
Alternative hypothesis H_1: $p_1 - p_2 \neq 0$

Method	Z-Value	P-Value
Normal approximation	0.65	0.515
Fisher's exact		1.000

The test based on the normal approximation uses the pooled estimate of the proportion (0.785714).
The normal approximation may be inaccurate for small samples.

Figure 33. Minitab results for the hypothesis test, j=1.

In Figure 33 the method describes the chosen parameters for the test. Descriptive statistics summarize the event parameters such as favorable events and total events (N), and sample probability. Estimation for difference provides reference values at 99.167% CI for the hypothesized difference.

The test section in Figure 33 shows the computed z-value and p-value based on normal approximation. Due to the model's sample size of 7, the normal approximation in the hypothesis test might be considered imprecise. Hence, Fisher's exact test was conducted [80]. P-values from the Fisher's exact for six tests, i.e., for six joints are presented in Table 10. P-value is the smallest level of significance, based on which we

can reject the null hypothesis. If the resultant p-value is less than the chosen alpha level, i.e., 0.00833, we have enough evidence to reject the null hypothesis.

Table 10. P-Value results based on Fisher's exact.

Body Joint	**P-Value**
Left Back	1.00
Right Back	0.592
Left Elbow	0.070
Right Elbow	0.592
Left Knee	0.103
Right Knee	0.266

The results show that the smallest p-value was attained for the left elbow joint. However, we were unable to reject the null hypothesis based on p-values. The analysis states that a larger sample size is required to reject the null hypothesis.

Analyzing the results based on CI, if the hypothesized difference, i.e., 0 lies between the achieved CI limits, it denotes the possibility that the difference in proportions between the two subjects is due to chance.

Minitab results for all six null hypotheses tests are presented in APPENDIX C. CI for all the null hypotheses, i.e., $j = 1, 2, 3, 4, 5, 6$ are summarized in Table 11.

Table 11.Confidence intervals for two proportions: six joints.

Body Joint	Lower Bound	Upper Bound
Left Back	-0.426982	0.712696
Right Back	-0.382482	0.95391
Left Elbow	0.077933	1
Right Elbow	-0.382482	0.95391
Left Knee	-1	-0.001589
Right Knee	-0.175834	1

From computed CI for all the joints, the reference value specified in the null hypothesis, i.e., 0 lies outside the CI for the left elbow and left knee joints. Therefore, the analysis provided evidence to state that the difference in proportions between subject 1 and subject 2 is not at all due to chance. With 99.167% confidence, an interval was estimated that does not disregard the possibility that the difference in proportions between subject 1 and subject 2 is due to chance.

Although based on the discussed p-values, there was not enough evidence to justify rejecting the null hypothesis. But the nature of CI shows that testing a larger sample size holds the possibility to reject the null hypothesis. Therefore, we reject the null hypothesis (Equation 1) and accept that *similar joints* cannot detect biomechanical fatigue using the proposed methodology for two individuals. Hence, verifying the need for personalized DT of an MMH operator to detect and analyze fatigue.

5. SUMMARY AND CONCLUSION

This study presented a digital twin framework for a manual material handling (MMH) operator to detect fatigue via variation in absolute joint angles. Two modules of development were presented to analyze fatigue in an operator while performing a lifting task. In the Data Collection Module, a motion capture system was used to collect the subject's precise joint positional data performing tasks. Left and right elbows, knees, and back joints were studied for the accumulation of fatigue. The coordinate data from the motion capture system was used to measure the joint angles using inverse kinematics concepts.

The Operator Analysis and Feedback Module compared and analyzed the change in joint angles for all the lifting experiment repetitions. The dynamic time warping (DTW) algorithm was used to compare the change in joint angles with time. Keeping the variation in the first lifting activity as a reference, all the other lifting motions performed by the individual in an experiment were compared and analyzed. The variation in DTW parameters was evaluated via an exponentially weighted moving average (EWMA) control chart. The proposed method was analyzed to detect the out of control points in the control chart as the subject reaches hard exertion of the activity on a Borg's RPE scale (RPE 15).

To test the proposed methodology, fourteen lifting and lowering experiments were performed by two healthy male individuals (seven experiments each), lifting a box of weight 24 kg at a time interval of 9 seconds. The subjects were allowed to perform the MMH activity until they reached an RPE level of 18. The fatigue detection methodology was tested on the experiments and evaluated via model sensitivity metric. The research

demonstrated that:

1. The proposed method was able to detect biomechanical fatigue in all fourteen experiments via at least one body joint.
2. Different individuals indicate signs of biomechanical fatigue via different body joints. Similar body joints cannot be used to analyze fatigue in subjects performing similar tasks.

This justifies the need for a personalized digital twin (DT) for an MMH operator to provide feedback on fatigue and activity statistics.

6. FUTURE SCOPE

The proposed framework methodology tends to fulfill the four dimensions of a true DT, as concluded by [81], i.e., connectivity, analyzability, visibility, and granularity.

The first component, ‘Connectivity,’ deals with the DT being a copy of the real system. In the framework, the Data Collection Module helps document the subject's actual moves in the activity area. The operator's real-time data collection on the factory floor with technologies like Inertial Motion capture Units (IMU) & 3D vision shall allow the concept's on-site implementation.

The second dimension, ‘Analyzability,’ assists the DT in decision making, assisting the human operator in real-time. Evaluating the motion data as discussed in the Operator Analysis & Feedback module allows the fulfillment of this true DT development component. As discussed by researchers, the proposed dynamic time warping (DTW) algorithm carries real-time capabilities. Additional parameter tuning, such as optimizing the ‘Reference Index,’ shall increase the model’s performance in detecting shifts in joint angles. The current use case focuses on the evaluation of joint angles for fatigue evaluation. Upon further development, body fatigue predictions can be made based on motion data [44]. The application of this approach is currently limited to operator fatigue. However, the framework includes model testing and implementation capabilities to make real-time decisions for optimized scheduling, human resource allocation, and operator-specific job tasks.

Various parameters used in the current methodology can be optimized to increase the model's sensitivity. The calibration point was decided in the EWMA control charts based on the subject’s RPE 10 level. Since RPE is subjective, research by Sudarshan [20]

conceptualizes how various physiological factors can be used to estimate RPE; hence, the calibration point. λ and L values in EWMA control charts can be tailored to the subject's change in joint angles.

The box plots for experiments 6, 7, 13, and 14 show lower variations than their preceding experiments. Considering muscle memory in humans, the lower variability in DTW values in later experiments remains a topic for future research.

The 'Visibility' element of operator DT development can be accomplished via advanced tools and dedicated software development kit dashboards with the ability to be customized on-demand. The current framework withholds the capability to integrate Qualisys and Unity software [82] to represent the operator's futuristic avatar with a real-time diagnosis of lifting motion and advanced training of the new generation workforce.

The discussed framework is a conceptual model with a high abstraction level, considering minimum details of the system about the development of a true DT. Whereas, the fatigue analysis of the operator sits at a lower abstraction level, considering the very specifics of the operator body fatigue based on body joint movements. With further incorporation of other body joints, forces, and torques acting on the body, joints can be studied for variation using the same methodology. Henceforth, fulfilling the initial requirement of the fourth dimension of DT development, i.e., 'Granularity.'

APPENDIX SECTION

APPENDIX A

The following section contains details on R script developed to implement the necessary analysis in the proposed methodology. The R script was implemented via IDE RStudio. Packages used to perform the analysis are plyr, qcc, dtw, ggplot2, and plotly.

```
#Load required library
library(plyr)

#  This program separates .tsv files into individual lifting or lowering motion segments.
#  This file works on all lifting, lowering, lift&Lowering files

#  The program outputs up to three files:
#       A segmented listing of under load lifting motions that is indexed
#       A segmented listing of under load lowering motions that is indexed
#       A summary file that identifies which marker was used to perform the segmentation
#      (segmentation is based on the maker with the most complete data set.)

###  Data variable definition area

# read in source ".tsv" file exported from QTM software
filename1 <- "C:/QTM_x-y-z_coordinate_data"
readfile1 <- paste(filename1, ".tsv", sep = "")
MoCap_data_load <- read.csv2(file=readfile1, header = TRUE, sep = "\t", dec = ".",skip=10, stringsAsFactors=FALSE)
MoCap_data_load[MoCap_data_load == 0] <- NA   #  Set all 0 values to NA
# read in subject's RPE data to align with QTM data
filename <- "C:/RPE_data"
readfile <- paste(filename, ".csv", sep = "")
RPE_data <- read.csv2(file=readfile, header = TRUE, sep = ",", dec = ".")
MoCap_data_load$RPE[1]<-RPE_data$RPE[1]
j<-1
for(i in 2:length(MoCap_data_load$Frame)){
  if(MoCap_data_load$Frame[i]%%6000==0){
    j=j+1
    MoCap_data_load$RPE[i]<-RPE_data$RPE[j]
    i=i+1
  }
  else {
    MoCap_data_load$RPE[i]<-RPE_data$RPE[j]
    i=i+1
  }
}
# read 6 angle files from QTM Analyze

filename2.1 <- "C:/LeftBackAngle"
readfile2.1 <- paste(filename2.1, ".tsv", sep = "")
LBackAngle <- read.csv2(file=readfile2.1, header = TRUE, sep = "\t", dec = ".",skip=7)

filename2.2 <- "C:/RightBackAngle"
readfile2.2 <- paste(filename2.2, ".tsv", sep = "")
RBackAngle <- read.csv2(file=readfile2.2, header = TRUE, sep = "\t", dec = ".",skip=7)

filename3 <- "C:/LeftElbowAngle"
readfile3 <- paste(filename3, ".tsv", sep = "")
LElbowAngle <- read.csv2(file=readfile3, header = TRUE, sep = "\t", dec = ".",skip=7)

filename4 <- "C:/LeftKneeAngle"
readfile4 <- paste(filename4, ".tsv", sep = "")
LKneeAngle <- read.csv2(file=readfile4, header = TRUE, sep = "\t", dec = ".",skip=7)

filename5 <- "C:/RightElbowAngle"
```

```
readfile5 <- paste(filename5, ".tsv", sep = "")
RElbowAngle <- read.csv2(file=readfile5, header = TRUE, sep = "\t", dec = ".",skip=7)

filename6 <- "C:/RightKneeAngle"
readfile6 <- paste(filename6, ".tsv", sep = "")
RKneeAngle <- read.csv2(file=readfile6, header = TRUE, sep = "\t", dec = ".",skip=7)

# creating a single data frame with coordinate, angles and RPE data
MoCap_data <- data.frame(MoCap_data_load, LBackAngle$LBackAngle, RBackAngle$RBackAngle, LElbowAngle$LElbowAngle,
LKneeAngle$LKneeAngle,
                RElbowAngle$RElbowAngle, RKneeAngle$RKneeAngle)
##############################   Step 1  ##############################

#Calculate percentage of complete data for determining segmenting control marker

##################### Naming convention ####################
nframe <- nrow(MoCap_data)
Perframe_RH <- sum(!is.na(MoCap_data$RHandOut.X))/nframe
Perframe_LH <- sum(!is.na(MoCap_data$LHandOut.X))/nframe
Perframe_RWO <- sum(!is.na(MoCap_data$RWristOut.X))/nframe
Perframe_LWO <- sum(!is.na(MoCap_data$LWristOut.X))/nframe
Perframe_RWI <- sum(!is.na(MoCap_data$RWristIn.X))/nframe
Perframe_LWI <- sum(!is.na(MoCap_data$LWristIn.X))/nframe
# identify the column set with the most data
v_name = c("RHandOut","LHandOut", "RWristIn","LWristIn", "RWristOut", "LWristOut")
motionpt1 <- v_name[which.max(c(Perframe_RH,Perframe_LH, Perframe_RWI,Perframe_LWI, Perframe_RWO, Perframe_LWO))]

MoCap_data["EVENTS"] <- NA   # add column called EVENTS
MoCap_data["INDEX"] <- NA   # add column called INDEX

#############################################################################
###     Part 2 - identify fixed point events
#############################################################################

#  create user identified column labels
#  motion tags
MP1X <- paste(motionpt1,".X", sep='')
MP1Y <- paste(motionpt1,".Y", sep='')
MP1Z <- paste(motionpt1,".Z", sep='')

#  iDentify user identfied column label locations
# motion tags
MP1Xc <- which( colnames(MoCap_data)==MP1X )
MP1Yc <- which( colnames(MoCap_data)==MP1Y )
MP1Zc <- which( colnames(MoCap_data)==MP1Z )

miny <- min(MoCap_data[,MP1Y], na.rm=T)
minz <- min(MoCap_data[,MP1Z], na.rm=T)

bary <- miny + 250
barz <- minz + 300

i <- 1

for (i in i:(nrow(MoCap_data)-4)){

  if(is.na(MoCap_data[i,MP1Yc])){ YA <- bary+1} else {YA <- MoCap_data[i,MP1Yc]}
  if(is.na(MoCap_data[i+1,MP1Yc])){ YB <- bary+1} else {YB <- MoCap_data[i+1,MP1Yc]}
  if(is.na(MoCap_data[i+2,MP1Yc])){ YC <- bary+1} else {YC <- MoCap_data[i+2,MP1Yc]}
  if(is.na(MoCap_data[i+3,MP1Yc])){ YD <- bary+1} else {YD <- MoCap_data[i+3,MP1Yc]}
  if(is.na(MoCap_data[i+4,MP1Yc])){ YE <- bary+1} else {YE <- MoCap_data[i+4,MP1Yc]}

  if(is.na(MoCap_data[i,MP1Zc])){ ZA <- barz+1} else {ZA <- MoCap_data[i,MP1Zc]}
  if(is.na(MoCap_data[i+1,MP1Zc])){ ZB <- barz+1} else {ZB <- MoCap_data[i+1,MP1Zc]}
  if(is.na(MoCap_data[i+2,MP1Zc])){ ZC <- barz+1} else {ZC <- MoCap_data[i+2,MP1Zc]}
  if(is.na(MoCap_data[i+3,MP1Zc])){ ZD <- barz+1} else {ZD <- MoCap_data[i+3,MP1Zc]}
  if(is.na(MoCap_data[i+4,MP1Zc])){ ZE <- barz+1} else {ZE <- MoCap_data[i+4,MP1Zc]}

  if((YC > 1500 ) & (YB <1500))
  {
```

```
   MoCap_data[i+2,"EVENTS"] <- "BREAK"
  }

  if(YC < bary)
  {
   if((YA > YC) & (YB > YC) & (YC < YD) & (YC < YE))
   {
    MoCap_data[i+2,"EVENTS"] <- "UPPER"
   }
  }
  if(ZC < barz)
  {
   if((ZA > ZC) & (ZB > ZC) & (ZC < ZD) & (ZC < ZE))
   {
    MoCap_data[i+2,"EVENTS"] <- "LOWER"
   }
  }
}

#writefile <- paste(filename,"_", Sys.Date(),"_",".csv", sep = "")
#write.table(MoCap_data, writefile, sep = ",", col.names = T, append = T)

table(MoCap_data$EVENTS)

#########################################################################
####   Part 3 -- Identify Segments
#########################################################################

#  a segment is defined as a series of motions between to points.  Intermediary points may exist, but the segment is defined by only
two points.

# Lower events signify the lower location
# Upper events signify the upper location

#  create sub set of identified events
Segments <- MoCap_data[ which(MoCap_data$EVENTS=='LOWER'| MoCap_data$EVENTS=='UPPER'|
MoCap_data$EVENTS=='BREAK'),  ]

table(Segments$EVENTS)

#writefile <- paste(filename,"Segments_", Sys.Date(),"_",".csv", sep = "")
#write.csv(Segments, writefile, sep = ",", col.names = T)

#  check for proper event patterns
#  remove out of sequence events
#   if two consecutive events, remove the first one, if two consecutive 'out' events, remove first one

cnt <- 0
k <- 1
for( k in 1:(nrow(Segments)-1)){
  if(Segments[k,"EVENTS"] == Segments[k+1,"EVENTS"]){cnt <- cnt +1}
}

repeat{

  for( i in 1:(nrow(Segments)-1)){
    #   both cells are UPPER
    if((toString(Segments[i,"EVENTS"]) == "UPPER") & (toString(Segments[i+1,"EVENTS"]) == "UPPER")){
      Segments <- Segments[-c(i+1),]
      cnt <- cnt - 1
    }
  }

  for( i in 1:(nrow(Segments)-1)){
    #   both cells are UPPER
    if((toString(Segments[i,"EVENTS"]) == "BREAK") & (toString(Segments[i+1,"EVENTS"]) == "BREAK")){
      Segments <- Segments[-c(i+1),]
      cnt <- cnt - 1
    }
  }
```

```
   for( i in 1:(nrow(Segments)-1)){
   #   both cells are LOWER
   if((toString(Segments[i,"EVENTS"]) == "LOWER") & (toString(Segments[i+1,"EVENTS"]) == "LOWER")){
     Segments <- Segments[-c(i),]
     cnt <- cnt - 1
   }
  }
  if(cnt == 0){break}
}

table(Segments$EVENTS)

#names(Segments) <- c("rowID", names(Segments)[1:ncol(Segments)-1])
#writefile <- paste(filename,"Segments_", Sys.Date(),"_",".csv", sep = "")
#write.table(Segments, writefile, sep = ",", col.names = T, append = T)

# create segment files

# segment files are defined by the first and last fixed point identifiers

# identify intentional lift motion segments

Y <- 1

if(Segments$EVENTS[1]== "LOWER" && Segments$EVENTS[2]== "UPPER" && Segments$EVENTS[3]== "BREAK"){
  startval <- Segments[1,"Frame"]
  endval <- Segments[2,"Frame"]

  LiftSegment <- MoCap_data[(startval:endval),]
  LiftSegment["INDEX"] <- Y

  writefile <- paste(filename1,"_LiftSegments_", Sys.Date(),"_",".csv", sep = "")
  write.table(LiftSegment, writefile, sep = ",", col.names = T, append = T, row.names = F)
  Y <- Y + 1
}

for(i in 3:(nrow(Segments)-3)){
  if(Segments$EVENTS[i]== "BREAK" && Segments$EVENTS[i+1]== "LOWER" && Segments$EVENTS[i+2]== "UPPER" &&
Segments$EVENTS[i+3]== "BREAK"){
    startval <- Segments[i+1,"Frame"]
    endval <- Segments[i+2,"Frame"]

    LiftSegment <- MoCap_data[(startval:endval),]
    LiftSegment["INDEX"] <- Y
    writefile <- paste(filename1,"_LiftSegments_", Sys.Date(),"_",".csv", sep = "")
    if(Y==1){
      write.table(LiftSegment, writefile, sep = ",", col.names = T, append = T, row.names = F)
    }  else {write.table(LiftSegment, writefile, sep = ",", col.names = F, append = T, row.names = F)}
    Y <- Y + 1
  }
}

# identify intentional lower motion segments

Z <- 1

if(Segments$EVENTS[1]== "UPPER" && Segments$EVENTS[2]== "LOWER" && Segments$EVENTS[3]== "BREAK"){
  startval <- Segments[1,"Frame"]
  endval <- Segments[2,"Frame"]

  LowerSegment <- MoCap_data[(startval:endval),]
  LowerSegment["INDEX"] <- Z

  writefile <- paste(filename1,"_LowerSegments_", Sys.Date(),"_",".csv", sep = "")
  write.table(LowerSegment, writefile, sep = ",", col.names = T, append = T, row.names = F)
  Z <- Z + 1
  flag <- 1
}

for(i in 3:(nrow(Segments)-3)){
```

```
 if(Segments$EVENTS[i]== "BREAK" && Segments$EVENTS[i+1]== "UPPER" && Segments$EVENTS[i+2]== "LOWER" &&
Segments$EVENTS[i+3]== "BREAK"){
   startval <- Segments[i+1,"Frame"]
   endval <- Segments[i+2,"Frame"]

   LowerSegment <- MoCap_data[(startval:endval),]
   LowerSegment["INDEX"] <- Z
   writefile <- paste(filename1,"_LowerSegments_", Sys.Date(),"_",".csv", sep = "")
   if(Z==1){write.table(LowerSegment, writefile, sep = ",", col.names = T, append = T, row.names=F)
   }  else {write.table(LowerSegment, writefile, sep = ",", col.names = F, append = T, row.names=F)}
   Z <- Z + 1
 }
}


SumDataOut <- array(,dim=c(10,2))
SumDataOut[1,1] <- 'Total of Identified segments'
SumDataOut[1,2] <- Y + Z -2
SumDataOut[2,1] <- 'Total number of Lift segments'
SumDataOut[2,2] <- Y -1
SumDataOut[3,1] <- 'Total number of Lower segments'
SumDataOut[3,2] <- Z -1
SumDataOut[4,1] <- '% of data for LHandOut'
SumDataOut[4,2] <- Perframe_LH*100
SumDataOut[5,1] <- '% of data for RHandOut'
SumDataOut[5,2] <- Perframe_RH*100
SumDataOut[6,1] <- '% of data for LWristOut'
SumDataOut[6,2] <- Perframe_LWO*100
SumDataOut[7,1] <- '% of data for RWristOut'
SumDataOut[7,2] <- Perframe_RWO*100
SumDataOut[8,1] <- '% of data for LWristIn'
SumDataOut[8,2] <- Perframe_LWI*100
SumDataOut[9,1] <- '% of data for RWristIn'
SumDataOut[9,2] <- Perframe_RWI*100
SumDataOut[10,1] <- "Marker used for segmentation"
SumDataOut[10,2] <- motionpt1

filename1 <- paste(filename1,"_Summary_", Sys.Date(),".csv", sep = "")
write.csv(SumDataOut, file=filename1, row.names=F)
# End of segmentation script

# DTW distance, EWMA control charts and model performance statistics

#Load required libraries
library(qcc)
library(ggplot2)
library(plotly)
library(dtw)
library(plyr)

#Read in segmented file for analysis
filename7 <- "C:/Lift_segments"
readfile7 <- paste(filename7, ".csv", sep = "")
Seg_data <- read.csv(file=readfile7, header = TRUE, ",")

filename1 <- "C:/Filename"

#plot RPE data vs lifting segments using ggplot2
Index_RPE_plot <- ggplot(data = Seg_data, aes(x= INDEX, y= RPE),)
Index_RPE_plot <- Index_RPE_plot + geom_point() + stat_smooth(color = "blue")
Index_RPE_plot <- ggplotly(Index_RPE_plot)

################ Save RPE Plot ################
file_name <- paste(filename1,"_RPE_", Sys.Date(),".html")
htmlwidgets::saveWidget(Index_RPE_plot, file = file_name)

#load file with EWMA calibration parameters for the experiments
filename17 <- "C:/EWMACalibration"
readfile17 <- paste(filename17, ".csv", sep = "")
Cali_data <- read.csv(file=readfile17, header = TRUE, ",")
```

```
#count total number of segments
Segments_Total <- max(Seg_data$INDEX)
n <- Segments_Total - 1

#################################################################
######## 1.1 LBackAngle DTW ##########################
#################################################################
w_data_col1.1 <- list()
for(i in names(table(Seg_data$INDEX))){
  temp <- Seg_data$LBackAngle.LBackAngle[Seg_data$INDEX== i]
  w_data_col1.1[[i]] <- as.data.frame(temp)
}

dist.mat1.1 <- dist(x = w_data_col1.1, method = "DTW")
dist.mat1.1
data_x1.1 <- c(1:n)
dtw_matrix1.1 <- data.frame(data_x1.1, (dist.mat1.1[1:n]))
#################################################################
colnames(dtw_matrix1.1) <- c("X","LBackAngle_DTW")
dtw_matrix1.1

#################################################################
######## 1.2 RBackAngle DTW ##########################
#################################################################
w_data_col1.2 <- list()
for(i in names(table(Seg_data$INDEX))){
  temp <- Seg_data$RBackAngle.RBackAngle[Seg_data$INDEX== i]
  w_data_col1.2[[i]] <- as.data.frame(temp)
}

dist.mat1.2 <- dist(x = w_data_col1.2, method = "DTW")
dist.mat1.2
data_x1.2 <- c(1:n)
dtw_matrix1.2 <- data.frame(data_x1.2, (dist.mat1.2[1:n]))
#################################################################
colnames(dtw_matrix1.2) <- c("X","RBackAngle_DTW")
dtw_matrix1.2

#################################################################
######## 2.1 LElbowAngle DTW ##########################
#################################################################
w_data_col2.1 <- list()
for(i in names(table(Seg_data$INDEX))){
  temp <- Seg_data$LElbowAngle.LElbowAngle[Seg_data$INDEX== i]
  w_data_col2.1[[i]] <- as.data.frame(temp)
}

dist.mat2.1 <- dist(x = w_data_col2.1, method = "DTW")
dist.mat2.1
data_x2.1 <- c(1:n)
dtw_matrix2.1 <- data.frame(data_x2.1, (dist.mat2.1[1:n]))
#################################################################
colnames(dtw_matrix2.1) <- c("X","LElbowAngle_DTW")
dtw_matrix2.1

#################################################################
######## 2.2 RElbowAngle DTW ##########################
#################################################################
w_data_col2.2 <- list()
for(i in names(table(Seg_data$INDEX))){
  temp <- Seg_data$RElbowAngle.RElbowAngle[Seg_data$INDEX== i]
  w_data_col2.2[[i]] <- as.data.frame(temp)
}

dist.mat2.2 <- dist(x = w_data_col2.2, method = "DTW")
dist.mat2.2
data_x2.2 <- c(1:n)
dtw_matrix2.2 <- data.frame(data_x2.2, (dist.mat2.2[1:n]))
#################################################################
colnames(dtw_matrix2.2) <- c("X","RElbowAngle_DTW")
```

```
dtw_matrix2.2

#############################################################
######## 3.1 LKneeAngle DTW ##########################
#############################################################
w_data_col3.1 <- list()
for(i in names(table(Seg_data$INDEX))){
  temp <- Seg_data$LKneeAngle.LKneeAngle[Seg_data$INDEX== i]
  w_data_col3.1[[i]] <- as.data.frame(temp)
}

dist.mat3.1 <- dist(x = w_data_col3.1, method = "DTW")
dist.mat3.1
data_x3.1 <- c(1:n)
dtw_matrix3.1 <- data.frame(data_x3.1, (dist.mat3.1[1:n]))
#############################################################
colnames(dtw_matrix3.1) <- c("X","LKneeAngle_DTW")
dtw_matrix3.1

#############################################################
######## 3.2 RKneeAngle DTW ##########################
#############################################################
w_data_col3.2 <- list()
for(i in names(table(Seg_data$INDEX))){
  temp <- Seg_data$RKneeAngle.RKneeAngle[Seg_data$INDEX== i]
  w_data_col3.2[[i]] <- as.data.frame(temp)
}

dist.mat3.2 <- dist(x = w_data_col3.2, method = "DTW")
dist.mat3.2
data_x3.2 <- c(1:n)
dtw_matrix3.2 <- data.frame(data_x3.2, (dist.mat3.2[1:n]))
#############################################################
colnames(dtw_matrix3.2) <- c("X","RKneeAngle_DTW")
dtw_matrix3.2

#create a single data frame of raw DTW values for all joint angles for the run 1

raw_dtw_matrix <- data.frame(dtw_matrix1.1$LBackAngle_DTW, dtw_matrix1.2$RBackAngle_DTW,
                             dtw_matrix2.1$LElbowAngle_DTW, dtw_matrix2.2$RElbowAngle_DTW,
                             dtw_matrix3.1$LKneeAngle_DTW, dtw_matrix3.2$RKneeAngle_DTW)
colnames(raw_dtw_matrix) <- c("R1_LBack", "R1_RBack", "R1_LElbow","R1_RElbow", "R1_LKnee", "R1_RKnee")
write.csv(raw_dtw_matrix, "DTW_data.csv")

#  Read in saved file with all DTW values
filename7 <- "C:/DTW_data"
readfile7 <- paste(filename7, ".csv", sep = "")
DTW_data <- read.csv(file=readfile7, header = TRUE, ",")

#defining parameters for EWMA control charts
Segments_Total <- length(which(DTW_data$R1_LBack != 0))
n <- Segments_Total
#calibration data at beginning of RPE 10
n_cali <- 60
#beginning of RPE 15
rpe15_start <- 104
#end of RPE 16
rpe16_end <- 126
#width of coltrol limits = L
sigma <- 3
#weight constant = lambda
lambda_val <- 0.2

############### EWMA_LBack1.1 ####################
ewma_LBack1.1 <-  ewma(DTW_data$R1_LBack[1:n_cali], lambda=lambda_val, nsigmas=sigma,
                       newdata = DTW_data$R1_LBack[61:n])

#using EWMA control chart to extract relevant information
#EWMA points
ewma_values_LBack <- data.frame(ewma_LBack1.1_sd$y)
```

```
#EWMA upper and lower control limits
ewma_limits_LBack <- data.frame(ewma_LBack1.1_sd$limits)
#create data frame
ewma_stats_LBack <- data.frame(1:n, ewma_values_LBack$ewma_LBack1.1_sd.y, ewma_limits_LBack$LCL,
ewma_limits_LBack$UCL)
#change column names
colnames(ewma_stats_LBack)<- c("Segment", "EWMA", "LCL", "UCL")
#creating subsets of points in RPE 15 to RPE 17 range
ewma_stats_15_16_LBack <- subset(ewma_stats_LBack, ewma_stats_LBack$Segment >= rpe15_start &
                          ewma_stats_LBack$Segment <= rpe16_end)
#creating subsets of points in RPE 10 to RPE 15 range
ewma_stats_ncali_15_LBack <- subset(ewma_stats_LBack, ewma_stats_LBack$Segment > n_cali &
                            ewma_stats_LBack$Segment < rpe15_start)
#performance metrics of the control charts
#calculating true positive points
tp_LBack <- nrow(subset(ewma_stats_15_16_LBack, ewma_stats_15_16_LBack$EWMA > ewma_stats_15_16_LBack$UCL))
#calculating false negative points
fn_LBack <- nrow(subset(ewma_stats_15_16_LBack, ewma_stats_15_16_LBack$EWMA <= ewma_stats_15_16_LBack$UCL))
#calculating true negative points
tn_LBack <- nrow(subset(ewma_stats_ncali_15_LBack, ewma_stats_ncali_15_LBack$EWMA <=
ewma_stats_ncali_15_LBack$UCL))
#calculating false positive points
fp_LBack <- nrow(subset(ewma_stats_ncali_15_LBack, ewma_stats_ncali_15_LBack$EWMA >
ewma_stats_ncali_15_LBack$UCL))
#creating a data frame with all necessary metrics for measuring performance
cmat_LBack <- data.frame(tp_LBack, tn_LBack, fp_LBack, fn_LBack)
#plot the control chart with relevant information using plotly library
fig_LBack <- plot_ly(x = ewma_stats_LBack$Segment ,y = ewma_stats_LBack$EWMA,
                type = "scatter", mode = "lines+markers", name="EWMA Left Back", color = I("mediumpurple"), showlegend = T)
fig_LBack <- fig_LBack %>% add_trace(y = ewma_stats_LBack$UCL, name="Upper Control Limit", mode = "lines", color =
I("dodgerblue"))
fig_LBack <- fig_LBack %>% add_trace(y = ewma_stats_LBack$LCL, name="Lower Control Limit", mode = "lines", color =
I("dodgerblue"))
fig_LBack <- fig_LBack %>% add_trace(x = rpe15_start, name="RPE 15", mode = "lines", color = I("orange"))
fig_LBack <- fig_LBack %>% add_trace(x = rpe16_end, name="RPE 17", mode = "lines",color = I("red"))
fig_LBack <- fig_LBack%>% add_trace(x = n_cali, name="Calibration point", mode = "lines",color = I("cyan"))
fig_LBack <- fig_LBack %>% layout(title = "EWMA Plot_LBack", xaxis = list(title = "Segment"),
                           yaxis = list(title = "EWMA point"))
fig_LBack
############### EWMA_RBack1.2 ####################
ewma_RBack1.2_sd <-  ewma(DTW_data$R1_Rback[1:n_cali], lambda=lambda_val, nsigmas=sigma,
                    newdata = DTW_data$R1_Rback[61:n])
ewma_values_RBack <- data.frame(ewma_RBack1.2_sd$y)
ewma_limits_RBack <- data.frame(ewma_RBack1.2_sd$limits)
ewma_stats_RBack <- data.frame(1:n, ewma_values_RBack$ewma_RBack1.2_sd.y, ewma_limits_RBack$LCL,
ewma_limits_RBack$UCL)
colnames(ewma_stats_RBack)<- c("Segment", "EWMA", "LCL", "UCL")
ewma_stats_15_16_RBack <- subset(ewma_stats_RBack, ewma_stats_RBack$Segment >= rpe15_start &
                          ewma_stats_RBack$Segment <= rpe16_end)
ewma_stats_ncali_15_RBack <- subset(ewma_stats_RBack, ewma_stats_RBack$Segment > n_cali &
                            ewma_stats_RBack$Segment < rpe15_start)
tp_RBack <- nrow(subset(ewma_stats_15_16_RBack, ewma_stats_15_16_RBack$EWMA > ewma_stats_15_16_RBack$UCL))

fn_RBack <- nrow(subset(ewma_stats_15_16_RBack, ewma_stats_15_16_RBack$EWMA <= ewma_stats_15_16_RBack$UCL))
tn_RBack <- nrow(subset(ewma_stats_ncali_15_RBack, ewma_stats_ncali_15_RBack$EWMA <=
ewma_stats_ncali_15_RBack$UCL))
fp_RBack <- nrow(subset(ewma_stats_ncali_15_RBack, ewma_stats_ncali_15_RBack$EWMA >
ewma_stats_ncali_15_RBack$UCL))
cmat_RBack <- data.frame(tp_RBack, tn_RBack, fp_RBack, fn_RBack)
fig_RBack <- plot_ly(x = ewma_stats_RBack$Segment ,y = ewma_stats_RBack$EWMA,
                type = "scatter", mode = "lines+markers", name="EWMA Right Back", color = I("mediumpurple"), showlegend = T)
fig_RBack <- fig_RBack %>% add_trace(y = ewma_stats_RBack$UCL, name="Upper Control Limit", mode = "lines", color =
I("dodgerblue"))
fig_RBack <- fig_RBack %>% add_trace(y = ewma_stats_RBack$LCL, name="Lower Control Limit", mode = "lines", color =
I("dodgerblue"))
fig_RBack <- fig_RBack %>% add_trace(x = rpe15_start, name="RPE 15", mode = "lines", color = I("orange"))
fig_RBack <- fig_RBack %>% add_trace(x = rpe16_end, name="RPE 17", mode = "lines",color = I("red"))
fig_RBack <- fig_RBack%>% add_trace(x = n_cali, name="Calibration point", mode = "lines",color = I("cyan"))
fig_RBack <- fig_RBack %>% layout(title = "EWMA Plot_RBack", xaxis = list(title = "Segment"),
                           yaxis = list(title = "EWMA point"))
```

```
fig_RBack
############### EWMA_LElbow2.1 ####################
ewma_LElbow2.1_sd <-  ewma(DTW_data$R1_LElbow[1:n_cali], lambda=lambda_val, nsigmas=sigma,
                    newdata = DTW_data$R1_LElbow[61:n])
ewma_values_LElbow <- data.frame(ewma_LElbow2.1_sd$y)
ewma_limits_LElbow <- data.frame(ewma_LElbow2.1_sd$limits)
ewma_stats_LElbow <- data.frame(1:n, ewma_values_LElbow$ewma_LElbow2.1_sd.y, ewma_limits_LElbow$LCL,
ewma_limits_LElbow$UCL)
colnames(ewma_stats_LElbow)<- c("Segment", "EWMA", "LCL", "UCL")
ewma_stats_15_16_LElbow <- subset(ewma_stats_LElbow, ewma_stats_LElbow$Segment >= rpe15_start &
ewma_stats_LElbow$Segment <= rpe16_end)
ewma_stats_ncali_15_LElbow <- subset(ewma_stats_LElbow, ewma_stats_LElbow$Segment > n_cali &
ewma_stats_LElbow$Segment < rpe15_start)
tp_LElbow <- nrow(subset(ewma_stats_15_16_LElbow, ewma_stats_15_16_LElbow$EWMA > ewma_stats_15_16_LElbow$UCL))
fn_LElbow <- nrow(subset(ewma_stats_15_16_LElbow, ewma_stats_15_16_LElbow$EWMA <=
ewma_stats_15_16_LElbow$UCL))
tn_LElbow <- nrow(subset(ewma_stats_ncali_15_LElbow, ewma_stats_ncali_15_LElbow$EWMA <=
ewma_stats_ncali_15_LElbow$UCL))
fp_LElbow <- nrow(subset(ewma_stats_ncali_15_LElbow, ewma_stats_ncali_15_LElbow$EWMA >
ewma_stats_ncali_15_LElbow$UCL))
cmat_LElbow <- data.frame(tp_LElbow, tn_LElbow, fp_LElbow, fn_LElbow)
fig_LElbow <- plot_ly(x = ewma_stats_LElbow$Segment ,y = ewma_stats_LElbow$EWMA,
                  type = "scatter", mode = "lines+markers", name="EWMA Left Elbow", color = I("mediumpurple"), showlegend = T)
fig_LElbow <- fig_LElbow %>% add_trace(y = ewma_stats_LElbow$UCL, name="Upper Control Limit", mode = "lines", color =
I("dodgerblue"))
fig_LElbow <- fig_LElbow %>% add_trace(y = ewma_stats_LElbow$LCL, name="Lower Control Limit", mode = "lines", color =
I("dodgerblue"))
fig_LElbow <- fig_LElbow %>% add_trace(x = rpe15_start, name="RPE 15", mode = "lines", color = I("orange"))
fig_LElbow <- fig_LElbow %>% add_trace(x = rpe16_end, name="RPE 17", mode = "lines",color = I("red"))
fig_LElbow <- fig_LElbow%>% add_trace(x = n_cali, name="Calibration point", mode = "lines",color = I("cyan"))
fig_LElbow <- fig_LElbow %>% layout(title = "EWMA Plot_LElbow", xaxis = list(title = "Segment"),
                           yaxis = list(title = "EWMA point"))
fig_LElbow
############### EWMA_RElbow2.2 ####################
ewma_RElbow2.2_sd <-  ewma(DTW_data$R1_RElbow[1:n_cali], lambda=lambda_val, nsigmas=sigma,
                    newdata = DTW_data$R1_RElbow[61:n])
ewma_values_RElbow <- data.frame(ewma_RElbow2.2_sd$y)
ewma_limits_RElbow <- data.frame(ewma_RElbow2.2_sd$limits)
ewma_stats_RElbow <- data.frame(1:n, ewma_values_RElbow$ewma_RElbow2.2_sd.y, ewma_limits_RElbow$LCL,
ewma_limits_RElbow$UCL)
colnames(ewma_stats_RElbow)<- c("Segment", "EWMA", "LCL", "UCL")
ewma_stats_15_16_RElbow <- subset(ewma_stats_RElbow, ewma_stats_RElbow$Segment >= rpe15_start &
ewma_stats_RElbow$Segment <= rpe16_end)
ewma_stats_ncali_15_RElbow <- subset(ewma_stats_RElbow, ewma_stats_RElbow$Segment > n_cali &
ewma_stats_RElbow$Segment < rpe15_start)
tp_RElbow <- nrow(subset(ewma_stats_15_16_RElbow, ewma_stats_15_16_RElbow$EWMA > ewma_stats_15_16_RElbow$UCL))
fn_RElbow <- nrow(subset(ewma_stats_15_16_RElbow, ewma_stats_15_16_RElbow$EWMA <=
ewma_stats_15_16_RElbow$UCL))
tn_RElbow <- nrow(subset(ewma_stats_ncali_15_RElbow, ewma_stats_ncali_15_RElbow$EWMA <=
ewma_stats_ncali_15_RElbow$UCL))
fp_RElbow <- nrow(subset(ewma_stats_ncali_15_RElbow, ewma_stats_ncali_15_RElbow$EWMA >
ewma_stats_ncali_15_RElbow$UCL))
cmat_RElbow <- data.frame(tp_RElbow, tn_RElbow, fp_RElbow, fn_RElbow)
fig_RElbow <- plot_ly(x = ewma_stats_RElbow$Segment ,y = ewma_stats_RElbow$EWMA,
                  type = "scatter", mode = "lines+markers", name="EWMA Right Elbow", color = I("mediumpurple"), showlegend = T)
fig_RElbow <- fig_RElbow %>% add_trace(y = ewma_stats_RElbow$UCL, name="Upper Control Limit", mode = "lines", color =
I("dodgerblue"))
fig_RElbow <- fig_RElbow %>% add_trace(y = ewma_stats_RElbow$LCL, name="Lower Control Limit", mode = "lines", color =
I("dodgerblue"))
fig_RElbow <- fig_RElbow %>% add_trace(x = rpe15_start, name="RPE 15", mode = "lines", color = I("orange"))
fig_RElbow <- fig_RElbow %>% add_trace(x = rpe16_end, name="RPE 17", mode = "lines",color = I("red"))
fig_RElbow <- fig_RElbow%>% add_trace(x = n_cali, name="Calibration point", mode = "lines",color = I("cyan"))
fig_RElbow <- fig_RElbow %>% layout(title = "EWMA Plot_RElbow", xaxis = list(title = "Segment"),
                           yaxis = list(title = "EWMA point"))
fig_RElbow
############### EWMA_LKnee3.1 ####################
ewma_LKnee3.1_sd <-  ewma(DTW_data$R1_LKnee[1:n_cali], lambda=lambda_val, nsigmas=sigma,
                    newdata = DTW_data$R1_LKnee[61:n])
ewma_values_LKnee <- data.frame(ewma_LKnee3.1_sd$y)
ewma_limits_LKnee <- data.frame(ewma_LKnee3.1_sd$limits)
```

```
ewma_stats_LKnee <- data.frame(1:n, ewma_values_LKnee$ewma_LKnee3.1_sd.y, ewma_limits_LKnee$LCL,
ewma_limits_LKnee$UCL)
colnames(ewma_stats_LKnee)<- c("Segment", "EWMA", "LCL", "UCL")
ewma_stats_15_16_LKnee <- subset(ewma_stats_LKnee, ewma_stats_LKnee$Segment >= rpe15_start &
ewma_stats_LKnee$Segment <= rpe16_end)
ewma_stats_ncali_15_LKnee <- subset(ewma_stats_LKnee, ewma_stats_LKnee$Segment > n_cali & ewma_stats_LKnee$Segment <
rpe15_start)
tp_LKnee <- nrow(subset(ewma_stats_15_16_LKnee, ewma_stats_15_16_LKnee$EWMA > ewma_stats_15_16_LKnee$UCL))
fn_LKnee <- nrow(subset(ewma_stats_15_16_LKnee, ewma_stats_15_16_LKnee$EWMA <= ewma_stats_15_16_LKnee$UCL))
tn_LKnee <- nrow(subset(ewma_stats_ncali_15_LKnee, ewma_stats_ncali_15_LKnee$EWMA <=
ewma_stats_ncali_15_LKnee$UCL))
fp_LKnee <- nrow(subset(ewma_stats_ncali_15_LKnee, ewma_stats_ncali_15_LKnee$EWMA >
ewma_stats_ncali_15_LKnee$UCL))
cmat_LKnee <- data.frame(tp_LKnee, tn_LKnee, fp_LKnee, fn_LKnee)
fig_LKnee <- plot_ly(x = ewma_stats_LKnee$Segment ,y = ewma_stats_LKnee$EWMA,
                type = "scatter", mode = "lines+markers", name="EWMA Left Knee", color = I("mediumpurple"), showlegend = T)
fig_LKnee <- fig_LKnee %>% add_trace(y = ewma_stats_LKnee$UCL, name="Upper Control Limit", mode = "lines", color =
I("dodgerblue"))
fig_LKnee <- fig_LKnee %>% add_trace(y = ewma_stats_LKnee$LCL, name="Lower Control Limit", mode = "lines", color =
I("dodgerblue"))
fig_LKnee <- fig_LKnee %>% add_trace(x = rpe15_start, name="RPE 15", mode = "lines", color = I("orange"))
fig_LKnee <- fig_LKnee %>% add_trace(x = rpe16_end, name="RPE 17", mode = "lines",color = I("red"))
fig_LKnee <- fig_LKnee%>% add_trace(x = n_cali, name="Calibration point", mode = "lines",color = I("cyan"))
fig_LKnee <- fig_LKnee %>% layout(title = "EWMA Plot_LKnee", xaxis = list(title = "Segment"),
                          yaxis = list(title = "EWMA point"))
fig_LKnee
################ EWMA_RKnee3.2 ####################
ewma_RKnee3.2_sd <-  ewma(DTW_data$R1_RKnee[1:n_cali], lambda=lambda_val, nsigmas=sigma,
                    newdata = DTW_data$R1_RKnee[61:n])
summary(ewma_RKnee3.2_sd)
ewma_values_RKnee <- data.frame(ewma_RKnee3.2_sd$y)
ewma_limits_RKnee <- data.frame(ewma_RKnee3.2_sd$limits)
ewma_stats_RKnee <- data.frame(1:n, ewma_values_RKnee$ewma_RKnee3.2_sd.y, ewma_limits_RKnee$LCL,
ewma_limits_RKnee$UCL)
colnames(ewma_stats_RKnee)<- c("Segment", "EWMA", "LCL", "UCL")
ewma_stats_15_16_RKnee <- subset(ewma_stats_RKnee, ewma_stats_RKnee$Segment >= rpe15_start &
ewma_stats_RKnee$Segment <= rpe16_end)
ewma_stats_ncali_15_RKnee <- subset(ewma_stats_RKnee, ewma_stats_RKnee$Segment > n_cali & ewma_stats_RKnee$Segment
< rpe15_start)
tp_RKnee <- nrow(subset(ewma_stats_15_16_RKnee, ewma_stats_15_16_RKnee$EWMA > ewma_stats_15_16_RKnee$UCL))
fn_RKnee <- nrow(subset(ewma_stats_15_16_RKnee, ewma_stats_15_16_RKnee$EWMA <= ewma_stats_15_16_RKnee$UCL))
tn_RKnee <- nrow(subset(ewma_stats_ncali_15_RKnee, ewma_stats_ncali_15_RKnee$EWMA <=
ewma_stats_ncali_15_RKnee$UCL))
fp_RKnee <- nrow(subset(ewma_stats_ncali_15_RKnee, ewma_stats_ncali_15_RKnee$EWMA >
ewma_stats_ncali_15_RKnee$UCL))
cmat_RKnee <- data.frame(tp_RKnee, tn_RKnee, fp_RKnee, fn_RKnee)
fig_RKnee <- plot_ly(x = ewma_stats_RKnee$Segment ,y = ewma_stats_RKnee$EWMA,
                type = "scatter", mode = "lines+markers", name="EWMA Right Knee", color = I("mediumpurple"), showlegend = T)
fig_RKnee <- fig_RKnee %>% add_trace(y = ewma_stats_RKnee$UCL, name="Upper Control Limit", mode = "lines", color =
I("dodgerblue"))
fig_RKnee <- fig_RKnee %>% add_trace(y = ewma_stats_RKnee$LCL, name="Lower Control Limit", mode = "lines", color =
I("dodgerblue"))
fig_RKnee <- fig_RKnee %>% add_trace(x = rpe15_start, name="RPE 15", mode = "lines", color = I("orange"))
fig_RKnee <- fig_RKnee %>% add_trace(x = rpe16_end, name="RPE 17", mode = "lines",color = I("red"))
fig_RKnee <- fig_RKnee%>% add_trace(x = n_cali, name="Calibration point", mode = "lines",color = I("cyan"))
fig_RKnee <- fig_RKnee %>% layout(title = "EWMA Plot_RKnee", xaxis = list(title = "Segment"),
                          yaxis = list(title = "EWMA point"))
fig_RKnee

#editing the row names of performance metrics
rownames(cmat_LBack) <- c("R1_LBack")
rownames(cmat_RBack) <- c("R1_RBack")
rownames(cmat_LElbow) <- c("R1_LElbow")
rownames(cmat_RElbow) <- c("R1_RElbow")
rownames(cmat_LKnee) <- c("R1_LKnee")
rownames(cmat_RKnee) <- c("R1_RKnee")
#editing the column names of performance metrics
colnames(cmat_LBack) <- c("TP", "TN", "FP", "FN")
colnames(cmat_RBack) <- c("TP", "TN", "FP", "FN")
colnames(cmat_LElbow) <- c("TP", "TN", "FP", "FN")
```

```
colnames(cmat_RElbow) <- c("TP", "TN", "FP", "FN")
colnames(cmat_LKnee) <- c("TP", "TN", "FP", "FN")
colnames(cmat_RKnee) <- c("TP", "TN", "FP", "FN")
#creating single dataframe
cmat_all <- data.frame(rbind(cmat_LBack, cmat_RBack, cmat_LElbow, cmat_RElbow, cmat_LKnee, cmat_RKnee))
#save data frame
write.csv(cmat_all, "R1_EWMA_performance.csv")
#measure parameters for confusion matrix
#creating functions for all four parameters
#precision
m_pr <- function(t) {
  n_p <- cmat_all$TP[t]
  d_p <- cmat_all$TP[t]+cmat_all$FP[t]
  p_r <- n_p / d_p
  return(p_r)
}
#recall / sensitivity
m_re <- function(t) {
  n_r <- cmat_all$TP[t]
  d_r <- cmat_all$TP[t]+cmat_all$FN[t]
  r_r <- n_r / d_r
  return(r_r)
}
#specificity
m_sp <- function(t) {
  n_s <- cmat_all$TN[t]
  d_s <- cmat_all$TN[t]+cmat_all$FP[t]
  s_r <- n_s / d_s
  return(s_r)
}
#accuracy
m_ac <- function(t) {
  n_a <- cmat_all$TP[t]+cmat_all$TN[t]
  d_a <- cmat_all$TP[t]+cmat_all$TN[t]+cmat_all$FP[t]+cmat_all$FN[t]
  a_r <- n_a / d_a
  return(a_r)
}
#calculating precision, sensitivity, specificity and accuracy of all
pr_LBack <- m_pr(1)
re_LBack <- m_re(1)
sp_LBack <- m_sp(1)
ac_LBack <- m_ac(1)
pr_RBack <- m_pr(2)
re_RBack <- m_re(2)
sp_RBack <- m_sp(2)
ac_RBack <- m_ac(2)
pr_LElbow <- m_pr(3)
re_LElbow <- m_re(3)
sp_LElbow <- m_sp(3)
ac_LElbow <- m_ac(3)
pr_RElbow <- m_pr(4)
re_RElbow <- m_re(4)
sp_RElbow <- m_sp(4)
ac_RElbow <- m_ac(4)
pr_LKnee <- m_pr(5)
re_LKnee <- m_re(5)
sp_LKnee <- m_sp(5)
ac_LKnee <- m_ac(5)
pr_RKnee <- m_pr(6)
re_RKnee <- m_re(6)
sp_RKnee <- m_sp(6)
ac_RKnee <- m_ac(6)
R1_precision <- c(pr_LBack, pr_RBack, pr_LElbow, pr_RElbow, pr_LKnee, pr_RKnee)
R1_recall <- c(re_LBack, re_RBack, re_LElbow, re_RElbow, re_LKnee, re_RKnee)
R1_specf <- c(sp_LBack, sp_RBack, sp_LElbow, sp_RElbow, sp_LKnee, sp_RKnee)
R1_accuracy <- c(ac_LBack, ac_RBack, ac_LElbow, ac_RElbow, ac_LKnee, ac_RKnee)
#create a cumulative dataframe for EWMA statistics
EWMA_model_stats <- data.frame(R1_precision, R1_recall, R1_specf, R1_accuracy)
rownames(EWMA_model_stats) <- c("R1_LBack", "R1_RBack",
                                "R1_LElbow", "R1_RElbow",
```

```
                    "R1_LKnee", "R1_RKnee")
#save
write.csv(EWMA_model_stats, "EWMA_model_stats.csv")
```

APPENDIX B

This section presents EWMA control charts for all the experiments. The plots are combined as per body joints i.e. back, elbow and knee. Hence, for each experiment three plots are presented.

Chart 1. EWMA chart for experiment 1 - Back joint.

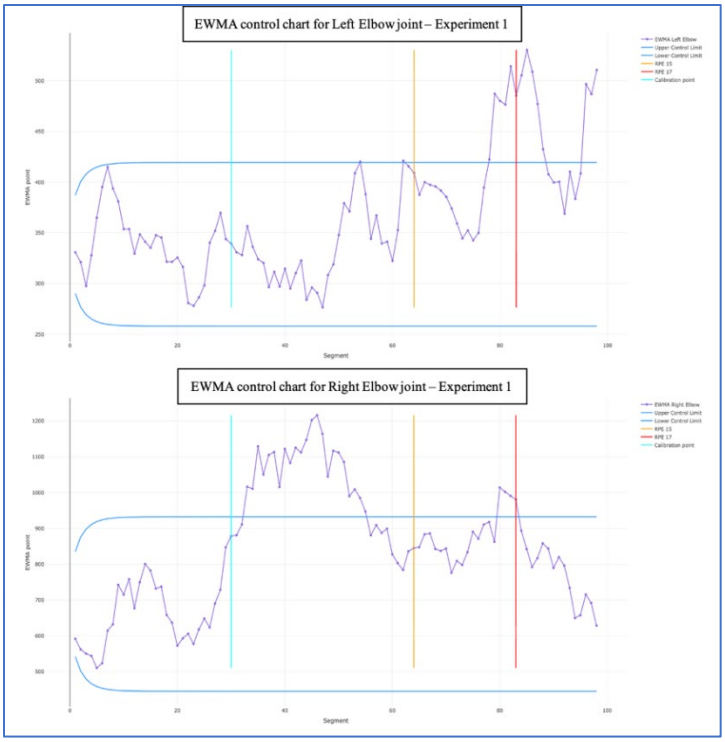

Chart 2. EWMA chart for experiment 1 - Elbow joint.

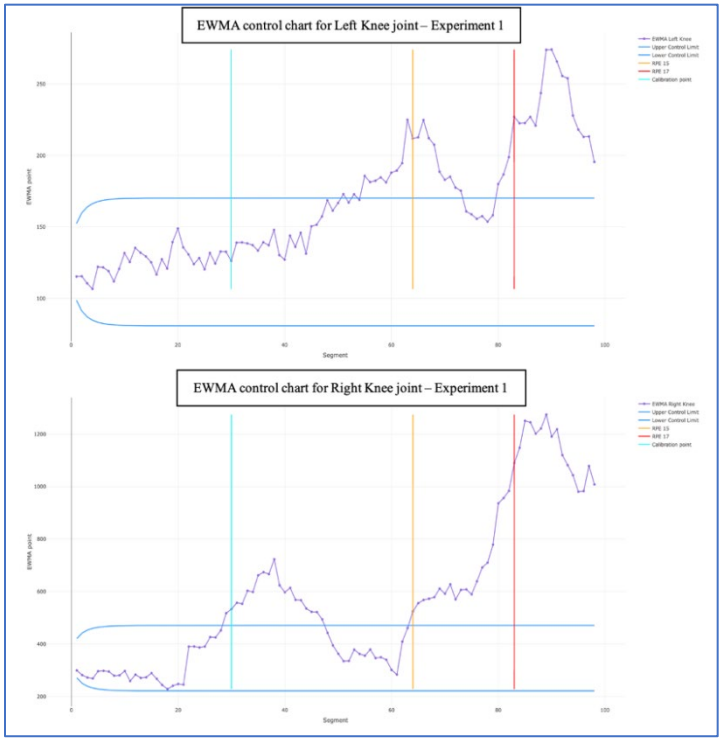

Chart 3. EWMA chart for experiment 1 - Knee joint.

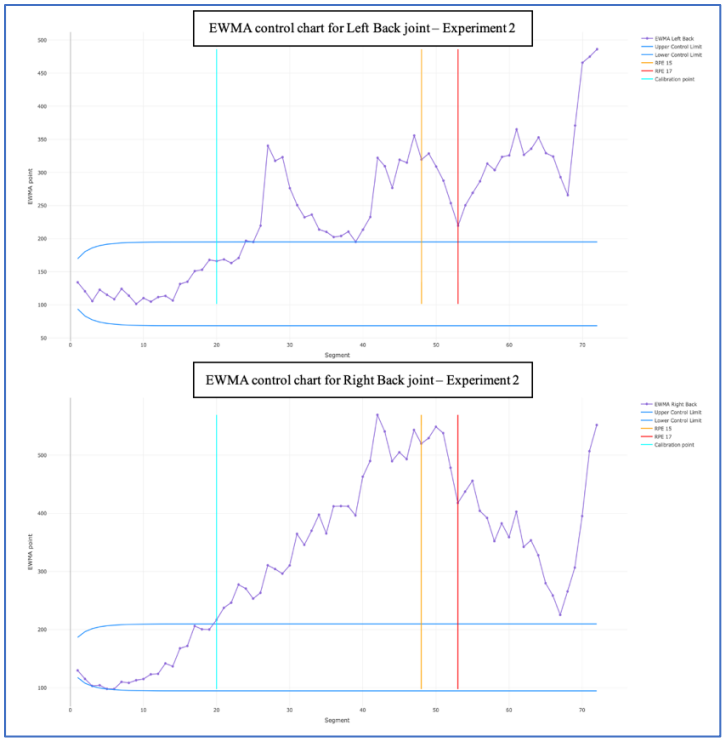

Chart 4. EWMA chart for experiment 2 - Back joint.

Chart 5. EWMA chart for experiment 2 - Elbow joint.

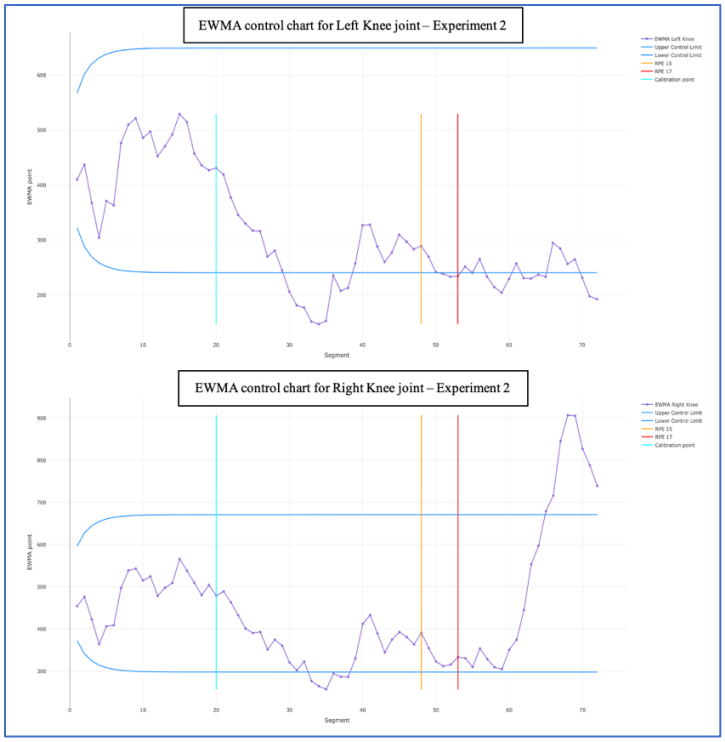

Chart 6. EWMA chart for experiment 2 - Knee joint.

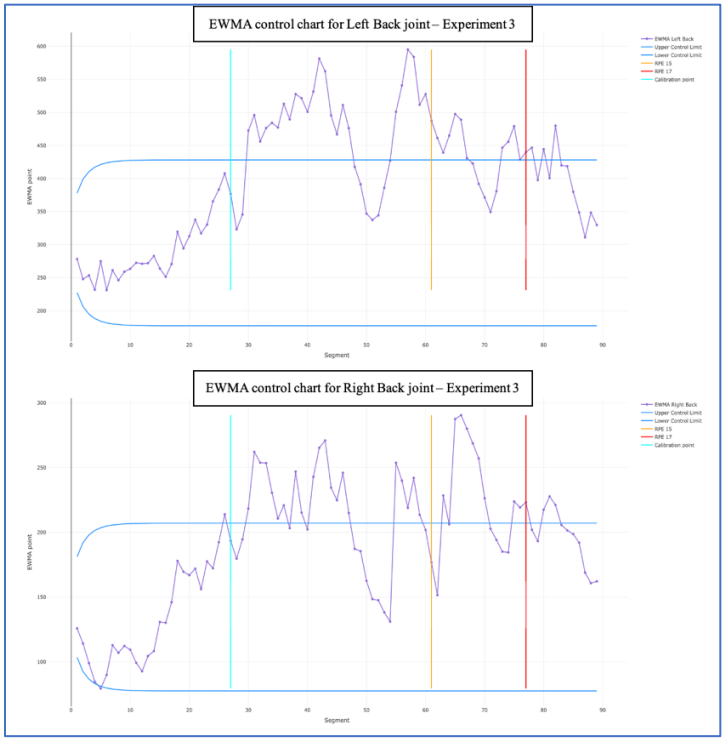

Chart 7. EWMA chart for experiment 3 - Back joint.

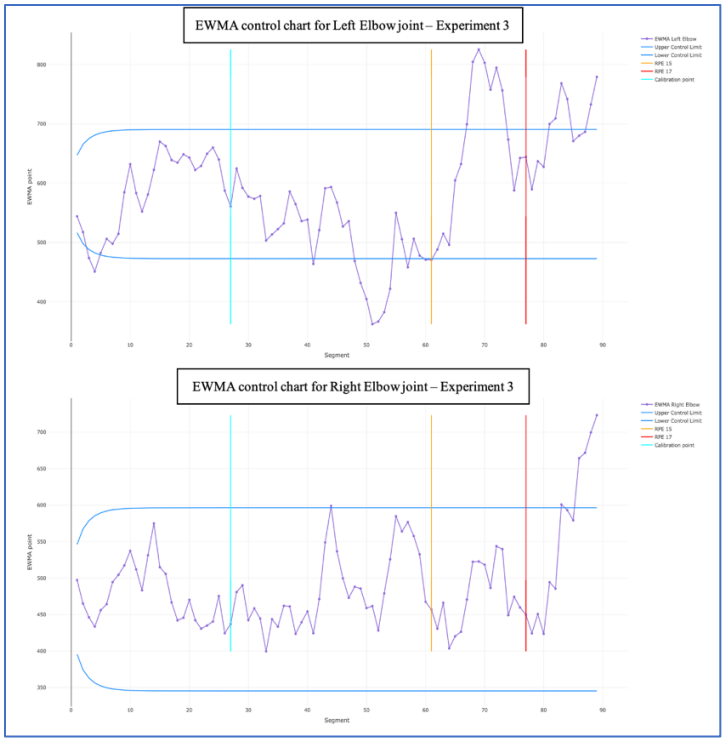

Chart 8. EWMA chart for experiment 3 - Elbow joint.

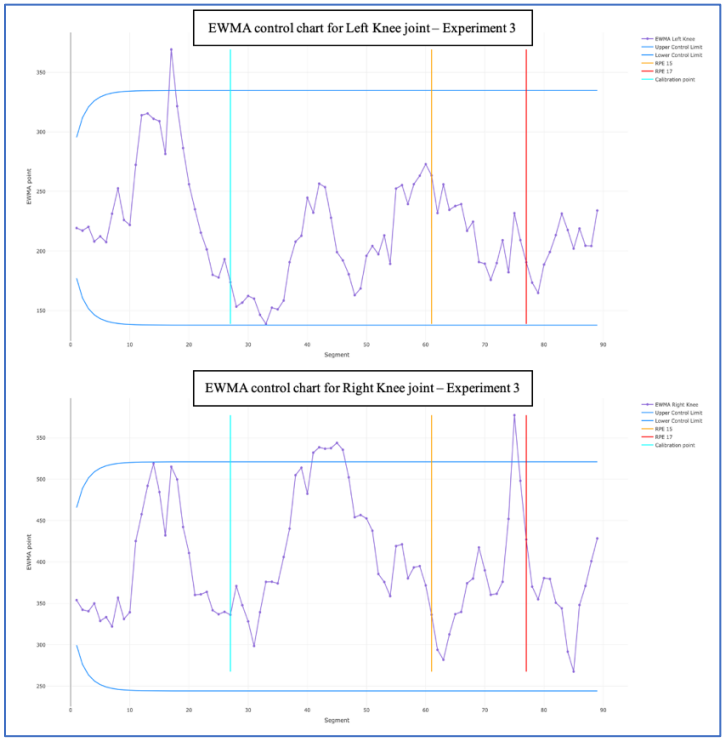

Chart 9. EWMA chart for experiment 3 - Knee joint.

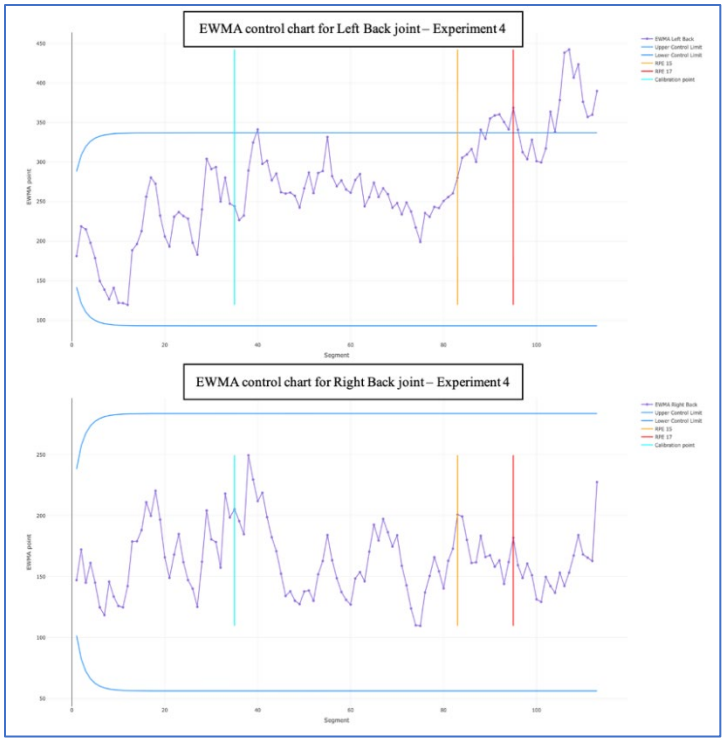

Chart 10. EWMA chart for experiment 4 - Back joint.

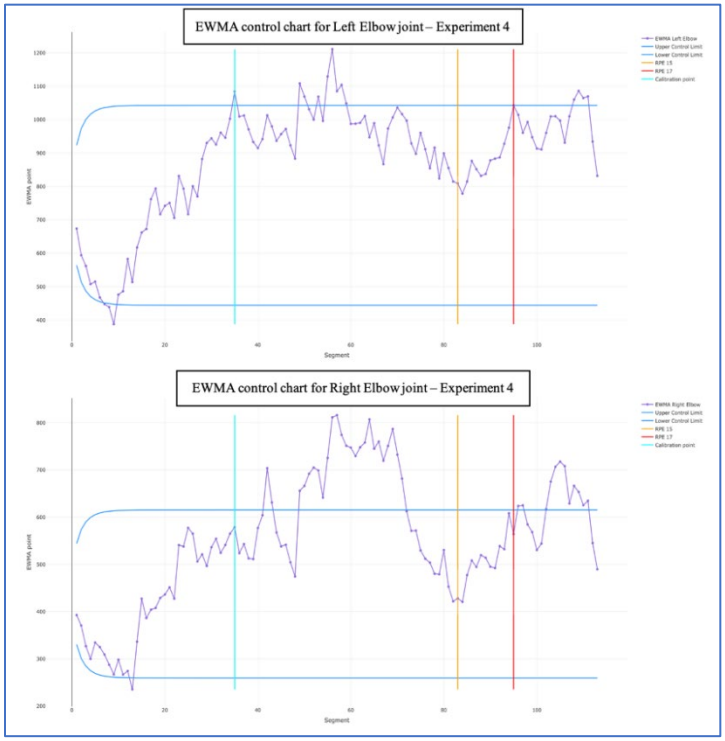

Chart 11. EWMA chart for experiment 4 - Elbow joint.

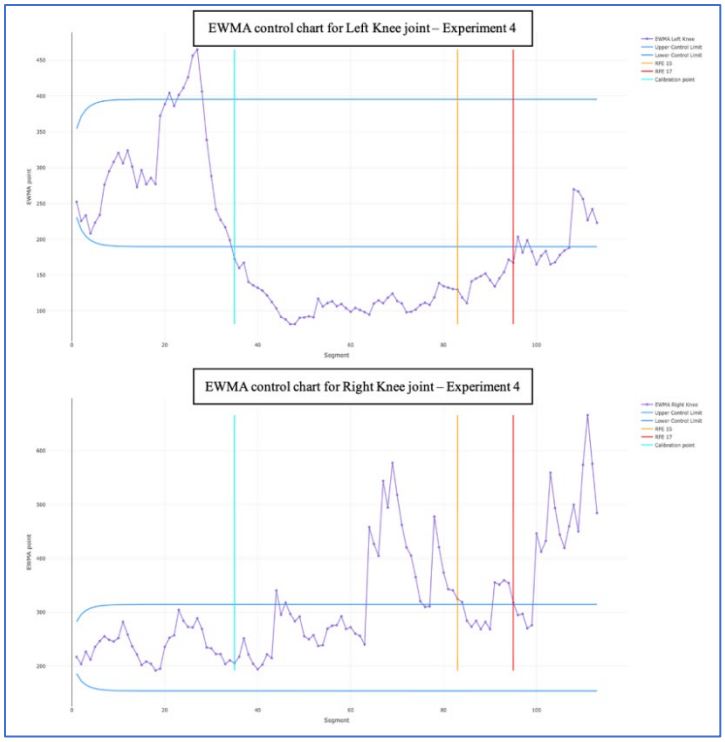

Chart 12. EWMA chart for experiment 4 - Knee joint.

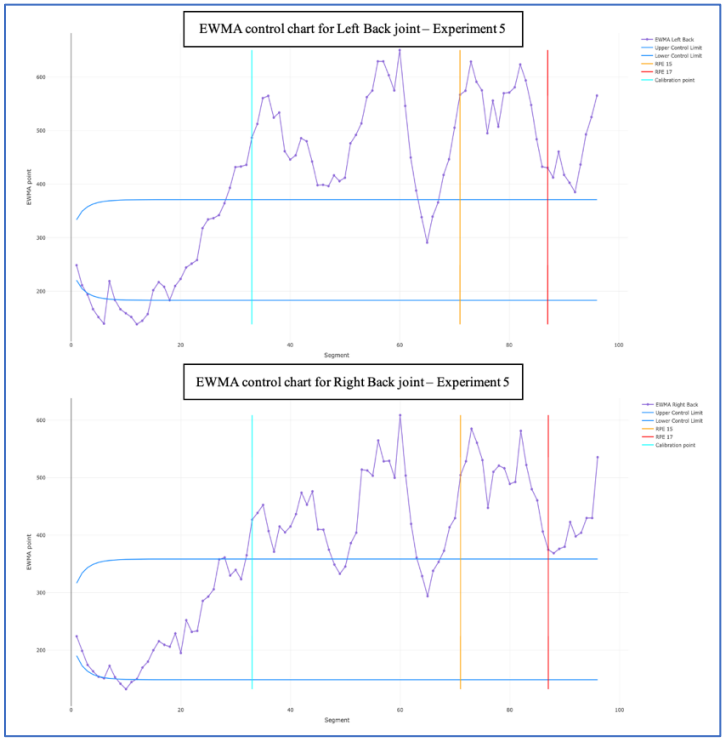

Chart 13. EWMA chart for experiment 5 - Back joint.

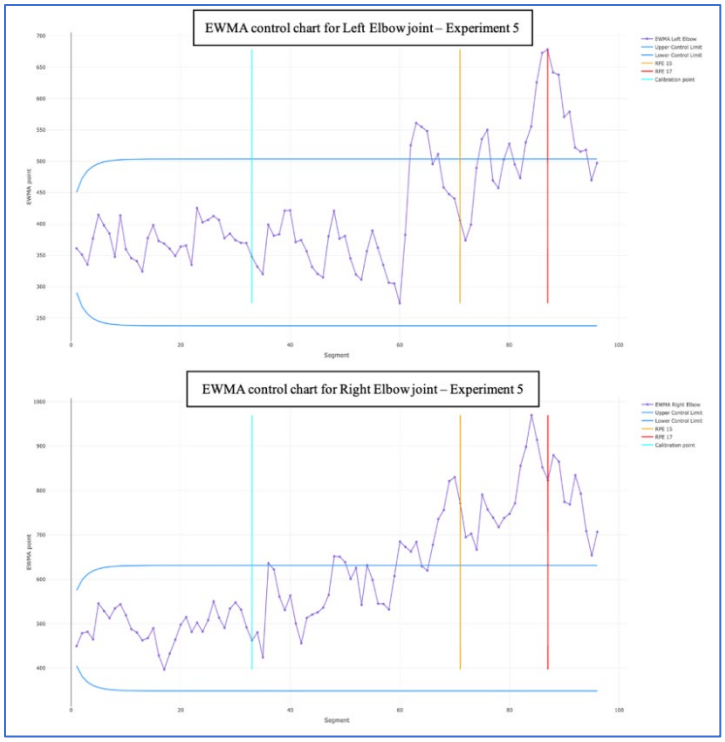

Chart 14. EWMA chart for experiment 5 - Elbow joint.

Chart 15. EWMA chart for experiment 5 - Knee joint.

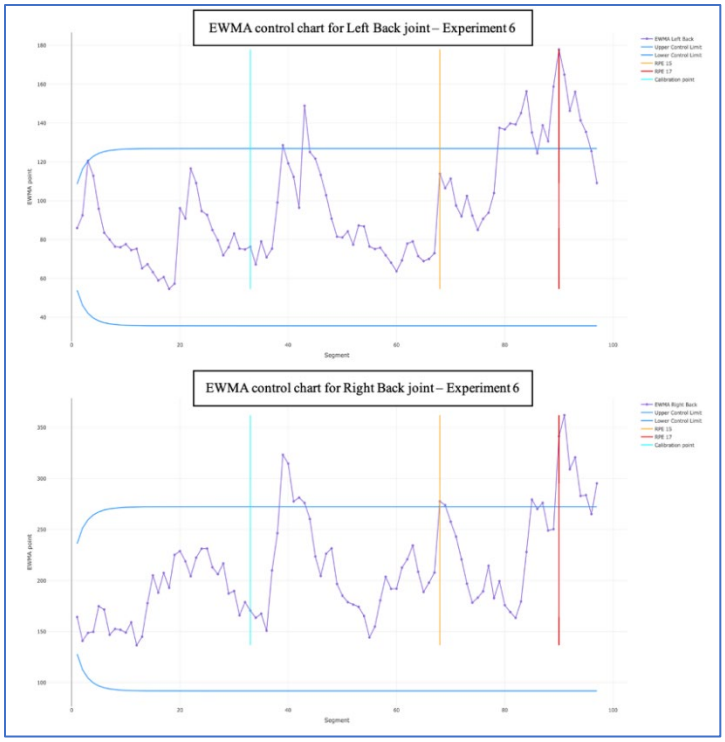

Chart 16. EWMA chart for experiment 6 - Back joint.

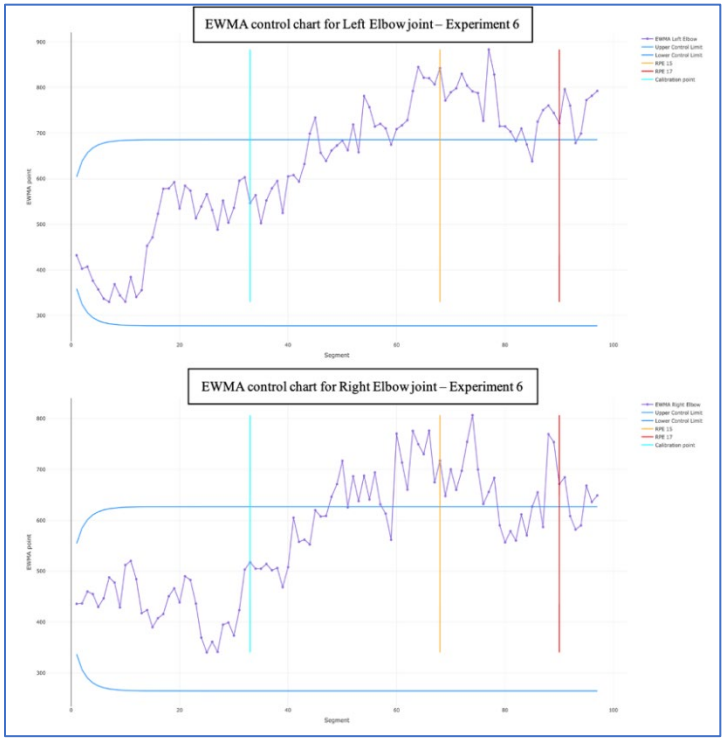

Chart 17. EWMA chart for experiment 6 - Elbow joint.

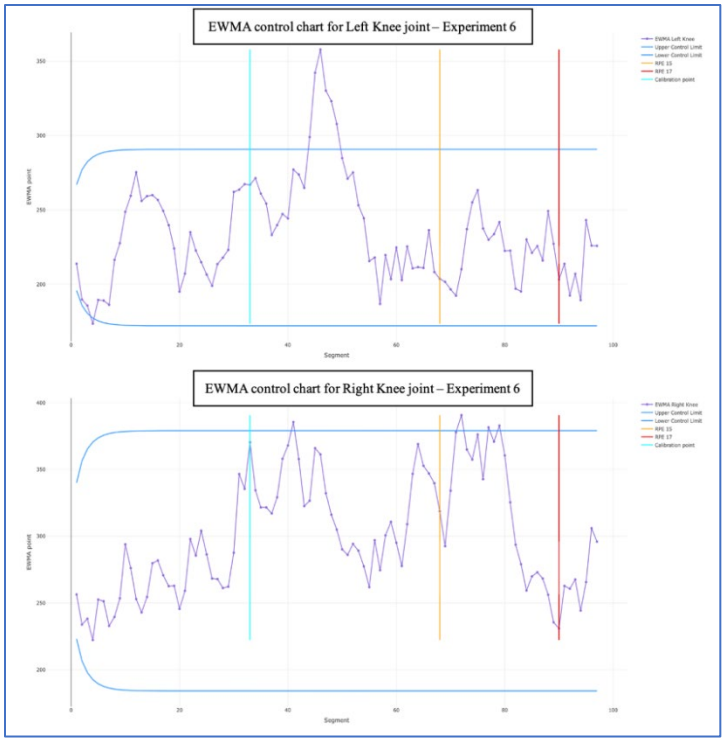

Chart 18. EWMA chart for experiment 6 - Knee joint.

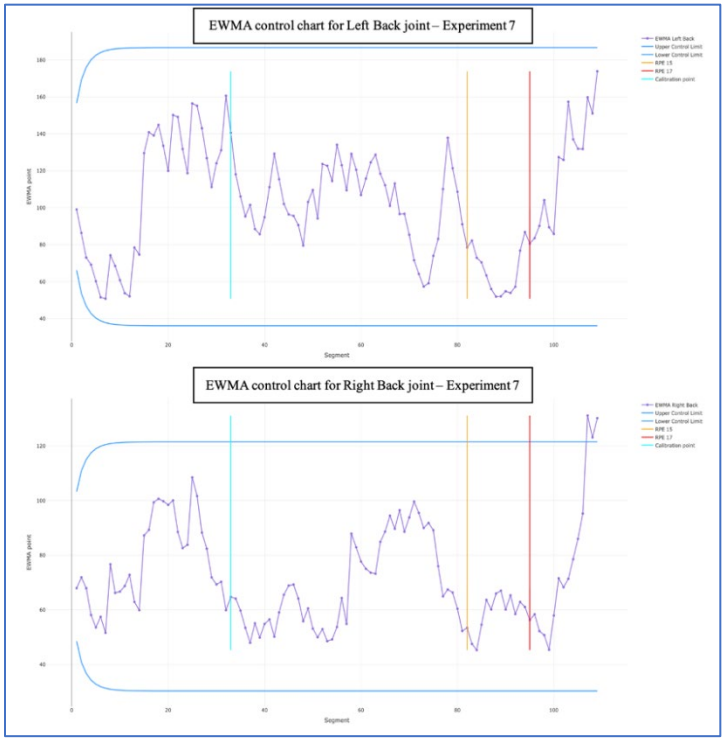

Chart 19. EWMA chart for experiment 7 - Back joint.

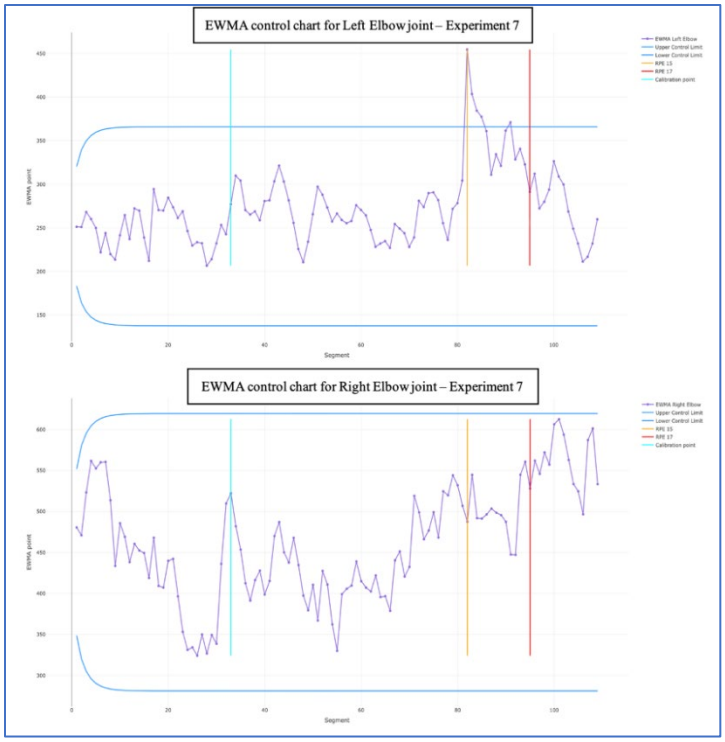

Chart 20. EWMA chart for experiment 7 - Elbow joint.

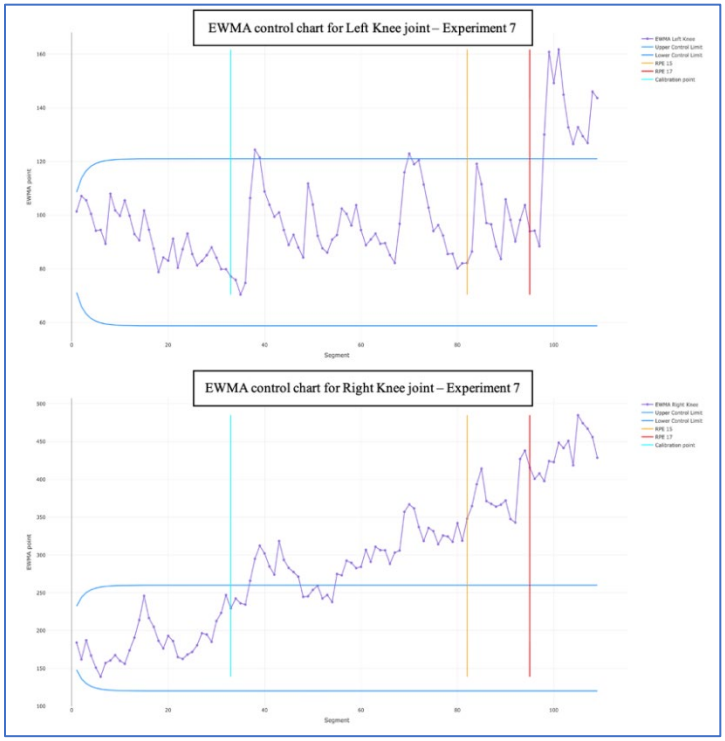

Chart 21. EWMA chart for experiment 7 - Knee joint.

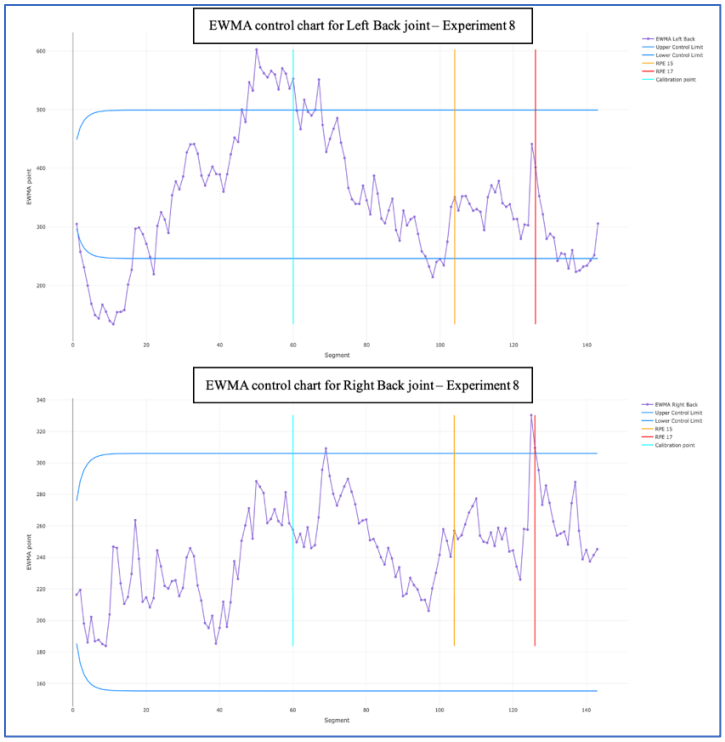

Chart 22. EWMA chart for experiment 8 - Back joint.

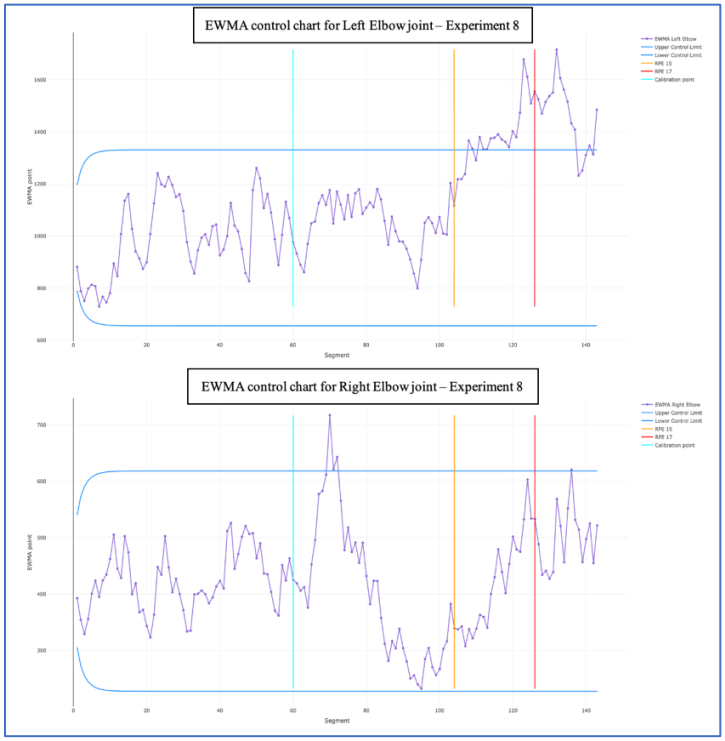

Chart 23. EWMA chart for experiment 8 - Elbow joint.

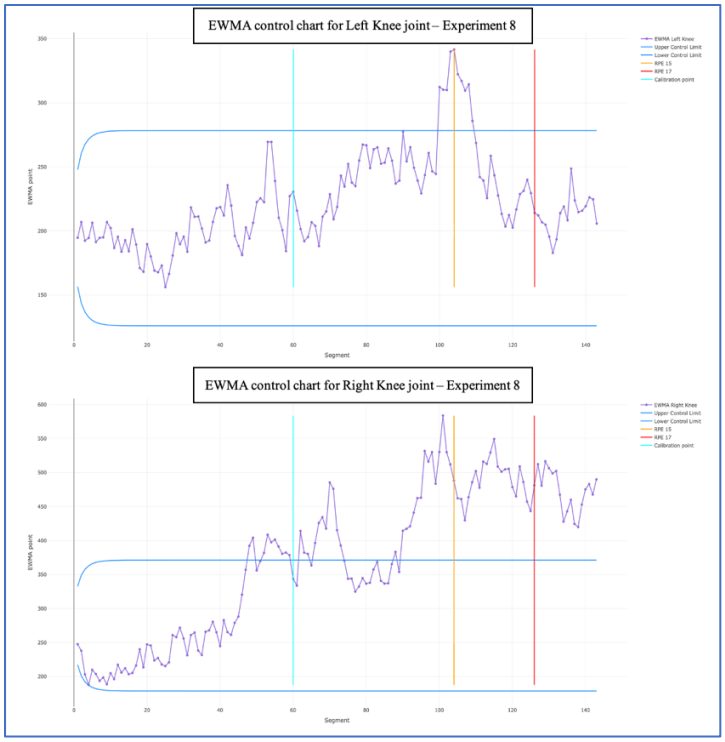

Chart 24. EWMA chart for experiment 8 - Knee joint.

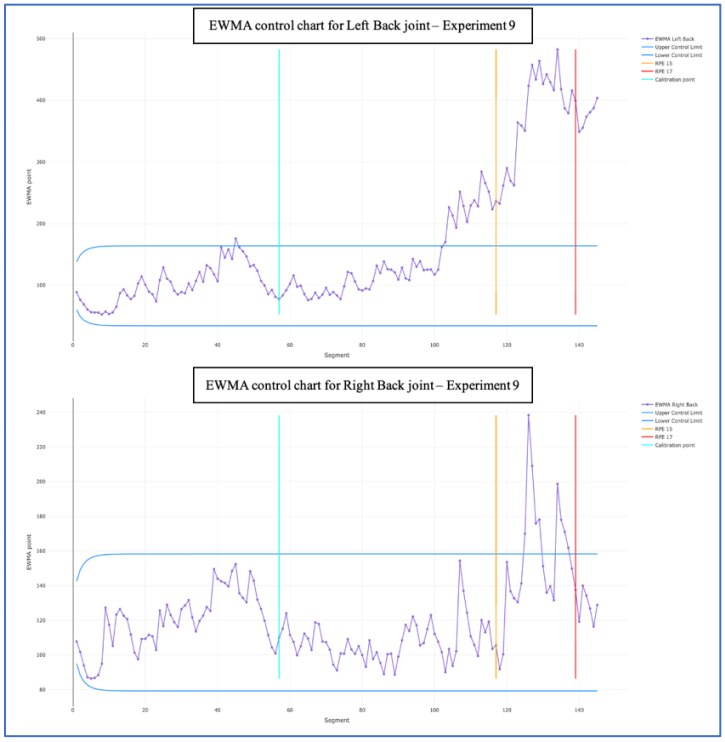

Chart 25. EWMA chart for experiment 9 - Back joint.

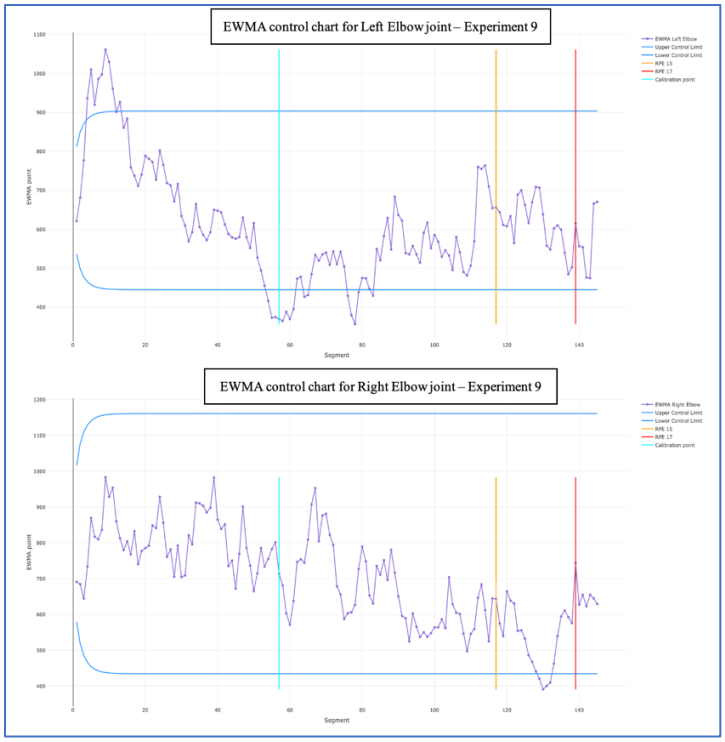

Chart 26. EWMA chart for experiment 9 - Elbow joint.

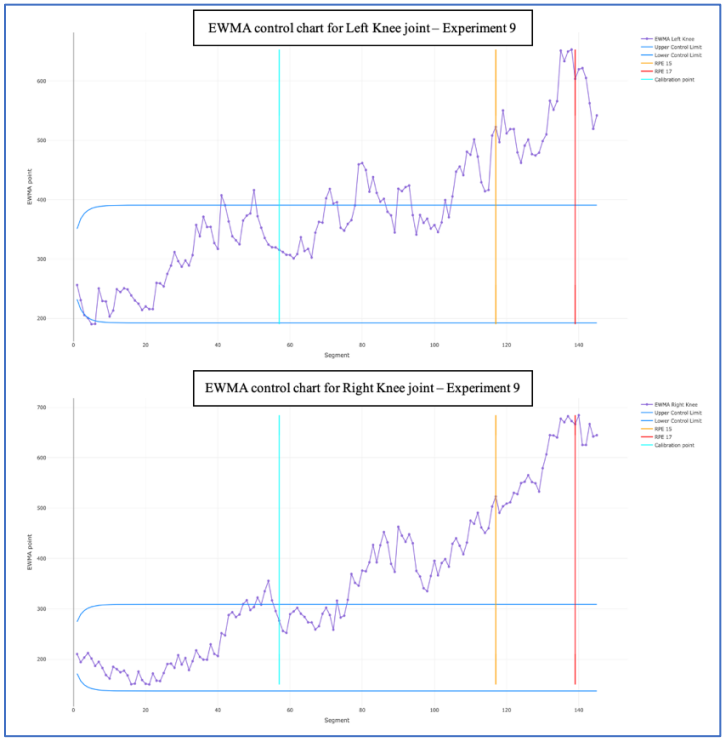

Chart 27. EWMA chart for experiment 9 - Knee joint.

Chart 28. EWMA chart for experiment 10 - Back joint.

Chart 29. EWMA chart for experiment 10 - Elbow joint.

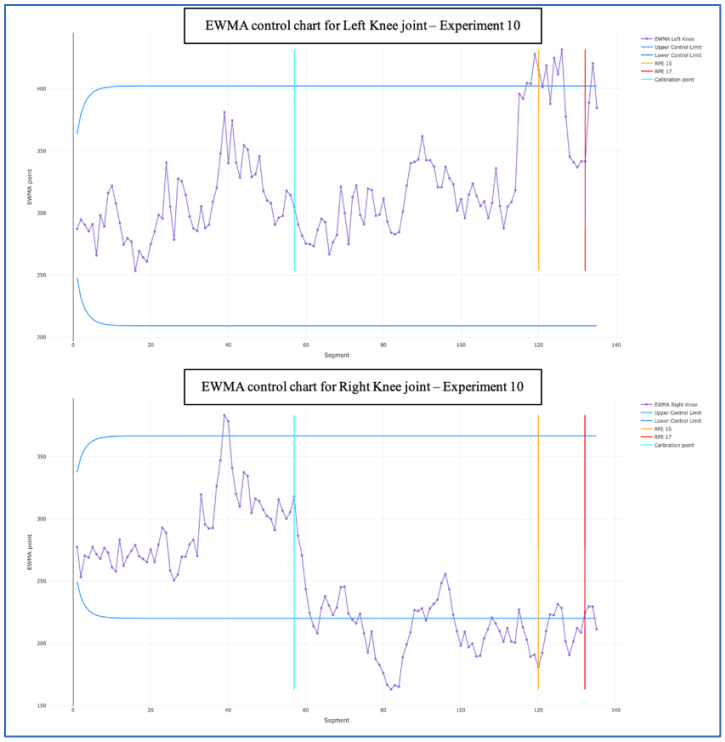

Chart 30. EWMA chart for experiment 10 - Knee joint.

Chart 31. EWMA chart for experiment 11 - Back joint.

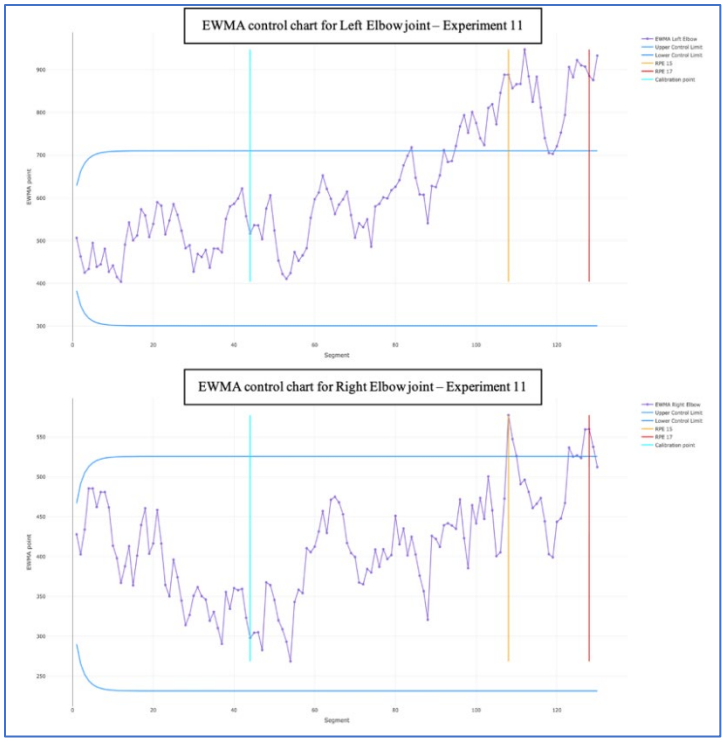

Chart 32. EWMA chart for experiment 11 - Elbow joint.

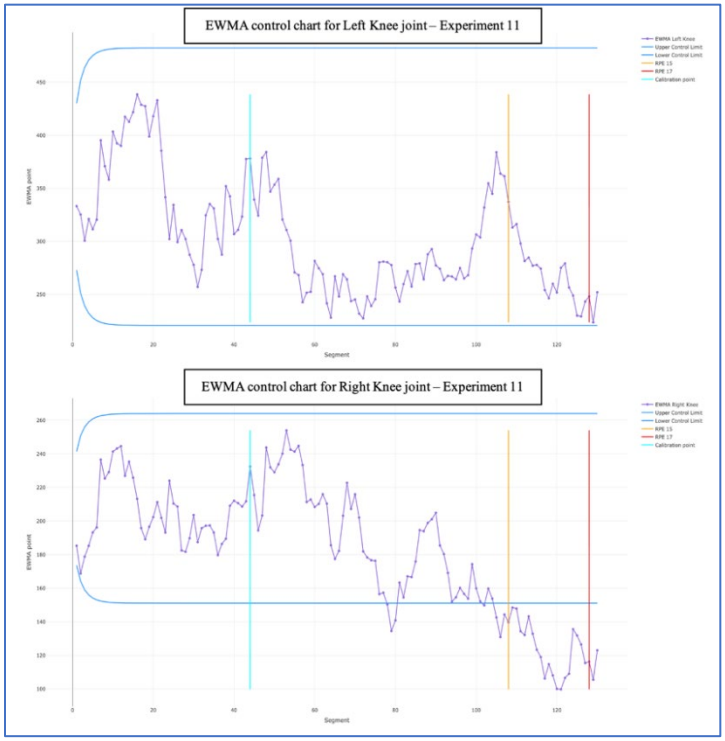

Chart 33. EWMA chart for experiment 11 - Knee joint.

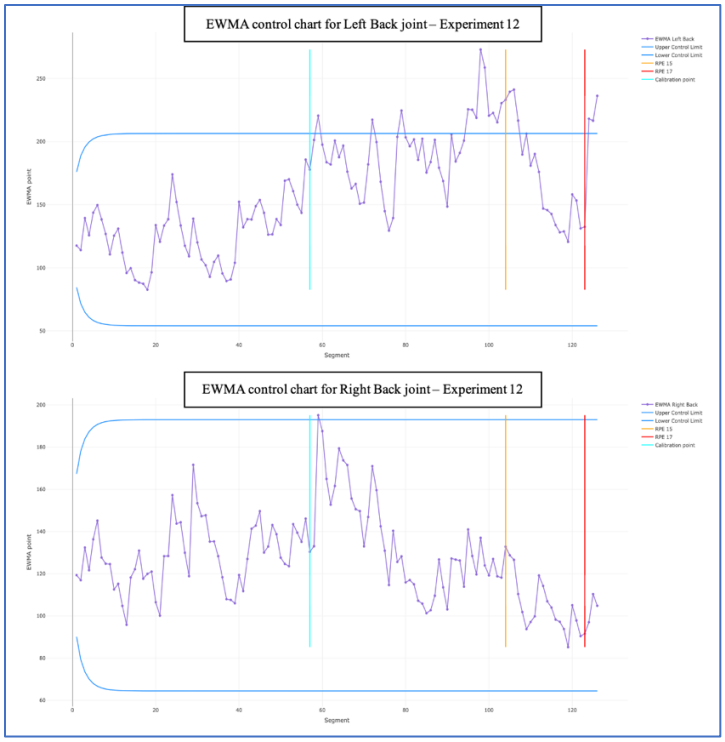

Chart 34. EWMA chart for experiment 12 - Back joint.

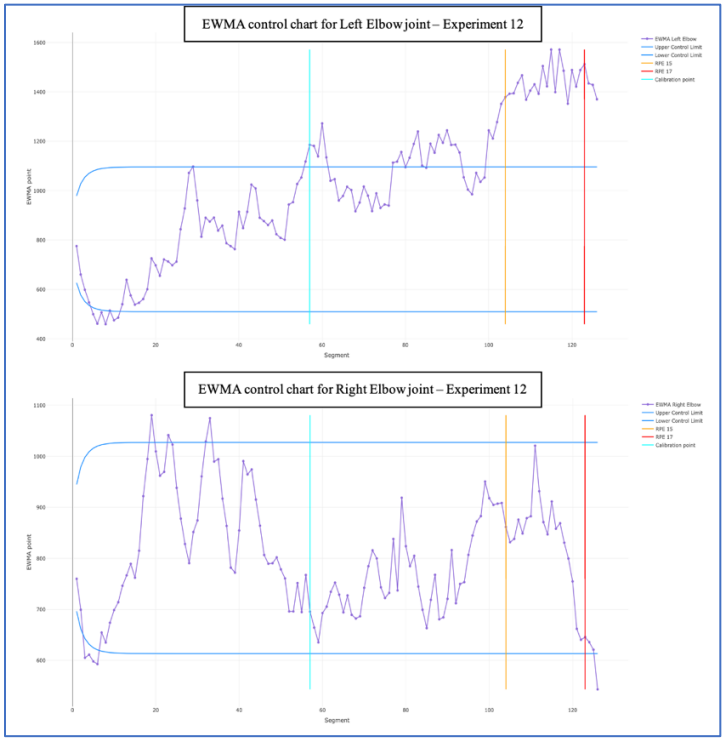

Chart 35. EWMA chart for experiment 12 - Elbow joint.

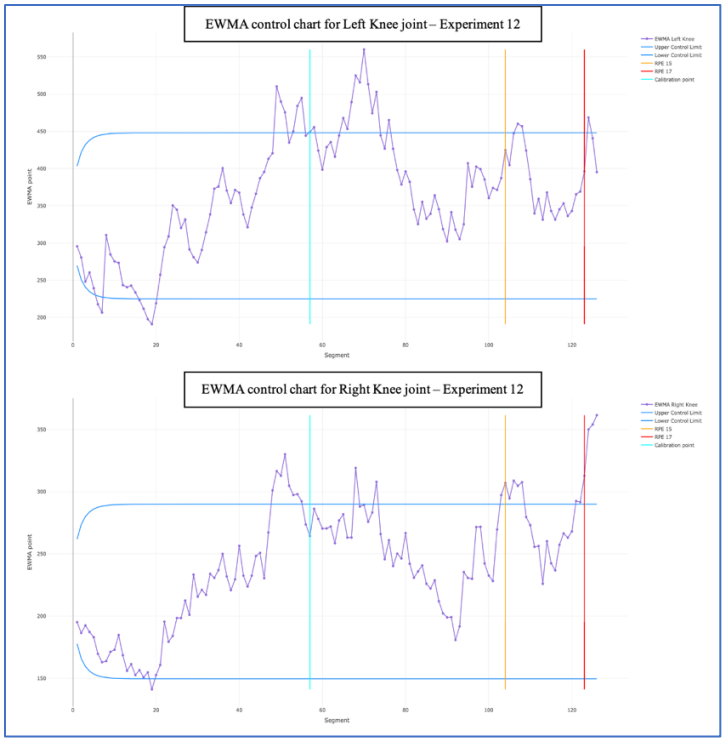

Chart 36. EWMA chart for experiment 12 - Knee joint.

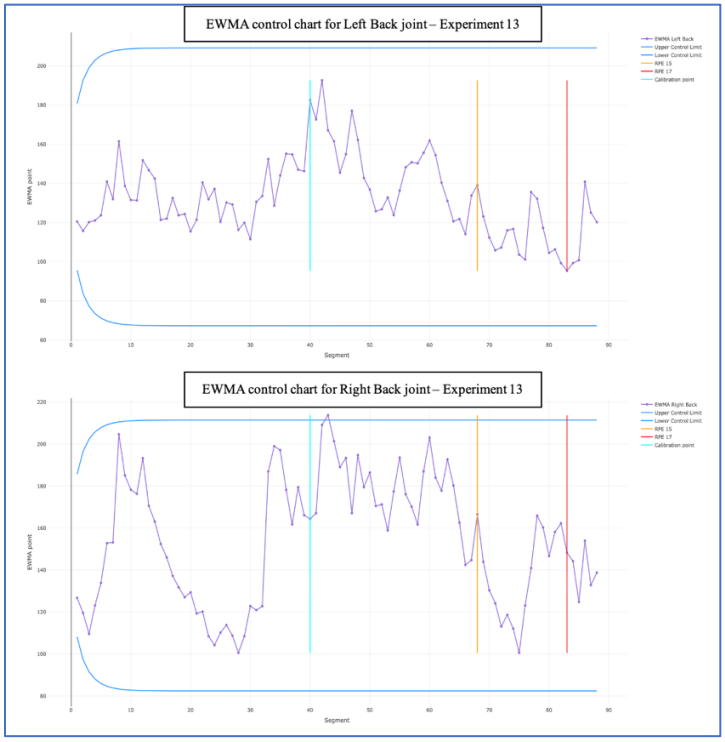

Chart 37. EWMA chart for experiment 13 - Back joint.

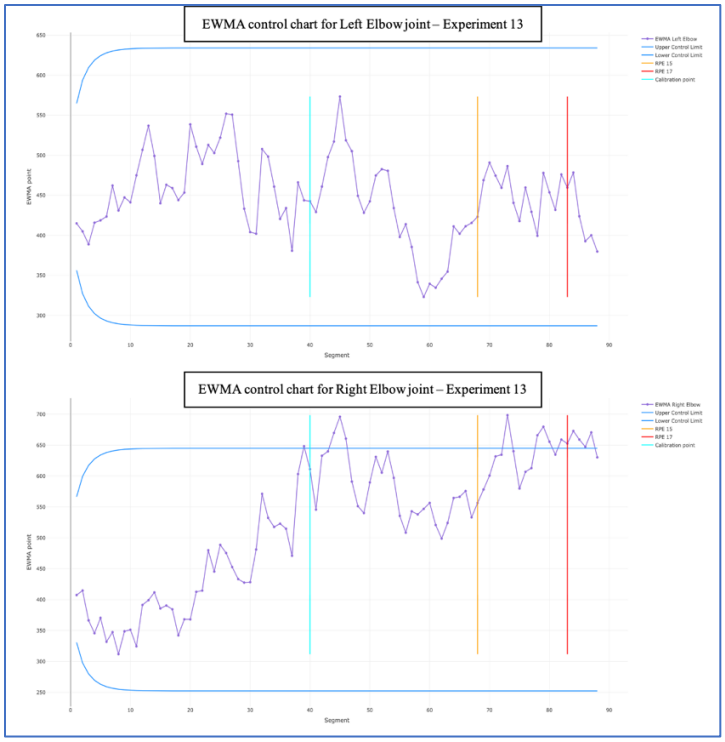

Chart 38. EWMA chart for experiment 13 - Elbow joint.

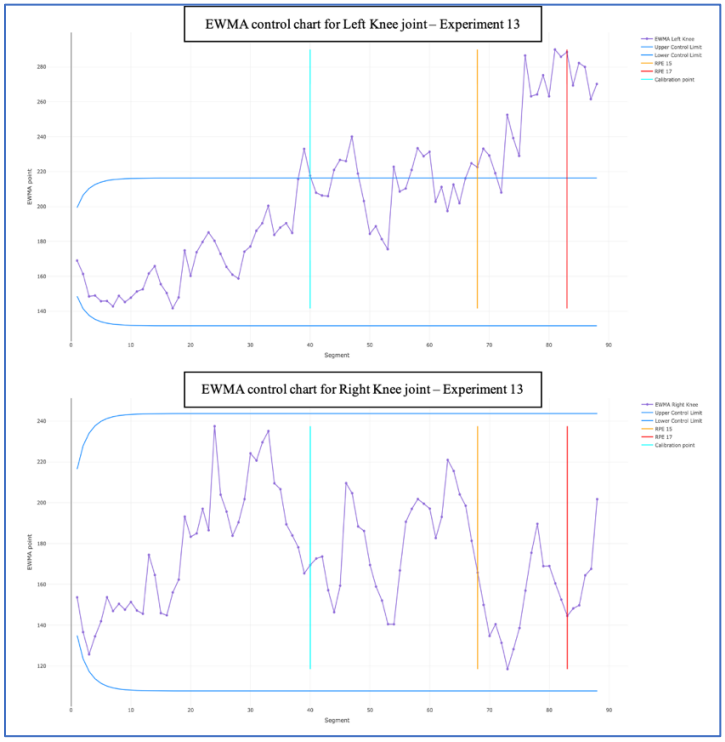

Chart 39. EWMA chart for experiment 13 - Knee joint.

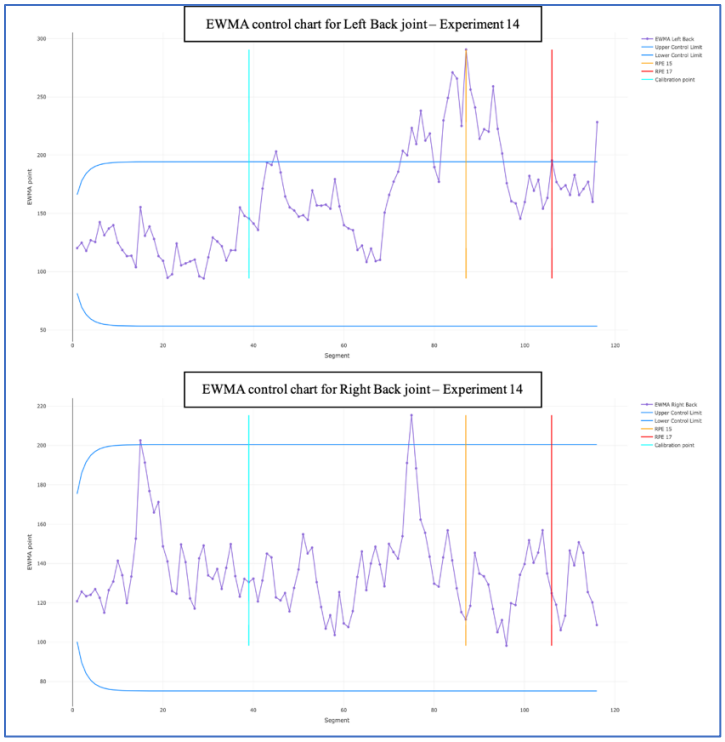

Chart 40. EWMA chart for experiment 14 - Back joint.

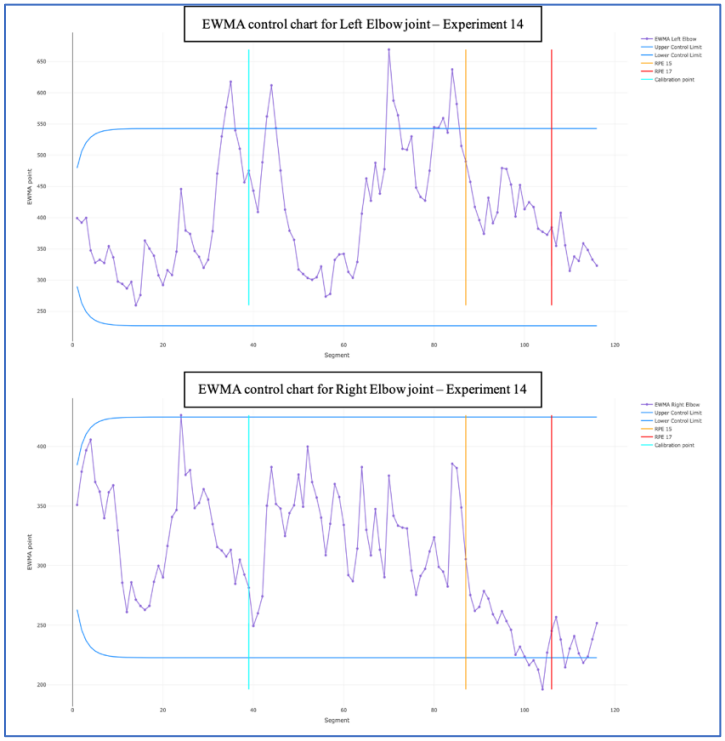

Chart 41. EWMA chart for experiment 14 - Elbow joint.

Chart 42. EWMA chart for experiment 14 - Knee joint.

APPENDIX C

This section presents the hypothesis tests conducted via Minitab Statistical Software® for each body joint.

WORKSHEET 1

Test and CI for Two Proportions: Left Back S1, Left Back S2

Method

Event: 1

p_1: proportion where Left Back S1 = 1

p_2: proportion where Left Back S2 = 1

Difference: $p_1 - p_2$

Descriptive Statistics

Sample	N	Event	Sample p
Left Back S1	7	6	0.857143
Left Back S2	7	5	0.714286

Estimation for Difference

Difference	99.167% CI for Difference
0.142857	(-0.426982, 0.712696)

CI based on normal approximation

Test

Null hypothesis H_0: $p_1 - p_2 = 0$

Alternative hypothesis H_1: $p_1 - p_2 \neq 0$

Method	Z-Value	P-Value
Normal approximation	0.65	0.515
Fisher's exact		1.000

The test based on the normal approximation uses the pooled estimate of the proportion (0.785714).

The normal approximation may be inaccurate for small samples.

Image 1. Minitab results for hypothesis test, j=1.

WORKSHEET 1

Test and CI for Two Proportions: Right Back S1, Right Back S2

Method

Event: 1

p_1: proportion where Right Back S1 = 1

p_2: proportion where Right Back S2 = 1

Difference: $p_1 - p_2$

Descriptive Statistics

Sample	N	Event	Sample p
Right Back S1	7	5	0.714286
Right Back S2	7	3	0.428571

Estimation for Difference

Difference	99.167% CI for Difference
0.285714	(-0.382482, 0.953910)

CI based on normal approximation

Test

Null hypothesis H_0: $p_1 - p_2 = 0$

Alternative hypothesis H_1: $p_1 - p_2 \neq 0$

Method	Z-Value	P-Value
Normal approximation	1.08	0.280
Fisher's exact		0.592

The test based on the normal approximation uses the pooled estimate of the proportion (0.571429).

The normal approximation may be inaccurate for small samples.

Image 2. Minitab results for hypothesis test, j=2.

WORKSHEET 1

Test and CI for Two Proportions: Left Elbow S1, Left Elbow S2

Method

Event: 1

p_1: proportion where Left Elbow S1 = 1

p_2: proportion where Left Elbow S2 = 1

Difference: $p_1 - p_2$

Descriptive Statistics

Sample	N	Event	Sample p
Left Elbow S1	7	7	1.000000
Left Elbow S2	7	3	0.428571

Estimation for Difference

Difference	99.167% CI for Difference
0.571429	(0.077933, 1.000000)

CI based on normal approximation

Test

Null hypothesis H_0: $p_1 - p_2 = 0$

Alternative hypothesis H_1: $p_1 - p_2 \neq 0$

Method	Z-Value	P-Value
Normal approximation	2.37	0.018
Fisher's exact		0.070

The test based on the normal approximation uses the pooled estimate of the proportion (0.714286).

The normal approximation may be inaccurate for small samples.

Image 3. Minitab results for hypothesis test, j=3.

WORKSHEET 1

Test and CI for Two Proportions: Right Elbow S1, Right Elbow S2

Method

Event: 1
p_1: proportion where Right Elbow S1 = 1
p_2: proportion where Right Elbow S2 = 1
Difference: $p_1 - p_2$

Descriptive Statistics

Sample	N	Event	Sample p
Right Elbow S1	7	4	0.571429
Right Elbow S2	7	2	0.285714

Estimation for Difference

Difference	99.167% CI for Difference
0.285714	(-0.382482, 0.953910)

CI based on normal approximation

Test

Null hypothesis H_0: $p_1 - p_2 = 0$
Alternative hypothesis H_1: $p_1 - p_2 \neq 0$

Method	Z-Value	P-Value
Normal approximation	1.08	0.280
Fisher's exact		0.592

The test based on the normal approximation uses the pooled estimate of the proportion (0.428571).
The normal approximation may be inaccurate for small samples.

Image 4. Minitab results for hypothesis test, j=4.

WORKSHEET 1

Test and CI for Two Proportions: Left Knee S1, Left Knee S2

Method

Event: 1
p_1: proportion where Left Knee S1 = 1
p_2: proportion where Left Knee S2 = 1
Difference: $p_1 - p_2$

Descriptive Statistics

Sample	N	Event	Sample p
Left Knee S1	7	1	0.142857
Left Knee S2	7	5	0.714286

Estimation for Difference

Difference	99.167% CI for Difference
-0.571429	(-1.000000, -0.001589)

CI based on normal approximation

Test

Null hypothesis H_0: $p_1 - p_2 = 0$
Alternative hypothesis H_1: $p_1 - p_2 \neq 0$

Method	Z-Value	P-Value
Normal approximation	-2.16	0.031
Fisher's exact		0.103

The test based on the normal approximation uses the pooled estimate of the proportion (0.428571).
The normal approximation may be inaccurate for small samples.

Image 5. Minitab results for hypothesis test, j=5.

WORKSHEET 1

Test and CI for Two Proportions: Right Knee S1, Right Knee S2

Method

Event: 1

p_1: proportion where Right Knee S1 = 1

p_2: proportion where Right Knee S2 = 1

Difference: $p_1 - p_2$

Descriptive Statistics

Sample	N	Event	Sample p
Right Knee S1	7	6	0.857143
Right Knee S2	7	3	0.428571

Estimation for Difference

Difference	99.167% CI for Difference
0.428571	(-0.175834, 1.000000)

CI based on normal approximation

Test

Null hypothesis $H_0: p_1 - p_2 = 0$

Alternative hypothesis $H_1: p_1 - p_2 \neq 0$

Method	Z-Value	P-Value
Normal approximation	1.67	0.094
Fisher's exact		0.266

The test based on the normal approximation uses the pooled estimate of the proportion (0.642857).

The normal approximation may be inaccurate for small samples.

Image 6. Minitab results for hypothesis test, j=6.

REFERENCES

[1] E. Howard, "The Evolution of the Industrial Ages: Industry 1.0 to 4.0," Simio LLC, 5 September 2018. [Online]. Available: https://www.simio.com/blog/2018/09/05/evolution-industrial-ages-industry-1-0-4-0/.

[2] H. Editors, "Ford's assembly line starts rolling," A&E Television Networks, 13 November 2009. [Online]. Available: https://www.history.com/this-day-in-history/fords-assembly-line-starts-rolling.

[3] D. A. Hounshell, "The Same Old Principles in the New Manufacturing," Harvard Business Review, November 1988. [Online]. Available: https://hbr.org/1988/11/the-same-old-principles-in-the-new-manufacturing.

[4] U. Karmarkar, "Getting Control of Just-in-Time," Harvard Business Review, September-October 1989. [Online]. Available: https://hbr.org/1989/09/getting-control-of-just-in-time.

[5] K. Schwab, "The Fourth Industrial Revolution: what it means, how to respond," World Economic Forum, 14 January 2016. [Online]. Available: https://www.weforum.org/agenda/2016/01/the-fourth-industrial-revolution-what-it-means-and-how-to-respond/.

[6] "What is Industry 4.0?," inray Industriesoftware GmbH, [Online]. Available: https://www.opc-router.com/what-is-industry-4-0/.

[7] M. Mikell and J. Clark, "Cheat sheet: What is Digital Twin?," 4 January 2018. [Online]. Available: https://www.ibm.com/blogs/internet-of-things/iot-cheat-sheet-digital-twin/.

[8] B. Schleich, N. Anwer, L. Mathieu and S. Wartzack, "Shaping the digital twin for design and production engineering," CIRP Annals - Manufacturing Technology, vol. 66, pp. 141-144, 2017.

[9] D. Gorecky, M. Schmitt, M. Loskyll and D. Zühlke, "Human-Machine-Interaction in the Industry 4.0 Era," in 12th IEEE International Conference on Industrial Informatics (INDIN), 2014.

[10] L. Lu, F. M. Megahed, R. F. Sesek and L. A. Cavuoto, "A survey of the prevalence of fatigue, its precursors and individual coping mechanisms among U.S. manufacturing workers," Applied Ergonomics, vol. 65, pp. 139-151, 2017.

[11] D. Romero, P. Bernus, O. Noran, J. Stahre and Å. Fast-Berglund, "The Operator 4.0: Human Cyber-Physical Systems & Adaptive Automation Towards Human-Automation Symbiosis Work Systems," in IFIP International Conference on Advances in Production Management Systems, 2016.

[12] V. Visentin, F. Sgarbossa, M. Calzavara and A. Persona, "Fatigue accumulation in the assignment of manual material handling activities to operators," IFAC-PapersOnLine, vol. 51, no. 11, pp. 826-831, 2018.

[13] "Data USA: Warehousing & storage," 2018. [Online]. Available: https://datausa.io/profile/naics/warehousing-storage.

[14] H. Reeve, S. Stephens, S. Pegula and R. Farrell, "25 Years Of Worker Injury, Illness, And Fatality Case Data," U.S. Bureau of Labor Statistics, 2019.

[15] M. Boocock, Y. Naude, S. Taylor, J. Kilby and G. Mawston, "Influencing lumbar posture through real-time biofeedback and its effects on the kinematics and kinetics of a repetitive lifting task," Gait & Posture , pp. 93-100, 2019.

[16] F. Mendez, D. Wierschem and J. Jimenez, "A Motion Capture System Framework for the Study of Human Manufacturing Repetitive Motions," in 15th IMHRC Proceedings , Savannah, Georgia. USA, 2018.

[17] A. Sharotry, J. Jimenez, D. Wierschem, F. Mendez, G. Koutitas, D. Valles, S. Aslan and K. RM, "A Digital Twin Framework of a Material Handling Operator in Industry 4.0 Environments," in 8th International Conference on Information Systems, Logistics and Supply Chain, Austin, 2020.

[18] A. Sharotry, J. A. Jimenez, D. Wierschem, F. A. M. Mediavilla, R. M. Koldenhoven, D. Valles, G. Koutitas and S. Aslan, "A Digital Twin Framework for Real-time Analysis and Feedback of Repetitive Work in the Manual Material Handling Industry," in Proceedings of the 2020 Winter Simulation Conference.

[19] V. S. Christopher, "Analysis of Repetitive Motion in Manual Material Handling Systems Using a Digital Twin Framework," December 2019. [Online]. Available: https://digital.library.txstate.edu/handle/10877/8979.

[20] M. Sudarsan, "Using Wearable Sensors to Evaluate Material Handling Operator's Fatigue in Repetitive Activities: A Design of Experiments Approach," July 2020. [Online]. Available: https://digital.library.txstate.edu/handle/10877/12265.

[21] Qualisys, "Qualisys Track Manager (QTM)," Qualisys AB, [Online]. Available: https://www.qualisys.com/software/qualisys-track-manager/.

[22] R. Team, "RStudio: Integrated Development Environment for R," RStudio, PBC, Boston, MA , 2020. [Online]. Available: http://www.rstudio.com/.

[23] G. Borg, "Psychophysical bases of perceived exertion.," Medicine and Science in Sports and Exercise, pp. 377-381, 1982.

[24] ABB, "Digital twins and simulations," ABB Review, 2019.

[25] A. Maloney, "The difference between a simulation and a digital twin," 23 October 2019. [Online]. Available: https://blogs.sw.siemens.com/mindsphere/the-difference-between-a-simulation-and-a-digital-twin/.

[26] E. Howard, "Digital Twin Technology: 5 Challenges Businesses Face by Overlooking It," Simio LLC, 13 September 2019. [Online]. Available: https://www.simio.com/blog/2019/09/13/digital-twin-technology-5-challenges-businesses-face-by-overlooking-it/.

[27] D. Woods, "Why Digital Twins Should be the CEO's Best Friend," 18 July 2018. [Online]. Available: https://www.forbes.com/sites/danwoods/2018/07/18/why-digital-twins-should-be-the-ceos-best-friend/.

[28] J. A. Jimenez, "HIGHER EDUCATION: Digital Twins," MHI Solutions, 2020.

[29] "DHL Press releases," DHL , July 2019. [Online]. Available: https://www.dpdhl.com/en/media-relations/press-releases/2019/dhl-supply-chain-partners-tetra-pak-implement-first-digital-twin-warehouse-asia-pacific.html.

[30] Grand View Research, "Global Digital Twin Market Size, Share & Trends Analysis Report by End Use , by Region and Segment Forecasts, 2018-2025," Grand View Research, 2018.

[31] J. Smith, "The Wall Street Journal," 15 July 2019. [Online]. Available: https://www.wsj.com/articles/unilever-uses-virtual-factories-to-tune-up-its-supply-chain-11563206402.

[32] T. Borangiu, D. Trentesaux, A. Thomas, P. Leitao and J. Barata, "Digital transformation of manufacturing through cloud services and resource virtualization," Computers in Industry, vol. 108, pp. 150-162, 2019.

[33] "Workplace Safety & Prevention Services," 2011. [Online]. Available: https://www.wsps.ca/Home.aspx.

[34] Y. Yu, H. Li, X. Yang, L. Kong, X. Luo and A. Y.L. Wong, "An automatic and non-invasive physical fatigue assessment method for construction workers," Automation in Construction , pp. 1-12, 2019.

[35] L. McAtamney and E. Corlett, "RULA: a survey method for the investigation of work-related upper limb disorders," Applied Ergonomics, vol. 24, no. 2, pp. 91-99, 1993.

[36] J. S. Moore and A. Garg, "The Strain Index: A Proposed Method to Analyze Jobs For Risk of Distal Upper Extremity Disorders," American Industrial Hygiene Association Journal, vol. 56, no. 5, pp. 443-458, 1995.

[37] S. Hignett and L. McAtamney, "Rapid Entire Body Assessment (REBA)," Applied Ergonomics, vol. 31, no. 2, pp. 201-205, 2000.

[38] G. B. Scott and N. R. Lambe, "Working practices in a perchery system, using the OVAKO Working posture Analysing System (OWAS)," Applied Ergonomics, pp. 281-284, 1996.

[39] W. TR, P.-A. V, G. A and F. LJ, "Revised NIOSH equation for the design and evaluation of manual lifting tasks," Ergonomics, vol. 36, no. 7, pp. 749-776, 1993.

[40] S. H. Snook, "The design of manual handling tasks," Ergonomics, vol. 21, no. 12, pp. 963-985, 1978.

[41] M. A. Greig, J. Village, F. A. Salustri, S. Zolfaghari and W. P. Neumann, "A tool to predict physical workload and task times from workstation layout design data," International Journal of Production Research, vol. 56, no. 16, pp. 5306-5323, 2018.

[42] N. Vignais, M. Miezal, G. Bleser, K. Mura and D. Gorecky, "Innovative system for real-time ergonomic feedback in industrial manufacturing," Applied Ergonomics, pp. 566-574, 2013.

[43] J. Alderson and W. Johnson, "The personalised 'Digital Athlete': An evolving vision for the capture, modellingand simulation of on-field athletic performance.," in Proceedings of the 34th International Conference of Biomechanics in Sport, Tsukuba, 2016.

[44] G. Hernandez, D. Valles, D. C. Wierschem, R. M. Koldenoven, G. Koutitas, F. A. Mendez, S. Aslan and J. Jimenez, "Machine Learning Techniques for Motion Analysis of Fatigue from Manual Material Handling Operations Using 3D Motion Capture Data," in 10th Annual Computing and Communication Workshop and Conference (CCWC), 2020.

[45] M. Karg, G. Venture, J. Hoey and D. Kulić, "Human Movement Analysis as a Measure for Fatigue: A Hidden Markov-Based Approach," IEEE Transactions on Neural Systems and Rehabilitation Engineering , vol. 22, no. 3, pp. 470-481, 2014.

[46] S. Ameli, F. Naghdy, D. Stirling, G. Naghdy and M. Aghmesheh, "Assessment of exercise induced fatigue through motion analysis," in TENCON 2015 - 2015 IEEE Region 10 Conference, Macao, 2015.

[47] M. Golan, Y. Cohen and G. Singer, "A framework for operator – workstation interaction in Industry 4.0," International Journal of Production Research, 2019.

[48] M. Peruzzini, F. Grandi and M. Pellicciari, "Exploring the potential of Operator 4.0 interface and monitoring," Computers & Industrial Engineering, 2018.

[49] W. R. Johnson, A. Mian, C. J. Donnelly, D. Lloyd and J. Alderson, "Predicting athlete ground reaction forces and moments from motion capture.," Medical & Biological Engineering & Computing, pp. 1781-1792, 2018.

[50] E. v. d. Kurk and M. M. Reijne, "Accuracy of human motion capture systems for sport applications; state-of-the-art review," European Journal of Sport Science, vol. 18, no. 6, pp. 806-819, 2018.

[51] S. L. Colyer, M. Evans, D. P. Cosker and A. I. T. Salo, "A Review of the Evolution of Vision-Based Motion Analysis and the Integration of Advanced Computer Vision Methods Towards Developing a Markerless System," Sports Med Open, vol. 4, no. 1, 2018.

[52] Vicon, "What is motion capture," Vicon, [Online]. Available: https://www.vicon.com/about-us/what-is-motion-capture/.

[53] Qualisys, Qualisys AB, [Online]. Available: https://www.qualisys.com.

[54] CCOHS, "MMH - Introduction," Canadian Centre for Occupational Health & Safety, 4 June 2019. [Online]. Available: https://www.ccohs.ca/oshanswers/ergonomics/mmh/mmhintro.html.

[55] CCOHS, "MMH - Health Hazards," Canadian Centre for Occupational Health & Safety, 15 October 2020. [Online]. Available: https://www.ccohs.ca/oshanswers/ergonomics/mmh/hlth_haz.html.

[56] S. v. Sint Jan, Color Atlas of Skeletal Landmark Definitions, Elsevier Health Sciences, 2007.

[57] Hexoskin, "Hexoskin Health Sensors & AI," Hexoskin (Carre Technologies inc.), [Online]. Available: https://www.hexoskin.com/.

[58] "SolidWorks," Dassault Systems, [Online]. Available: https://www.solidworks.com.

[59] Z. Cheung, M. Feletto, J. Galante and T. Waters, "Ergonomic Guidelines for Manual Material Handling," Cal/OSHA Consultation Service, Research and Education Unit, Division of Occupational Safety and Health, California Department of Industrial Relations, 2007.

[60] "The Borg Scale of Perceived Exertion," Harvard T.H. Chan School of Public Health, [Online]. Available: https://www.hsph.harvard.edu/nutritionsource/borg-scale/.

[61] R. C. Team, "R: A Language and Environment for Statistical Computing," R Foundation for Statistical Computing, Vienna, Austria., 2013. [Online]. Available: http://www.R-project.org/.

[62] D. C. Wierschem, J. A. Jimenez and F. A. M. Mediavilla, "A motion capture system for the study of human manufacturing repetitive motions," The International Journal of Advanced Manufacturing Technology, vol. 110, pp. 813-827, 2020.

[63] H. Wickham, "The Split-Apply-Combine Strategy for Data Analysis," Journal of Statistical Software, vol. 40, no. 1, pp. 1-29, 2011.

[64] H. Sakoe and S. Chiba, "A Dynamic Programming Approach to Continuous Speech Recognition," in Proceedings of the Seventh International Congress on Acoustics, Budapest, 1971.

[65] X. Hu, S. Mo, D. Peng, F. Shen, C. Luo and X. Qu, "Automatic Activity Classification Based on Human Body Kinematics and Dynamic Time Wrapping," in 2018 IEEE 23rd International Conference on Digital Signal Processing (DSP), Shanghai, China, 2018.

[66] X. Yu and S. Xiong, "A Dynamic Time Warping Based Algorithm to Evaluate Kinect-Enabled Home-Based Physical Rehabilitation Exercises for Older People," Sensors, vol. 19, no. 13, p. 2882, 2019.

[67] P. A. Semblantes, V. H. Andaluz, J. Lagla, F. A. Chicaiza and A. Acurio, "Visual feedback framework for rehabilitation of stroke patients," Informatics in Medicine Unlocked, vol. 13, pp. 41-50, 2018.

[68] T. Hachaj and M. Piekarczyk, "Advanced human motion trajectories comparison using Dynamic PathWarping approach," WSEAS TRANSACTIONS on COMPUTERS, vol. 18, pp. 31-45, 2019.

[69] R. H. Osgouei, D. Soulsby and F. Bello, "An objective evaluation method for rehabilitation exergames," in 2018 IEEE Games, Entertainment, Media Conference, Galway, 2018.

[70] T. Giorgino, "Computing and Visualizing Dynamic Time Warping Alignments in R: The dtw Package," Journal of Statistical Software, vol. 31, no. 7, pp. 1-24, 2009.

[71] D. C. Montgomery, Introduction to Statistical Quality Control, Sixth Edition, John Wiley & Sons, Inc., 2009.

[72] L. Scrucca, " qcc: an R package for quality control charting and statistical process control," R News, vol. 4, no. 1, pp. 11-17, 2004.

[73] M. S. Software, Minitab, Inc., 2020. [Online]. Available: www.minitab.com.

[74] C. Yang, S. Leitkam and J. N. Côté, "Effects of different fatigue locations on upper body kinematics and inter-joint coordination in a repetitive pointing task," PLoS ONE, vol. 14, no. 12, 2019.

[75] P. J. Sparto, M. Parnianpour, T. E. Reinsel and S. Simon, "The Effect of Fatigue on Multijoint Kinematics and Load Sharing During a Repetitive Lifting Test," Spine, vol. 22, no. 22, pp. 2647-2654, 1997.

[76] A. D. Banks and F. Aghazadeh, "Progressive Fatigue Effects on Manual Lifting Factors," Human Factors and Ergonomics in Manufacturing, vol. 19, no. 5, p. 361–377, 2009.

[77] I. H. Witten, E. Frank, M. A. Hall and C. J. Pal, "Credibility," in Data Mining : Practical Machine Learning Tools and Techniques, Morgan Kaufmann, 2017.

[78] R. A. Armstrong, "When to use the Bonferroni correction," Ophthalmic Physiol Opt, vol. 34, p. 502– 508, 2014.

[79] IBM, "The calculation of Bonferroni-adjusted p-values," IBM SPSS Statistics, 16 April 2020. [Online]. Available: https://www.ibm.com/support/pages/calculation-bonferroni-adjusted-p-values.

[80] 2020 Minitab, LLC., "Methods that Minitab uses to calculate a 2 proportions test," Minitab, 2019. [Online]. Available: https://support.minitab.com/en-us/minitab-express/1/help-and-how-to/basic-statistics/inference/supporting-topics/tests-of-proportions-and-variances/methods-for-a-2-proportions-test/.

[81] G. Shao, S. Jain, C. Laroque, L. H. Lee, P. Lendermann and O. Rose, "Digital Twin for Smart Manufacturing: The Simulation Aspect," in Proceedings of the 2019 Winter Simulation Conference, 2019.

[82] "Unity," [Online]. Available: https://unity.com/.